creative commons
COMMONS DEED

저작자표시-비영리-변경금지 2.0 대한민국

이용자는 아래의 조건을 따르는 경우에 한하여 자유롭게

- 이 저작물을 복제, 배포, 전송, 전시, 공연 및 방송할 수 있습니다.

다음과 같은 조건을 따라야 합니다:

저작자표시. 귀하는 원저작자를 표시하여야 합니다.

비영리. 귀하는 이 저작물을 영리 목적으로 이용할 수 없습니다.

변경금지. 귀하는 이 저작물을 개작, 변형 또는 가공할 수 없습니다.

- 귀하는, 이 저작물의 재이용이나 배포의 경우, 이 저작물에 적용된 이용허락조건을 명확하게 나타내어야 합니다.
- 저작권자로부터 별도의 허가를 받으면 이러한 조건들은 적용되지 않습니다.

저작권법에 따른 이용자의 권리는 위의 내용에 의하여 영향을 받지 않습니다.

이것은 이용허락규약(Legal Code)을 이해하기 쉽게 요약한 것입니다.

Disclaimer

dCollection

A THESIS

FOR THE DEGREE OF DOCTOR OF PHILOSOPHY

Boundary Estimation in EIT using Oppositional Biogeography-Based Optimization

Ahmar Rashid

Major of Electronic Engineering

Faculty of Applied Energy System

GRADUATE SCHOOL

JEJU NATIONAL UNIVERSITY

2011. 06

Boundary Estimation in EIT using Oppositional Biogeography-Based Optimization

Ahmar Rashid

(Supervised by Professor Kyung Youn Kim)

A thesis submitted in partial fulfillment of the requirement for the degree of Doctor of Philosophy

2011. 06

The thesis has been examined and approved.

Thesis director, Sin Kim, Professor, Department of Nuclear and Energy Engineering, Jeju National University

B. Y. Choi

Bong Yeol Choi, Professor, Department of Electronic Engineering, Kyung Pook National University

Seok Jun Ko, Assistant Professor, Department of Electronic Engineering, Jeju National University

Min Jae Kang, Professor, Department of Electronic Engineering, Jeju National University

Kyung Youn Kim, Professor, Department of Electronic Engineering, Jeju National University

2011.07

Date

Major of Electronic Engineering
Faculty of Applied Energy System
GRADUATE SCHOOL
JEJU NATIONAL UNIVERSITY
REPUBLIC OF KOREA

dCollection @ jeju

Acknowledgements

All the praises are for Almighty Allah the sole creator of the universe. I would not have progressed even an inch further without his will.

I am so thankful to my parents who raised me with excessive love and affection. All my professional and academic achievements, whatsoever, have been the result of their enormous efforts to make me a successful person in life.

I would like to thank Professor Kyung Youn Kim for accepting me as a PhD student and supervising me with acumen throughout the entire course of the doctoral program. His continuous guidance helped me stay focused and his high expectations always made me work harder. I have found Professor Kyung Youn Kim very kind, caring and approachable. His contribution towards my personal life, making sure that my stay in Jeju remains comfortable and memorable, has been enormous and does not require explicit acknowledgement.

I am very grateful to Professor Sin Kim for his continuous scrutiny of my research work. His expert knowledge in the field of EIT and his resolve to bring quality to the work carried out at our research group and adherence to strict standards ensured that my PhD research work was always up to the mark.

I would like to express my gratitude towards all the remaining members of my PhD advisory committee, namely, Prof. Bong Yeol Choi, Prof. Min Jae Kang, Prof. Seok Jun Ko, for agreeing to review my thesis and providing me the feedback to further improve my research work.

I am thankful to Dr. Anil Kumar Khambampati for his nonstop support and help, professional and otherwise, during the whole period of my stay in Jeju. I would always remember him for the deeply involved discussions we have had during this time. I am much thankful to Dr Bong Seok Kim for his help and advice during my research work. I have found Dr. Kim, sincere, kind and a dedicated researcher in our inverse problems in engineering research group.

I am so thankful to all my friends, lab mates and peers including Umer, Nauman, Khalid, Murtuza, Arshad, Adnan, Saleem, RongLi, Liudong, Yoon Jeong, Boan Li, Min Seok and all others for their help and support, in and outside the lab.

Last, but not the least, I thank my wife, sister and brothers for all their moral and material support during the course of my work.

Collection @ jeju

Abbreviations and notations

AI	Artificial intelligence
BBO	Biogeography-based optimization
BBO/ES	Biogeography-based optimization combined with evolutionary strategy
CEM	Complete electrode model
DE	Differential evolution
DEA	Dynamic evolutionary algorithm
DOP	Dynamic optimization problem
EIT	Electrical impedance tomography
EM	Expectation maximization
EKF	Extended Kalman filter
EA	Evolutionary algorithm
EP	Evolutionary programming
ES	Evolutionary strategy
FEM	Finite element method
GA	Genetic algorithm
GP	Genetic programming
HSI	Habitat suitability index
SIV	Suitability index variable
MAE	Mean absolute error
MES	Mean error squared
MSE	Mean square error
mNR	Modified Newton-Raphson
OBBO	Oppositional biogeography-based optimization
OBL	Opposition-based learning
RMSE	Root mean square error
$RMSE_{Heart}$	Root mean square error of the Fourier coefficients aggregated for *Heart*
$RMSE_{Lung_1}$	Root mean square error of the Fourier coefficients aggregated for $Lung_1$
$RMSE_{Lung_2}$	Root mean square error of the Fourier coefficients aggregated for $Lung_2$
$RMSE_{Overall}$	Root mean square error of the Fourier coefficients aggregated for all the three organs
$RMSE_{Voltage}$	Root mean square for computed voltages
SIV	Suitability index variable
UKF	Unscented Kalman filter
Δf	Evolutionary progress in the fitness of a solution
$\overline{\Delta f}$	Cumulative average evolutionary progress in the fitness of a solution
ΔR	Relocation radius
Δr_c	Relocation radius for the cth decision variable

Collection @ jeju

$\Delta r_c^{\max}$	Maximum value of the relocation radius allowed in the cth decision variable
$\Delta r_c^{\min}$	Minimum value of the relocation radius allowed in the cth decision variable
$\overline{\Delta X}$	Average evolutionary progress in the decision space of a solution
Δx_c	Evolutionary progress in cth decision variable of a solution
$\overline{\Delta x_c}$	Cumulative average evolutionary progress in the cth decision variable of a solution
Φ	EIT cost functional
Ω	Object to be imaged
$\partial\Omega$	Boundary of the object
Ω_m	Mesh elements which cross the boundary
α	Used as a superscript with the basis function $\theta_n(s)$ $(\alpha = x / y)$
α_i, β_i	Parameters used in FEM formulation
$\hat{\gamma}$	Estimated value of the Fourier coefficient
$\gamma_j^{x_i}$	jth Fourier coefficient in the x-axis direction of the ith boundary
$\gamma_j^{y_i}$	jth Fourier coefficient in the y-axis direction of the ith boundary
γ_k^{α}	Fourier coefficients representing closed boundary
γ_{true}	True value of the Fourier coefficient
ε	Permittivity of the medium, precision variable
η	Number of Monte Carlo runs
θ_n	Periodic and smooth basis function, orthogonal to each other
λ	BBO immigration rate
μ	Permeability of the medium, BBO emigration rate
ν	Outward unit normal vector
σ	Conductivity of the medium
σ_e	Area weighted conductivity
$\sigma(x,y)$	Conductivity at $(x,y) \subset \Omega$
ϕ_i	Two-dimensional first order basis function
A	Magnetic vector potential, Stiffness matrix,
A_k	Disjoint region, enclosed inside a domain
B	Magnetic induction, Component of stiffness matrix
C	Component of stiffness matrix
$C_l(s)$	Boundary of any enclosed region
$C_k(s)$	Closed boundary
CR	Probability of crossover in DE algorithm
D	Electric displacement, Component of stiffness matrix
E	Electric field
$\mathbf{E}$	Maximum emigration rate in BBO

Collection @ jeju

F	Mutation scaling factor in DE algorithm
H	Magnetic field, habitat in a BBO population
$H_i(c)$	cth decision variable of the ith habitat
H^{N_P}	BBO population comprising of a group of N_P habitats
I	Identity matrix
$\mathbf{I}$	Maximum immigration rate in BBO
I_ℓ	Current applied to the ℓth electrode
J	Current density
J_r	Quasi-reflection jumping probability
J^s	Source current density
L	Number of electrodes
M	Number of closed boundaries inside the domain
N	Number of nodes in the finite element mesh
N_θ	Order of the Fourier coefficients to represent a closed boundary
N_c	Number of Fourier coefficients to represent an enclosed region
N_{ch}	Number of offspring solutions generated using an EA
N_G	Number of parent and offspring solutions combined
N_P	Number of candidate solutions in an EA population
P	Number of current patterns, Population of candidate solutions in an EA
Q_k	Process noise covariance
R_k	Measurement noise covariance
S_1, S_2	HSI islands in BBO
S_{max}	Maximum possible number of species in a BBO island
$\overline{S^X}$	Average sensitivity of decision space to change in objective space
T	Transpose of a matrix
U_ℓ	Boundary voltage measured on ℓth electrode
V	Boundary voltage calculated using the FEM formulation
$X_i(c)$	cth coefficient of the ith parent solution in DE
$Y_i(c)$	cth coefficient of the ith offspring solution in DE
e_ℓ	ℓth electrode
$\lvert e_j \rvert$	Area of the electrode j
f^{e_1}	Fitness values of an individual solution in old environment e_1
f^{e_2}	Fitness values of an individual solution in new environment e_2
$f_{best}^{e_2}$	Fitness value of the best fit solution in new environment e_2
i, j, k	indices
k	Discrete time step
ℓ	Electrode index
l	Enclosed region boundary index
n	Basis functions index
$nGen$	Total number of generations so far

Collection @ jeju

r_j	Uniformly distributed random number
s	Curve parameter $\in [0,1]$
s_e	Error standard deviation
$\overline{s_c^x}$	Average sensitivity of the cth decision variable to change in the objective space
$u(x,y)$	Electric potential at $(x,y) \subset \Omega$
w	Relative weight given to the past evolutionary progress compared to the most recent one
w_i	Reflection weight for the ith individual solution
w_k	Process noise
$\hat{x}$	An estimated solution
$\hat{x}_0$	Opposite of the estimated solution $\hat{x}$
$\hat{x}_{q0}$	Quasi-opposite of $\hat{x}$
$\hat{x}_{qr}$	Quasi-reflected of $\hat{x}$
x_c^{new}	cth decision variable after relocation step
x_c^{old}	cth decision variable before relocation step
$x_l(s)$	x-coordinates of the enclosed boundary, represented as coefficients of truncated Fourier series
$y_l(s)$	y-coordinates of the enclosed boundary, represented as coefficients of truncated Fourier series
z_ℓ	Contact impedance of lth electrode

Collection @ jeju

Contents

dCollection @ jeju

Collection @ jeju

List of figures

dCollection @ jeju

Collection @ jeju

Collection @ jeju

Collection @ jeju

Collection @ jeju

List of tables

Collection @ jeju

초 록

전기 임피던스 단층촬영법(EIT)은 비침습성 영상 방법으로, 산업 분야뿐만 아니라 의료 분야에서도 활발히 연구되어 왔다. 그러나 EIT를 사용하여 도전율 분포를 복원하기 위한 역문제 알고리즘들의 성능은 종종 차선(sub-optimal)이 된다. 측정 잡음에 대한 EIT의 높은 민감도, 반올림 오차(rounding-off errors), EIT 문제가 갖는 고유의 부정치성 성질 그리고 전역 최소치 대신에 국부 최소치로의 수렴 등등 이런 요소들로 인해 낮은 성능을 보인다. 게다가, 대부분의 역문제 알고리즘들의 성능은 초기치의 선택뿐만 아니라 gradient matrix의 정확한 계산에 크게 좌우한다. 이런 요인들을 고려해 보면, 정확한 해에 도달하기 위한 효과적인 최적화 알고리즘이 요구된다. 본 논문에서는 2D EIT를 사용하여 대상 도메인 내부에서 표적들의 경계면에 대한 모양과 크기 그리고 위치를 추정하기 위해 oppositional biogeography 기반의 최적화(OBBO) 기법을 제시하고 있다. 표적들의 경계면은 truncated 푸리에 급수의 계수로 표현되는데, 이 때 표적들의 도전율 값은 선험적으로 알려져 있다고 가정한다. OBBO 기법은 흉부와 같은 구조 내부에서 정적 조직의 경계면들을 복원하는데 처음으로 적용된다. 그리고 나서 움직이는 심장의 경계면을 추정하는데 동적 OBBO 기법이 적용된다. 그리고 정적뿐만 아니라 동적 경우에 대해, 반복적인 수치적 시뮬레이션과 실험 데이터를 사용하여 알고리즘의 강인성(robustness)을 입증하였다. OBBO 기법을 사용하여 추정된 파라미터들에 대해 폭넓은 통계학적 분석을 하였고 전형적인 mNR 알고리즘과 EKF 알고리즘과 비교하였다. 전형적인 알고리즘들과 비교했을 때 OBBO 기법이 우수한 성능을 보였다. 게다가, OBBO 기법은 측정 잡음과 경계면의 크기와 위치에 대한 초기치에 강인하였고 도전율의 선험적 지식이 정확하지 않을 때도 타당한 해를 제공하였다.

dCollection @ jeju

1. Introduction

1.1 Motivation and problem description

Electrical impedance tomography (EIT) is a non-invasive imaging modality in which a cross sectional image of the conductivity distribution inside an object can be obtained by injecting a set of current patterns and measuring boundary voltages across the electrodes attached to the surface of the object (McArdle 1992, Vauhkonen 1997). There are several applications of EIT in the fields of medical imaging and process industry. In medical imaging, EIT can be used to detect certain anomalies such as breast cancer cells (Kim *et al*. 2007a) and monitor several physiological phenomena, such as cardiac, pulmonary and respiratory functions (Harris 1991, Brown 1994, Kim *et al*. 2006, Deibele 2008). The applications of EIT in the process industry include monitoring the multi-phase flow in the process pipelines, monitoring of the mixing phenomenon, sedimentation monitoring and etc. (Mann *et al*. 1997, Kim *et al*. 2005, Khambampati *et al*. 2009, Rashid at al. 2010a). The conductivity estimation using EIT is a nonlinear ill-posed problem. In medical imaging we are often interested in the estimation of organ boundaries rather than the conductivity distribution inside the human body. The poor spatial resolution of EIT makes it difficult to estimate the organ boundaries, thus undermining its anatomical significance. If the conductivity values inside a specific region of the human body, such as that of thorax region, are assumed to be known *a priori* then the inverse problem in EIT becomes the estimation of shape, size and location of the internal organs. Such an approach is known as the boundary estimation problem in EIT. It consequently leads to a much lesser ill-posed problem and significantly reduces the dimension of the solution space. It also results in marked improvement in the estimation performance of the EIT inverse problem in terms of spatial resolution.

1.2 Boundary estimation in EIT

Several boundary estimation approaches have been devised in the literature (Han and Prosperetti 1999, Ikehata and Siltanen 2000, Kolehmainen *et al*. 2001). In closely related studies, Vauhkonen *et al*. (1998) and Rashid *et al*. (2010b) considered to

Collection @ jeju

reconstruct the elliptic boundaries, represented using only six Fourier coefficients. They assumed that the boundaries of the lungs are known *a priori* and the estimation problem was reduced to the estimation of heart (ventricle) boundary. Similarly, Khambampati *et al*. (2010) assumed the heart boundary to be known, while the dynamic boundaries of the elliptic lungs were recovered using the expectation maximization algorithm. The *a priori* knowledge of the boundaries of some of the organs, while reconstructing the others, may be inaccurate potentially leading to large estimation errors in realistic situations. Kolehmainen *et al*. (2001) considered a more general case, i.e., simultaneous estimation of three non-elliptic region boundaries (resembling two lungs and a heart) inside a circular domain using extended Kalman filter (EKF). They also attempted to reconstruct the boundaries using the traditional Gauss-Newton method; however, it exhibited severe convergence problems and a tendency to produce self-intersecting boundaries when the number of Fourier coefficients to express the boundaries is high. Even EKF reconstructions, besides a very close initial guess, sometimes showed deviations from the true boundaries, especially in the case of non-elliptic lungs. All these facts necessitate further research into EIT boundary estimation, more specifically in the case of multiple non-elliptic targets in which the inverse algorithms usually exhibit poor performance.

EIT reconstruction can be classified as either static imaging or dynamic imaging. In the case of static imaging, a full frame of independent measurements is available while the conductivity distribution inside the domains remains constant. In the case of dynamic imaging, however, a full measurement frame may not be obtained before the conductivity inside the domain changes. The static imaging algorithms usually fail to track the fast conductivity changes inside the domain. The dynamic imaging algorithms, on the other hand, enhance the temporal resolution of the EIT image when the conductivity distribution inside the body changes rapidly (Kim *et al*. 2001, Kim *et al*. 2007b). Extended Kalman filter (EKF) is one of the most frequently used dynamic estimation algorithms for nonlinear systems. EKF, however, is only accurate up to second order for Gaussian distribution. Moreover, the performance of EKF heavily relies on the calculation of Jacobain to linearize the inherently non-linear EIT problem. The unscented Kalman filter (UKF), which

Collection @ jeju

propagates mean and covariance information through a nonlinear transformation, does not require to calculate Jacobian and potentially offers superior performance compared to EKF (Julier and Uhlmann 2004). Remarkably, the computational complexity of the UKF is of the same order as that of EKF. Considering these advantages, Khambampati *et al*. (2009) employed UKF as an inverse solver to estimate the sharp interfacial phase boundaries in three-dimensional sedimentation monitoring using 3D EIT.

A major challenge while applying EIT to dynamic image reconstruction is that a state evolution based estimation technique is required. The evolution model, along with the observation model, constitutes the state-space representation of the system. In the state-space model, the evolution of state parameters is modelled as a stochastic process. The knowledge of the stochastic nature of the state evolution is instrumental in order to apply EIT for dynamic image reconstruction. A number of state evolution models have been proposed to monitor dynamic processes using EIT (Vauhkonen *et al.* 1998, Tossavainen *et al.* 2006, Kim *et al.* 2004, Khambampati *et al*. 2009). The simplest of these models is the so-called random-walk model in which the state parameters evolve by a predetermined covariance of the added white noise (Vauhkonen *et al.* 1998, Kim *et al.* 2007). However, application of this model is based on the fact that no prior knowledge of the process is available therefore it is not considered as an accurate evolution model. For processes which evolve with constant velocity or constant acceleration, the kinematic models offer a better solution (Tossavainen *et al.* 2006, Khambampati *et al*. 2009]. The kinematic models have originated from target tracking problems (Li 1997). In a comparative study, Tossavainen *et al*. (2006) showed that the kinematic models had better estimation of the settling curves, settling velocities and the conductivities of the phase layers than the random-walk model. Another evolution model which is commonly used to monitor the flow of a fluid in a pipeline is based on the convection diffusion equation (Seppanen *et al.* 2001a, 2001b). Rashid *et al*. (2010a) proposed a state evolution model developed for three-layer sedimentation based on the solids flux theory for batch sedimentation. It is essentially based upon a kinematical theory of sedimentation based on the propagation of sedimentation waves in the suspension and assumes that the settling velocity of the particles is a function of the

Collection @ jeju

concentration alone. The model is simple, computationally inexpensive and incorporates the dynamics of actual sedimentation phenomenon.

In realistic environments, the dynamics of the evolution are complex and it may be very difficult to model them in a prior form. The coefficients of noise covariance in the dynamic algorithms such as EKF and UKF need to be manually tuned and may lead to suboptimal performance, if not tuned well. It is, nevertheless, possible to estimate the dynamic state transition matrix, the noise covariance matrices and the initial states with the help of expectation-maximization (EM) algorithm. The EM algorithm is a method of finding a mode of the proposed likelihood function through the expectation and maximization steps (Dempster *et al*. 1977, Shumway and Stoffer 1982). Khambampati *et al*. (2011) proposed a dynamic estimation scheme to track the void boundaries in the flow process based on the assumption that the prior knowledge of the model parameters is not known with certainty. The problem was treated as state estimation problem to estimate the non-stationary boundaries represented using the Fourier coefficients.

The performance of the inverse algorithms for image reconstruction using EIT is often sub-optimal. Several factors contribute to this poor performance including high sensitivity of EIT to the measurement noise, the rounding-off errors, the inherent ill-posed nature of the problem and the convergence to a local minimum instead of the global minimum. Moreover, the performance of many of these inverse algorithms heavily relies on the selection of initial guess as well as the accurate calculation of a gradient matrix. Considering these facts the need of an efficient optimization algorithm to reach the correct solution cannot be overstated.

This thesis presents an oppositional biogeography-based optimization (OBBO) technique to estimate the shape, size and location of non-stationary region boundaries inside an object domain using two-dimensional electrical impedance tomography (2D EIT). The region boundaries are expressed as coefficients of truncated Fourier series and the conductivity distribution inside the domain is assumed to be known *a priori* (Kolehmainen *et al*. 2001). First of all, a static scenario has been considered such that all the organ boundaries are assumed be constant while a full frame of independent measurement data is obtained. In the second situation, the boundaries of the lungs are fixed while a heart expansion/contraction cycle is considered. The

Collection @ jeju

scenarios are analogous to the situation in which a patient is told to hold his/her breathe while EIT measurements are taken. In the second case, a partial subset of the full measurement frame is assumed to be available at each instance. A dynamic version of the OBBO is used to reconstruct the non-stationary organ boundaries in this case. An extensive statistical analysis of the estimated parameters using OBBO and its comparison with the traditional modified Newton-Raphson (mNR) and EKF algorithms is presented.

The main advantage of the proposed estimation technique over the traditional techniques is that it does not require the calculation of the Jacobain matrix. Furthermore, the dynamic version of the OBBO is very simple to derive and implement. Finally, in contrast to the aforementioned dynamic algorithms (EKF/UKF), the dynamic OBBO does not require much manual tuning, potentially leading to far superior results with little tuning effort.

1.3 Dissertation outline

This thesis consists of seven chapters. The first chapter gives a brief introduction and a literature survey of the boundary estimation in electrical impedance tomography. The second chapter gives an overview of electrical impedance tomography and its constituents. i.e., the forward problem and the inverse problem. Chapter three presents a literature survey of standard and advanced evolutionary algorithms (EAs). Chapter four applies the selected evolutionary algorithm, namely OBBO, to reconstruct static organ boundaries in human thorax using EIT. An extensive statistical analysis of the technique with the help of numerical simulations as well as with an experimental setup resembling human chest is presented. Chapter five introduces the dynamic optimization problem (DOP), discusses its important features and the related issues, presents the desired characteristics of a dynamic evolutionary algorithm (DEA) suitable to solve DOPs and concludes with the most common evolutionary approaches to solve them. Chapter six presents the dynamic OBBO with variable relocation. Finally, chapter seven presents a study of the dynamic OBBO applied to dynamic heart boundary estimation using EIT.

Collection @ jeju

2. Electrical impedance tomography

2.1 EIT forward problem

Electrical impedance tomography is an imaging modality in which the internal electrical conductivity distribution is reconstructed based on the imposed currents and the measured voltages across the electrodes placed on the surface of an object. The physical relationship between the internal conductivity $\sigma(x,y)$ and the electrical potential $u(x,y)$ on the object $\Omega \subset \Re^2$ is governed by a partial differential equation, derived from Maxwell's equations (Isaacson and Cheney 1990, Malmivuo and Plonsey 1995, Somersalo *et al*. 1992). Let E be an electric field, B be used to denote magnetic induction, H used for magnetic field, J used to denote the current density and D be the electric displacement, then the electromagnetic field in a domain $\Omega \in \Re^2$ can be described as

$$\nabla \times E = -\frac{\partial B}{\partial t} \tag{2.1}$$

$$\nabla \times H = J + \frac{\partial D}{\partial t}, \tag{2.2}$$

If the domain Ω is assumed to consist of a linear and isotropic medium then it follows that

$$D = \varepsilon E \tag{2.3}$$

$$J = \sigma E \tag{2.4}$$

$$\mathrm{B} = \mu H \tag{2.5}$$

where ε is the permittivity, μ is the permeability and σ is conductivity of the medium. If the injected currents are assumed to be time harmonic with frequency ω then after cancelling out the oscillatory exponential and separating the current density J into two components, ohmic current ($J^0 = \sigma E$) and current source (J^s), the Maxwell's equations can be written as

$$\nabla \times E = -i\omega\mu H \tag{2.6}$$

$$\nabla \times H = (\sigma + i\omega\varepsilon)E + J^s \tag{2.7}$$

Assuming static conditions such that the effect of magnetic induction as well as the capacitive effects $i\omega\varepsilon E$ are neglected (Barber and Brown 1984) and using the fact

Collection @ jeju

that J^s is zero in the given EIT frequency range, the following equations can be derived

$$E = -\nabla u \tag{2.8}$$

$$\nabla \times E = -i\omega\mu H \tag{2.9}$$

$$\nabla \times H = \sigma E \tag{2.10}$$

$$\nabla \cdot (\nabla \sigma u) = 0 \tag{2.11}$$

where $u = u(x, y)$ is the electric potential at $(x, y) \subset \Omega$. Equation (2.11) is known as the EIT governing equation and can be solved with appropriate boundary conditions, such as the so-called complete electrode model (CEM) which considers the shunting effects of the measurements as well as the contact impedance between the electrodes and the medium

$$\int_{e_\ell} \sigma \frac{\partial u}{\partial \nu} dS = I_\ell, \qquad (x, y) \subset e_\ell, \ \ell = 1, 2, \cdots, L \tag{2.12}$$

$$\sigma \frac{\partial u}{\partial \nu} = 0, \qquad (x, y) \subset \partial\Omega \setminus \bigcup_{\ell=1}^{L} e_\ell \tag{2.13}$$

$$u + z_\ell \sigma \frac{\partial u}{\partial \nu} = U_\ell, \qquad (x, y) \subset e_\ell, \ \ell = 1, 2, \cdots, L \tag{2.14}$$

where L is the number of electrodes, ν is the outward normal unit vector, z_ℓ is the effective contact impedance and U_ℓ is the measured boundary potential. Here, (2.12) represents the electrical current I_ℓ injected to the object Ω through the ℓth electrode e_ℓ while (2.13) shows that the current is zero in the regions between the electrodes. The equation (2.14), which represents the voltage U_ℓ measured across the electrodes $\ell = 1, 2, \cdots, L$, considers the shunting effect (i.e., the potential on the surface of each electrode is constant) and the contact impedance between the electrode and electrolyte inside the domain. The details of the different electrode models used in EIT can be found in the reference (Cheng *et al*. 1989). In addition to the boundary conditions, described before, two additional constraints are also imposed to solve the governing equation given in (2.11).

$$\sum_{\ell=1}^{L} I_\ell = 0 \ \text{ and } \ \sum_{\ell=1}^{L} U_\ell = 0 \tag{2.15}$$

Collection @ jeju

The first constraint enforces the conservation of charge which is needed for the existence of the solution while the second constraint enforces a condition on the voltages to specify the ground potential and is needed to ensure the uniqueness of the solution (Somersalo *et al*. 1992). The calculation of the boundary voltages using (2.11) – (2.15) is called the EIT forward problem. The forward problem is solved using the finite element method (FEM). The detailed FEM formulation of EIT can be found in the dissertation of Vauhkonen (1997). In FEM, the domain is divided into a number of small triangular elements. The conductivity value inside each finite element is assumed to be constant. Let N be the number of nodes in the finite element mesh. The finite element formulation gives the following system of linear equations (Vauhkonen 1997)

$$\mathbf{Ab} = \tilde{\mathbf{I}} \tag{2.16}$$

where

$$\mathbf{A} = \begin{pmatrix} \mathbf{B} & \mathbf{C} \\ \mathbf{C}^T & \mathbf{D} \end{pmatrix}, \qquad \mathbf{b} = \begin{pmatrix} \alpha \\ \beta \end{pmatrix} \quad \text{and} \quad \tilde{\mathbf{I}} = \begin{pmatrix} \mathbf{0} \\ \bar{\mathbf{I}} \end{pmatrix} \tag{2.17}$$

Here, $\alpha = (\alpha_1, \alpha_2, \cdots, \alpha_N)^{\mathrm{T}} \in \Re^{N\times 1}$ and $\beta = (\beta_1, \beta_2, \cdots, \beta_{L-1})^{\mathrm{T}} \in \Re^{(L-1)\times 1}$. $\bar{\mathbf{I}} = (I_1 - I_2, I_1 - I_3, \cdots, I_1 - I_L)^{\mathrm{T}} \in \Re^{(L-1)\times 1}$ is the reduced current matrix and $\mathbf{0} = (0, ..., 0)^{\mathrm{T}} \in \Re^{N\times 1}$. The system matrix $\mathbf{A} \in \Re^{(N+L-1)\times(N+L-1)}$ is of the form

$$B(i,j) = \int_\Omega \sigma \nabla \phi_i \cdot \nabla \phi_j \mathrm{d}\Omega + \sum_{\ell=1}^{L} \frac{1}{z_\ell} \int_{e_\ell} \phi_i \phi_j \mathrm{d}S, \; i,j = 1,2,\cdots,N \tag{2.18}$$

$$C(i,j) = -\frac{1}{z_1} \int_{e_1} \phi_i \mathrm{d}S + \frac{1}{z_{j+1}} \int_{e_{j+1}} \phi_i \mathrm{d}S, \; i = 1,2,\cdots,N, \; j = 1,2,\cdots,L-1 \tag{2.19}$$

$$C(i,j) = \begin{cases} \dfrac{|e_1|}{z_1} & i \neq j \\ \dfrac{|e_1|}{z_1} + \dfrac{|e_{j+1}|}{z_{j+1}} & i = j \end{cases}, \; i,j = 1,2,\cdots,L-1 \tag{2.20}$$

where ϕ_i is the two-dimensional first-order basis function and $|e_j|$ is the area of the electrode j.

A schematic description a 2D EIT measurement setup is shown ion figure 2.1.

Collection @ jeju

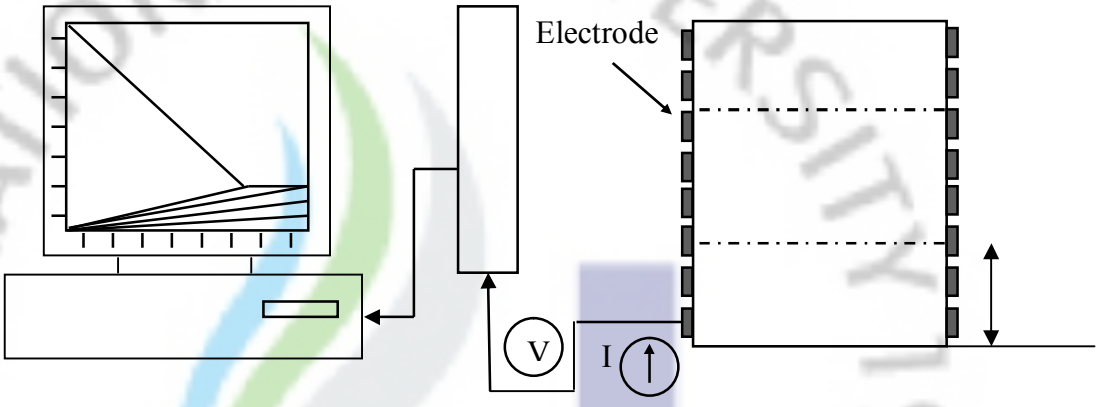

Figure 2.1. EIT schematic diagram.

2.2 EIT inverse problem

The EIT image reconstruction consists of forward and inverse problems. While the forward problem calculates the boundary voltages based on the given conductivity distribution, the inverse problem reconstructs the conductivity distribution minimizing the difference between the measured and the calculated boundary voltages.

$$\Phi = \frac{1}{2}[V-U]^T[V-U] \tag{2.21}$$

where U is the actual voltage measurements across the boundary electrodes and V is denotes the calculated voltages obtained through the FEM formulation. The objective of this thesis, however, is the estimation of the size and location of the internal organs rather than the conductivity estimation. If the conductivities of the organs are assumed to be known then the inverse problem is reduced to the reconstruction of organ boundaries (expressed as Fourier coefficients) inside the human chest. The cost functional (2.11), in turn, is expressed in terms of the Fourier coefficients γ_k as follows

$$\Phi(\gamma_k) = \frac{1}{2}[V(\gamma_k)-U]^T[V(\gamma_k)-U] \tag{2.22}$$

where $V(\gamma_k) \in \Re^{LK\times 1}$ are the calculated voltages based on given Fourier coefficients γ_k, $U \in \Re^{LK\times 1}$ are the measured voltages, k represents the iteration number and LK is the number of measurements at each iteration.

The conventional inverse algorithms in EIT, such as mNR and EKF, often show sub-optimal performance when used to solve the EIT inverse problem. The

Collection @ jeju

transformation of the conductivity estimation problem into a boundary estimation problem significantly reduces the ill-posedness of EIT inverse problem. However, the highly nonlinear nature of the inverse problem, the presence of the measurement noise, the discretization errors and the possibility of its convergence to a local minimum around the global minimum make it an extremely difficult problem to be solved in realistic conditions. Since an analytical solution to the EIT boundary estimation problem is very difficult to achieve, the selection of an efficient and reliable numerical minimization technique is paramount to reach the optimum solution. An algorithm which offers fast convergence to the optimum solution, effectively bypassing/filtering out the local minima, is desired. An algorithm combining the features of a global search method to a local search technique would be best suited to solve this problem. The evolutionary algorithms (EAs) are one class of such algorithms. In contrast to the traditional inverse algorithms applied to EIT these algorithms do not require the calculation of a Jacobian and, due to a large number of potential solutions available, often outperform the gradient-based methods. The application of a few EAs to EIT image reconstruction has been studied before (Rolnik and Seleghim 2006, Eckel H 2008, Rashid *et al*. 2010c). A recently introduced class of evolutionary algorithms offering aforementioned characteristics is the biogeography-based optimization (Simon 2008). The hybrid evolutionary algorithms usually outperform the autonomous evolutionary algorithms. (Tseng and Liang 2006, Grosan *et al*. 2007, Du *et al*. 2009). Du *et al*. (2009) have incorporated the features of evolutionary strategy (ES) (Beyer and Schwefel 2002) into biogeography-based optimization (BBO) and suggested the hybrid algorithm namely biogeography-based optimization combined with evolutionary strategy (BBO/ES). Ergezer *et al*. (2009) have incorporated the opposition-based learning (OBL) into the BBO algorithm to introduce the hybrid algorithm named oppositional biogeography-based optimization (OBBO). This thesis considers the application of OBBO to solve the EIT boundary estimation problem.

Collection @ jeju

2.2.1 The boundary representation

Let us consider a domain schematically shown in figure 1. The outer boundary $\partial\Omega$ of the object is assumed to be known. The boundary $C_l(s)$ of any enclosed region is assumed to be sufficiently smooth to be expressed as coefficients of truncated Fourier series $\gamma_k \in \Re^{2MN_\theta}$ (Kolehmainen *et al*. 2001)

$$C_l(s) = \begin{pmatrix} x_l(s) \\ y_l(s) \end{pmatrix} = \sum_{n=1}^{N_\theta} \begin{pmatrix} \gamma_n^{x_l} \theta_n^x(s) \\ \gamma_n^{y_l} \theta_n^y(s) \end{pmatrix}, \; l = 1,2,\cdots,M \tag{2.23}$$

where M is the number of boundaries, N_θ is the order of Fourier coefficients and $\theta_n(s)$ is the periodic and smooth basis function of the form

$$\begin{aligned} \theta_n^\alpha &= 1, && n = 1 \\ \theta_n^\alpha &= \sin(2\pi \frac{n}{2} s), && n = 2,4,6,\cdots \\ \theta_n^\alpha &= \cos(2\pi \frac{n-1}{2} s), && n = 3,5,7,\cdots \end{aligned} \tag{2.24}$$

The basis functions $\theta_n(s)$ are orthogonal to each other. The curve parameter $s \in [0,1]$ and α denotes x or y.

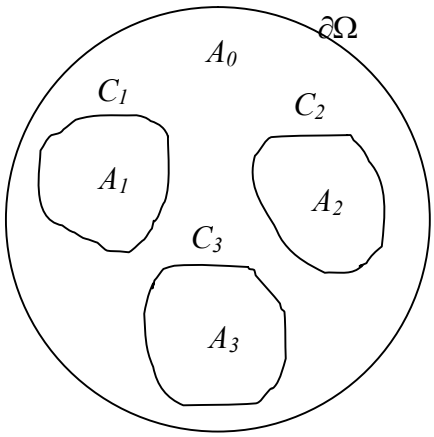

Figure 2.2. A schematic view of an object with three regions (M = 3) enclosed inside it. The boundary of the background region A_0 is $\partial\Omega$ while the boundaries of the enclosed regions A_1, A_2 and A_3 are denoted by C_1, C_2 and C_3, respectively.

Expanding (2.23) and (2.24), the boundaries C_l can be represented as γ of the shape coefficients, i.e.

$$\gamma = (\gamma_1^{x_1},\ldots,\gamma_{N_\theta}^{x_1},\gamma_1^{y_1},\ldots,\gamma_{N_\theta}^{y_1},\ldots,\ldots\gamma_1^{x_M},\ldots,\gamma_{N_\theta}^{x_M},\gamma_1^{y_M},\ldots,\gamma_{N_\theta}^{y_M})^{\mathrm{T}} \tag{2.25}$$

Collection @ jeju

The truncated Fourier series reduce to a centre point, circle and ellipse for N_θ=1, 2 and 3, respectively. This paper considers the problem of estimating the boundaries of two lungs and the heart (M = 3) with the conductivities of the organs and the background assumed to be known *a priori*. The inverse problem, therefore, becomes the estimation of $2MN_\theta$ Fourier coefficients γ given in (2.25). A schematic view of an object with three regions (M = 3) enclosed inside it is shown in figure 2.2.

Collection @ jeju

3. Evolutionary algorithms

Any optimization problem which is aimed at finding the best global solution among a possible set of local optima is known as the global optimization problem. One of the most popular examples of global optimization problems is the traveling salesman problem. These problems are often nonlinear, non-differentiable, exist in higher dimension of space and often fail reach the global optimum due to the presence of local minima. The analytical solution of these problems usually does not exist and thus require an algorithm equipped with a global search mechanism. Evolutionary algorithms (EAs) are well known population-based global optimization algorithms which work on the principal of mutation and recombination, the latter often referred to as the crossover (Bäck and Schwefel 193). The crossover creates new candidate solutions by combining two or more existing solutions, while the mutation corresponds to the erroneous duplication of the previous solutions. The crossover steps tends to increase the correlation among the current set of candidate solutions, whereas the mutation keeps the search space open to new solutions, thus increasing the population diversity. Both the approaches have their own advantages and disadvantages and the right balance between them has been studied before (Spears 1992).

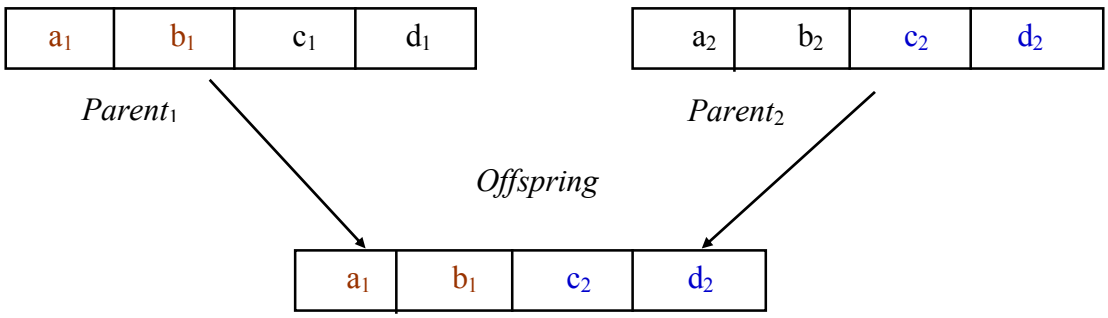

Figure 3.1. Schematic description of a simple crossover operation involving two parents. The characteristic variables a_1, b_2, from *Parent*$_1$ combine with the variables a_3, b_4 of *Parent*$_2$ to generate the new *Offspring*.

A major advantage of the EAs is their ability to incorporate *a priori* information into the problem solution. This is particularly beneficial in the case of EIT boundary estimation, which usually suffers from large measurement and round-off errors and under realistic conditions it is often impossible to be solved without

Collection @ jeju

any prior information. The *a priori* information can be incorporated in several ways. One way to do it is simply rejecting all the infeasible solutions (e.g., in the case of multi-region boundary estimation, the boundaries cannot cross each other). However, this can be computationally expensive. Another way to do it is the use of such mutation and crossover schemes which make sure that only feasible solutions are generated.

3.1 Basics of evolutionary algorithms

Using an evolutionary algorithm to address a problem requires choosing at least five elements:

- population initialization
- representation for the solution
- variation operators to apply
- evaluation criteria, and
- selection method

One of the most critical considerations for an evolutionary algorithm is the selection of the initial population. A population is a group of individuals belonging to the same species, resembling more closely to each other in terms of their genetics than any other group of individuals of the same species. In terms of the evolutionary algorithms, an initial population is a set of preliminary candidate solutions to the given problem. Each candidate solution is represented using some form of data structure. The selection for the data structure to store the candidate solutions is subject to reduction of computational complexity and ease of implementation. The data structure should be able to support the fundamental operations required for the implementation of the evolutionary algorithms such as sorting, variational operations/perturbations applied to evolve the current solutions into new solutions, the statistical analysis of the solutions based upon probability distributions and etc. The evaluation criteria measure the quality of the candidate solutions. The selection method uses the fitness of the solutions to select and eliminate a subset of the candidate solutions at each generation. The solutions which survive are termed as the

Collection @ jeju

parents. Figure 3.1 provides a flowchart of the process, while the key steps of the an evolutionary algorithm are as follows (Weicker 2003)

1. Initialize the algorithm parameters such as the size of population, the number of decision variables required to characterize an individual solution and etc.
2. Initialize a set of N_P potential solutions for the problem, referred to as the initial population P. Also, compute the cost Φ for each of the solution in the initial population set.
3. Select parents form offspring generation from the population P.
4. Generate offsrpings using combination/crossover operations.
5. Perform mutation based upon the mutation probability.
6. Calculate the cost Φ of each new solution.
7. Compare the newly generated solutions (steps 3-6) and select the N_P most feasible solutions for the next generation.
8. Go to step 3 for the next iteration, if needed.

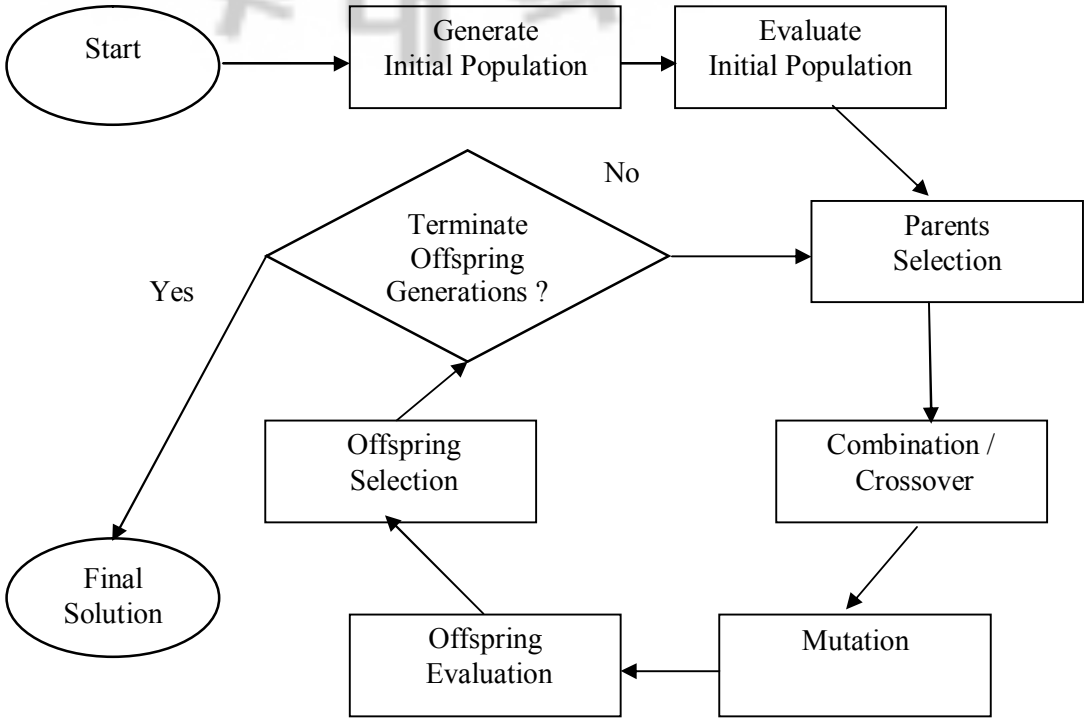

Figure 3.2. Flow chart description of offspring generations in evolutionary algorithms.

Collection @ jeju

Like any other algorithm, an evolutionary algorithm starts with the initialization of the necessary parameters regarding the algorithm. The first step after the initialization/start of the algorithm is the selection of an initial population. The size and the range of the initial population are problem dependent and strongly affect the performance of the algorithm. The initialization of an evolutionary algorithm can be arbitrary, completely at random, or can be based upon some historical data acquired though other sources. One of the most important characteristics of a good initial population is its diversity. In biology, the population diversity is usually measured in terms of the variation in the genetic features defining the population, or in terms of the populations' demographics, such as the number and proportion of individuals belonging to different age groups, genders, races and etc. In evolutionary computation, the diversity of the population is a measure of variation in the candidate solutions present in the population. The diversity can be measured either in terms of the variation in the fitness of the solutions or in terms of the variation in values of the characteristic features of each individual in the population.

Before entering into the generation loop of the algorithm, the fitness of each candidate solution in the initial population is evaluated. The fitness of an individual solution is the measure of the quality of that solution and forms the basis of selection procedures, for parents as well as the offsprings. The fitness evaluation criterion in the optimization problems, in general, is based upon the minimization of a predefined objective function. The objective function, also referred to as the cost functional, can be expressed either in terms of maximizing fitness, or minimizing error, or some combination of potentially conflicting criteria. Within each iteration, the population is sorted and ranked based upon the cost of the candidate solutions. The rank information is subsequently used for the selection of parents and the offsprings in the later part of the algorithm.

The role of the parent selection step is to select a number of individuals in the current population which lead to the creation of offsprings for the next generation. The selection of parents is qualitative and is often based upon probability distributions of the individuals in the population. Thus the individuals with higher fitness values have better chances of becoming parents as compared to the individuals which are least fit. In most of the evolutionary algorithms, an offspring is

Collection @ jeju

generated from two parents only; however, in some algorithms more than two parents may participate in the generation of a new offspring.

The combination/crossover step combines the features of two or more parents to generate a new offspring. The implementation of the crossover operator varies for different types of evolutionary algorithms. It can be as simple as a binary crossover between two parents or can be a complex probabilistic combination of two or more than two parents. A simple crossover operation involving two parents is depicted in figure 3.1. A number of offspring solutions are generated this way. Some of the offsrpings will be better (more fit) than their parents while others may not be better, or even worse than their parents. Selecting the best individuals for the next generation is the job of forthcoming steps in the algorithm. The dissertation by LaTorre (2009) gives an overview of common crossover operators and some of the selection schemes.

As the EA proceeds, the solutions with a high probability of success, i.e., the best fit solutions, tend to dominate the least fit solutions. This would be unfair in the sense that the solutions with a lower fitness (consequently of higher cost) value will not get much chance to improve even if they have more potential than the other solutions. In EAs, there is a remedy available for this in the form of mutation. The mutation step aims to keep the search space open to new solutions, thus maximizing the chance to reach at the best solution.

The fitness evaluation of an offspring is similar to the fitness evaluation step for the initial population, explained before. The only difference is that the objective of former step was to select the best parents for the offspring generation whereas the latter step is aimed at selecting the best offsprings for the next generation step.

The selection the offspring solutions to be carried to the next evolutionary cycle can be done in a number of ways

- *Steady state selection*: Only one offspring is generated and takes the place of one individual in the parent population.
- *Generational selection*: All the individuals in the parent population are replaced by a new generation of offspring solutions.

Collection @ jeju

- *Hybrid selection*: Some of the individual solutions in the parent population are replaced by new offspring solutions, while the others parents are retained. This strategy is aimed at selecting the best of all individuals among the parents and their offsprings.

In general, the hybrid selection scheme results in a better selection of the individual solutions as compared to other schemes and often leads to more optimized results. However, the selection and consequently the performance of the best scheme is problem dependent.

For the problems which are known to have an optimum solution, the termination criterion can be that the best solution has a fitness value with a give precision □ > 0. However, in order to avoid the scenario in which the algorithm may get stuck in an infinite loop, a stopping condition has to be enforced. Such a condition could be

- the maximum number of fitness evaluations allowed
- the maximum number of generation steps allowed
- the maximum number of generation steps during which the improvement in the value of the best solution does not exceed a certain threshold
- the maximum CPU time allowed to be elapsed, or
- the population diversity decreases below a certain threshold

3.2. Standard evolutionary algorithms

This section summarizes the characteristic features and the working of some standard evolutionary algorithms. Following algorithms have been considered

- genetic algorithms
- evolutionary strategies
- evolutionary programming
- genetic programming

3.2.1 Genetic algorithms

Genetic algorithms (GAs) are one of the most popular classes of EAs and have been introduced in mid twentieth century (Barricelli 1957, Fraser 1957). However, the book written by Holland (1975) is much responsible of the popularity of GAs. GAs

Collection @ jeju

are inspired by natural evolution and, like any other EA, solve the optimization problems using standard EA operation such as inheritance, mutation, selection, and crossover. Simple generational genetic algorithm procedure is as follows:

1) Select an initial set of candidate solutions, termed as the initial population.
2) Calculate the fitness/cost of each solution in the initial population.
3) Repeat the following steps until some termination criteria is met
   a) Select suitable pairs of parent solutions from the current population.
   b) Probabilistically perform the crossover operation on the selected parents to generate new offsprings.
   c) Probabilistically perform mutation for a selected set of individuals.
   d) Evaluate the fitness/cost of newly generated solutions.
   e) Select and replace the worst fit solutions in the old population with the new solutions.

3.2.2 Evolutionary strategies

The evolution strategies (ESs) were proposed and developed in sixties and seventies by P. Bienert, Ingo Rechenberg, Hans-Paul Schwefel and others (Rechenberg 71, Schwefel 74). Although ESs and GAs resemble each other in terms of general structure (i.e. repetition of mutation and selection procedures in a loop), they differ from each other significantly in terms of the selection scheme, the genetic representation and the adaptation of the strategy parameters (Hoffmeister 1991).The main difference is that, in contrast to the GAs, only the best fit individuals are allowed to reproduce in the ESs. The basic steps of an evolutionary strategy algorithm can be described as follows (Beyer Schwefel 2002)

1) Initialize a population comprising of N_P individual solutions.
2) Perform the recombination operation on N_P parents to generate N_{ch} children.
3) Mutate all the children, using strategy parameters.
4) Evaluate the cost of $N_G \in [N_P, N_P + N_{ch}]$ individuals.
5) Select the best N_P out of N_G solutions generated using the ES, to constitute the population for the next generation step.
6) Repeat the steps 3-6 until the termination criterion is met.

Collection @ jeju

In ES either all the $N_P + N_{ch}$ individuals can be evaluated or just the N_{ch} children can be evaluated instead. Choosing $N_P = N_{ch}$ and evaluating all the $N_P + N_{ch}$ individual solutions dramatically increases the probability of getting better solutions for the next generation step.

3.2.3 Evolutionary programming

Evolutionary programming (EP) was first employed by Lawrence J. Fogel in the US in 1960 as an artificial intelligence (AI) learning process. EP shares many common features with ES, such as the representation of search points, normally distributed random mutation, and more specifically, the self-adaptation of strategy parameters. However, the two techniques differ significantly from each other in the sense that EP does not have any recombination/crossover operator and it used simplistic selection procedures. Therefore, the performance of EP, in general, is inferior to that of ES (Bäck *et al*. 1993). EP consists of three steps, repeated until an adequate termination criterion is met

1) Select/generate an appropriate number of individual solutions to serve as the initial population.
2) Replicate and mutate each individual solution. The mutation can vary from minor to major. The degree of mutation is determined based on the extent of functional change imposed on the parents.
3) Evaluate the cost of each individual solution. Probabilistically decide to select and retain a subset of the current population for the next generation cycle. Neither the size of the population nor the number of offspring solutions to be generated from each parent solution is fixed.

3.2.4 Genetic programming

Genetic programming (GP) is yet another class of EA, and is a specialization of genetic algorithms (GA) in which each individual can be considered a computer program (Banzhaf *et al*. 1998). It was first used by Barricelli (1954). GP is a systematic optimization scheme which is used to tune a number of computer programs, based on their ability to perform certain tasks, termed as the fitness of

Collection @ jeju

programs. The population of programs thus progressively evolves over a series of generation steps. Like most of the other EAs, the GP uses crossover and mutation operators to generate now computer programs from the existing programs. The basic steps of GP are as follows

1) Randomly generate an initial population of computer programs.
2) Execute the computer programs and calculate the fitness of each program.
3) Select up to two programs, based their fitness values, to participate in the genetic operations (crossover/mutation).
4) Probabilistically perform crossover and mutation operations on the selected programs to generate new programs.
5) Repeat the above procedure (2-5) until the termination criterion is met.

3.3 Advanced evolutionary algorithms

This section discusses a few evolutionary algorithms with some advanced features, such as complex mutation or crossover steps and the participation of more than two parents in an offspring generation. In particular, two of the most recently introduced evolutionary algorithms are presented here

- differential evolution algorithm
- biogeography based optimization.

3.3.1 Differential evolution algorithm

The Differential evolution (DE) algorithm is an evolutionary algorithm which uses the distance and direction information derived from the current population to explore the search space (Storn and Price 1997). DE employs three control parameters for its operation: N_P, the size of the population, F, the mutation scaling factor and CR, the probability of crossover. Although DE is a simple, yet powerful evolutionary algorithm, its optimum performance is dependent upon the fine tuning of its control parameters. This issue, however, can be resolved by using self adaptive variants of DE (Brest *et al*. 2006, 2007). In DE, a new solution replaces the previous solution only if the former is more suitable than the latter. Although it follows a greedy

Collection @ jeju

selection schemes, DE is an extremely efficient algorithm to establish the global minimum and often performs better than other evolutionary algorithms.

The general mechanism of DE resembles that of the genetic algorithms (GAs) (Goldberg 1989, Rolnik and Seleghim 2006) which constitute another popular class of EAs, nonetheless, it has certain distinctive features of its own. For example, the GA replaces a small subset of all candidate solution whereas DE attempts to replace all the previous solutions in each generation. Another key difference is that in GA, the mutation step consists of a small modification in each of the selected individual solution while the DE mutation comprises of a more complex arithmetic combination of the individuals. A comparison of the DE with other EAs including GA can be found in the reference (Ali and Törn 2004). The pseudo-code of the DE algorithm applied to EIT boundary estimation is given below (Rashid *et al*. 2010c).

Generate the initial population P
Evaluate the fitness for each individual in P
while Exit condition is not satisfied **do**
  for i = 1 to N_P (for all population) **do**
    Select uniformly distributed random numbers
    $r_1 \neq r_2 \neq r_3 \neq i$
    for c = 1 to N_C **do**
      if rand[0, 1] < CR or $c = C_{\text{rand}}$ **then**
        $Y_i(c) = X_{r_1}(c) + F \times (X_{r_2}(c) - X_{r_3}(c))$
      else
        $Y_i(c) = X_i(c)$
      end if
    end for
  end for
  for i = 1 to N_P **do**
    Evaluate the offspring Y_i
    if Y_i is better than the parent X_i **then**
      $X_i = Y_i$

Collection @ jeju

end if
end for
end while

Here, N_c is the number characteristic features of each individual $X_i(c)$ is the cth variable of the individual solution, X_i and Y_i are the ith parent and offspring solutions respectively, and rand[0, 1] is a uniformly distributed random real number between 0 and 1.

It should be noted that DE algorithm is very good at exhausting the global search space in order to establish the location of the global minimum. However, it fails to properly exploit the solution, which can result in convergence to a local minimum around the global minimum. This issue can be addressed with the use of a hybrid algorithm, combining DE with another algorithm such as BBO which is good in exploitation of the solution space (Gong *et al*. 2010).

3.3.2 Biogeography based optimization

Biogeography is the study of nature's way of distribution of biological species. Several algorithms have been developed and mathematical models have been incorporated to describe the evolution of species over time and space. Biogeography-based optimization (BBO) is a recently proposed application of biogeography to optimization problems (Simon 2008). BBO is basically a population-based heuristic algorithm which consists of a set of distinctive candidate solutions to a problem. The set of candidate solutions, referred to as "habitats", consequently evolve to reach the best solution. The feasibility of each solution is measured by a habitat suitability index (HSI) and is characterized by the suitability index variables (SIVs). Here, SIVs are the independent variables while the HSI is the dependent variable. A good solution is expected to have a high HSI while a bad solution shall have a low HSI. While the HSI of a rich habitat sharing its solution with a poor habitat will remain unaffected, the HSI of the latter will change due to this transition. The evolution of the population i.e., the candidate solutions in BBO is analogous to the concept of immigration and emigration.

Collection @ jeju

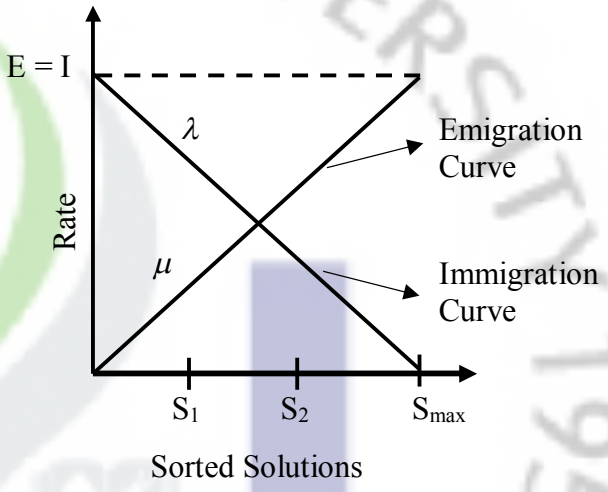

Figure 3.3. Linear immigration and emigration curves for candidate solutions to some problem, sorted by fitness. S_1 is like a low HSI island; it has a high immigration rate and a low emigration rate whereas S_2 is like a high HSI island that has a low immigration rate and a high emigration rate. S_{max} is the maximum possible number of species in the habitat (adapted from Simon 2008).

In figure 3.3, μ is the emigration rate, λ is the immigration rate, **E** is the maximum emigration rate, **I** is the maximum immigration rate and S_{max} is equal to the maximum possible number of species in the habitat. Here, S_1 is like a low HSI island. It has a high immigration rate and a low emigration rate, as it is more likely to share its features with relatively poorer solutions. S_2 is like a high HSI island. It has a low immigration rate and a high emigration rate as it is more likely to accept features from more suitable solutions. The emigration rate μ_k and the immigration rate λ_k for the *k*th individual can be calculated as follows (Simon 2008)

$$\mu_k = \frac{Ek}{N} \tag{3.1}$$

$$\lambda_k = I\left(1 - \frac{k}{N}\right) \tag{3.2}$$

where $N \equiv S_{max}$. The immigration and emigration curves in figure 3.3 are shown as straight lines. Although more complicated migration curves are possible, this thesis considers the simplest model in which the two migration curves are similar to each other, i.e., **E** = **I**, which consequently leads to

$$\lambda_S + \mu_S = \mathbf{E} \tag{3.3}$$

Further details regarding the BBO algorithm can be found in the reference (Simon 2008).

Collection @ jeju

3.3.2.1 BBO algorithm

Let H^{N_P} be a group of N_P habitats, also referred to as the BBO population, such that $H \in \mathrm{SIV}^m$ is a vector of size m representing a suitable solution to a problem. A suitability index variable SIV is any number that is allowed in a habitat. For $i, j \in \{1,2,...,N_P\}$, the probability of modification in a habitat H_i is proportional to its immigration rate λ_i while the emigration probability μ_j is proportional to the likelihood that the habitat H_j is the source of this modification. As stated before, it is assumed that λ_i and μ_j are linear with the same maximum values, i.e., E = I. Of course, better optimization can be achieved if these assumptions are relaxed, nonetheless, at the cost of increased complexity.

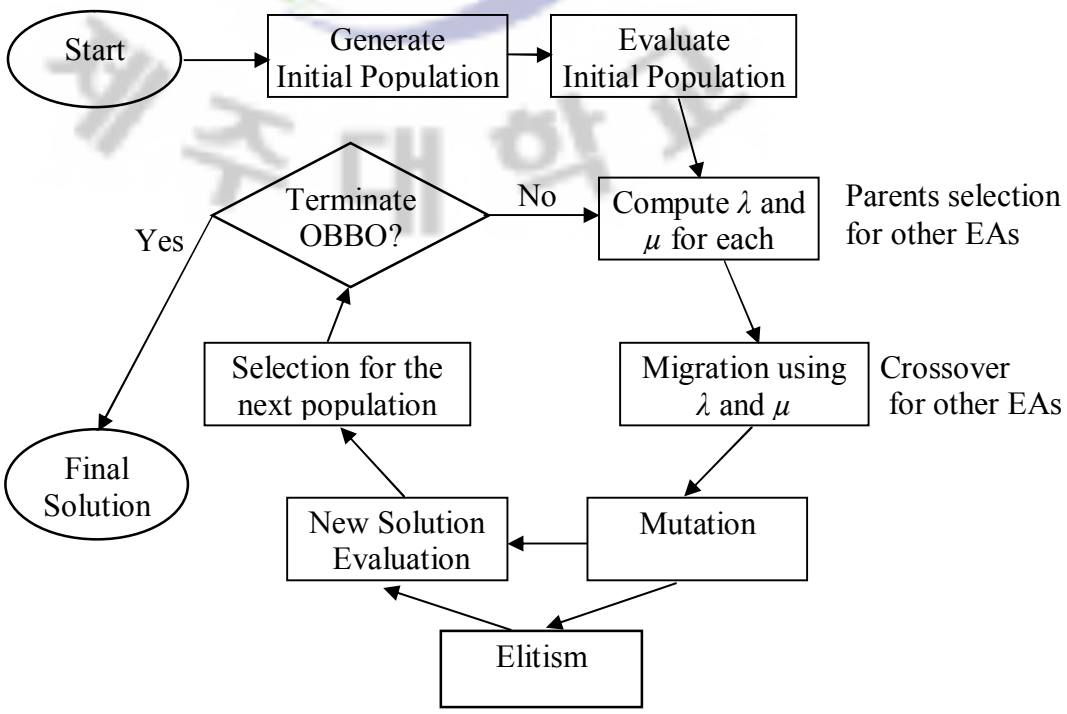

Figure 3.4. Flow chart description of BBO algorithm.

Figure 3.4 gives a Flow chart description of BBO algorithm, while the basic steps of BBO are as follows

Collection @ jeju

1) Initialize the BBO parameters (i.e., S_{max}, E, I and etc. The SIVs are mapped to the decision variables, while the cost functional is chosen as the habitat suitability index, HSI.)
2) Initialize a set of N_P potential solutions (habitats) for the problem. Also, compute the cost for each of the habitat in the initial population set.
3) Compute the immigration rate λ and emigration rate μ for each solution.
4) Probabilistically perform immigration and emigration to modify non-elite habitats.
5) Perform mutation on non-elite habitats based upon the mutation probability.
6) Calculate the cost of each new solution.
7) Go to step 3 for the next iteration, if needed.

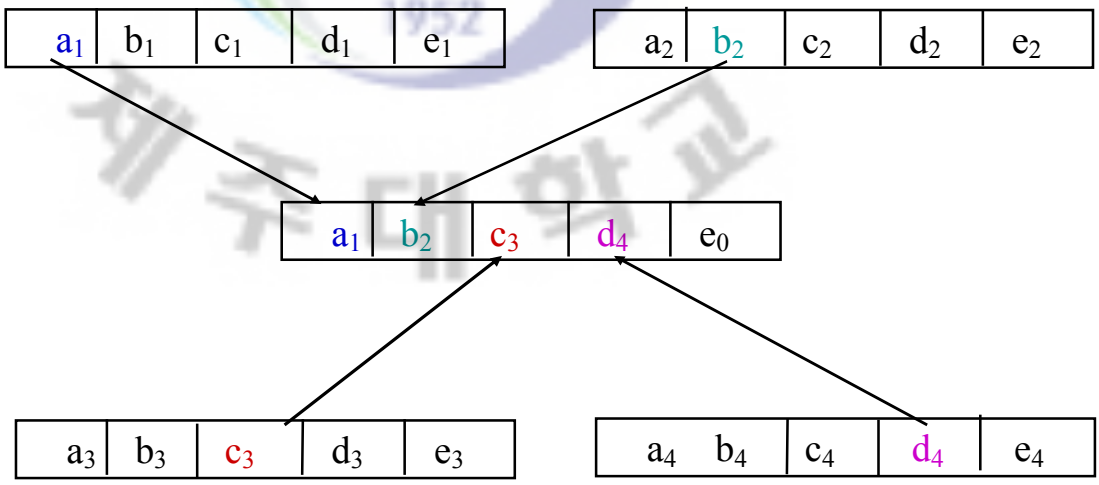

Figure 3.5. Schematic description of a BBO migration step. The immigrating solution (in the middle) is accepting characteristic (decision) variables (a_1, b_2, c_3 and c_4, respectively) from four emigrating sol utions, scattered around it. The decision variable e_0 belongs to the immigrating solution and is retained in the new solution.

The concept of migration/HSI modification (step 4) can be implemented in several ways. This thesis retains the concept prescribed in the original BBO paper, known as the partial immigration-based BBO (Simon 2008, 2009a, Simon *et al.* 2009b). In this approach, the migration is based on the immigration rate of each island and it is probabilistically decided whether or not to immigrate each SIV independently. The migration step is elaborated in the algorithmic way as follows

Collection @ jeju

for i = 1 to N_P (for each habitat)

for c = 1 to m (m is the number of decision variables)

Use the probability λ_i to decide whether to immigrate to island H_i

If island H_i selected for immigration

Randomly pick an island H_i with emigration probability μ_i

$H_i(c) = H_j(c)$ (replace the decision variable c in H_i with the respective variable c in H_j)

end if

end for

end for

It should be noted that in BBO the migration steps involves more than two parents, i.e., the immigrating solution is probabilistically combined with a number of emigrating solutions to generate a new solution (see figure 3.5 for schematic description).

3.4 Hybrid evolutionary algorithms

The hybrid evolutionary algorithms usually outperform the autonomous evolutionary algorithms. (Tseng and Liang 2006, Grosan *et al*. 2007, Du *et al*. 2009). This section looks at two hybrid versions of the most recently introduced and an increasingly popular evolutionary algorithm, i.e. biogeography-based optimization. They are

- biogeography-based optimization combined with evolutionary strategies
- oppositional biogeography-based optimization

3.4.1 Biogeography-based optimization combined with evolutionary strategies

Du *et al*. (2009) have incorporated the features of evolutionary strategy (Beyer and Schwefel 2002) into BBO and suggested the hybrid algorithm namely biogeography-based optimization combined with evolutionary strategy (BBO/ES). They applied the BBO/ES algorithm to several benchmarks and after carrying out an extensive statistical analysis, they concluded that the BBO/ES has statistically better performance as compared to that of the original BBO. The main idea behind BBO/ES

Collection @ jeju

algorithm is that while executing the migration step, for a given generation, N_P habitats form the previous generation remain unaltered while the immigration/emigration results into N_P new habitats. This is in contrast to the original BBO algorithm in which the original habitats are modified as a result of the migration step. After the completion of the current generation step, N_P most feasible habitats are retained out of a total of 2 N_P (N_P parents and N_P children) habitats for the next generation. This is especially suitable for the problems for which the cost functional calculation is computationally expensive and accounts for the major portion of the running time of the algorithm. With the given approach the feasibility of the N_P parents has already been calculated in the previous generation. Therefore, the burden of cost function calculation does not increase relative to the original BBO algorithm, resulting in a superior performance due to a larger pool of feasible solutions at its disposal. The key steps of the BBO/ES algorithm are as follows

1) Initialize the BBO parameters.
2) Initialize a set of N_P habitats and compute the cost for each of the habitat in the initial population.
3) Compute the immigration rate λ and emigration rate μ for each solution.
4) Probabilistically perform immigration and emigration on N_P parent habitats to generate N_P new child habitats.
5) Perform mutation based upon the mutation probability for each child habitat.
6) Calculate the cost of each child habitat.
7) Retain the N_P most feasible habitats out of a total of $2N_P$ (N_P parents and N_P children) habitats for the next generation. Keep the elite habitats in the new population by replacing the least feasible habitats.
8) Go to step 3 for the next iteration, if needed.

3.4.2 Oppositional-biogeography-based optimization

Ergezer *et al.* (2009) have incorporated the opposition-based learning (OBL) into the BBO algorithm to introduce the hybrid algorithm named oppositional biogeography-based optimization (OBBO). The OBL makes use of the opposite numbers to fast approach the solution. It is claimed by its inventors that a number's opposite is closer

Collection @ jeju

to the solution as compared to a random number, thus the use of opposite numbers significantly reduces the search space required to reach at the correct solution. FurtHermore, Ergezer *et al* (2009) have introduced a new opposition method named quasi-reflection and have mathematically demonstrated that a quasi-reflected number has the highest expected probability of being closer to the correct solution among all OBL methods. Figure 3.6 illustrates the schematic description of the quasi-reflection.

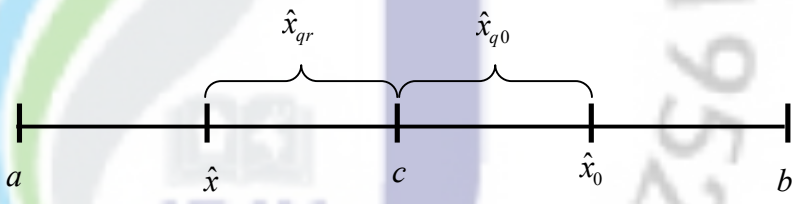

Figure 3.6. The schematic description of an estimated point $\hat{x} \in \{a, b\}$, its opposite $\hat{x}_0$, its quasi-opposite $\hat{x}_{q0}$ and the quasi-reflected point $\hat{x}_{qr}$, respectively. c is the centre of the domain $\{a, b\}$ (adapted from Ergezer *et al*. 2009).

Here, $\hat{x} \in \{a, b\}$ is an estimated solution, $\hat{x}_0 = a + b - x$ is the opposite of $\hat{x}$, and $\hat{x}_{q0} = \text{rand}(c, x_0)$ and $\hat{x}_{qr} = \text{rand}(c, x)$ are the quasi-opposite and the quasi-reflected points of $\hat{x}$, respectively. c is the centre of the domain $\{a, b\}$.

3.4.2.1 OBBO algorithm

The key steps of the OBBO algorithm for EIT boundary estimation are as follows

1) Initialize the BBO parameters.
2) Initialize a set of N_P potential solutions (habitats) for the problem and compute the cost for each of the habitat in the initial population set.
3) Compute the immigration rate λ and emigration rate μ for each candidate solution.
4) Probabilistically perform immigration and emigration to modify non-elite habitats.
5) Perform mutation based upon the mutation probability.
6) Calculate the cost of each new solution.
7) Generate a quasi-reflected opposition population and calculate the cost of each opposite solution.

Collection @ jeju

8) Compare the BBO generated solutions (steps 3-6) with their quasi-reflected solutions and retain the N_P most feasible solutions for the next generation. Keep the elite habitats in the new population by replacing the least feasible solutions.
9) Go to step 3 for the next iteration, if needed.

The migration/HSI modification (step 4) is similar to the one explained in the BBO algorithm. The step 7 i.e., the generation of a quasi-reflected population can be elaborated in the algorithmic form as follows

a) Decide with a (randomly generated) jumping probability, J_r, whether to skip the quasi-reflection step.
if $J_r >$ rand
skip the quasi-reflection step
end if
b) Calculate the minimum, maximum and the median of the current population.
c) Generate a reflection weight w_i based upon the fitness of each candidate solution
d) Now execute the quasi-reflection step
for i = 1 to N_P (for each habitat)
for c = 1 to m
if $H_i(c) <$ Median(c)
$OH_i(c) = H_i(c) +$ (Median(c) $- H_i(c))w_i$
else
$OH_i(c) =$ Median(c) + ($H_i(c) -$ Median(c))w_i
end if
end for
end for

where OH_i denotes the ith solution in the opposite population and Median(c) denotes the median of the population for the cth Fourier coefficient γ_c. The reflection weight w_i for the ith individual solution H_i is calculated based upon the fitness of that

Collection @ jeju

solution. A simple way to do this would be to calculate w_i using the index i of the given solution. More specifically, w_i can be calculated as follows

if $H_i(c) < \text{Median}(c)$

$$w_i = (i / N_P) \times rand$$

else

$$w_i = [(N_P - i) / N_P] \times rand$$

end if

where the random number $rand \in [0, 1]$ has been incorporated into the weight w_i in order to generate a different quasi-reflected solution in each subsequent repeat step, in case an individual solution was found to be infeasible in the previous quasi-reflection step. Since the population (before entering the quasi-reflection step) has been sorted with respect to the cost of each solution, the above approach will make sure that the (BBO generated) best fit individual solutions will generate quasi-reflected solutions in their close proximity whereas the least fit solutions will be reflected to the farthest possible solutions.

Collection @ jeju

4. OBBO applied to reconstruct organ boundaries in human thorax using EIT

Cardiac imaging plays a significant role in the diagnosis and treatment of the cardiac diseases and thus remains the focus of many researchers. Although most of the cardiac-related research has been concentrated on the characteristics of the individual cardiac chambers, the estimation of the total size of the heart has its own physiological significance and has been studied well by many researchers (Ziegler *et al*., 1962, Cotes *et al*., 1980). Total heart size variations have been linked to the efficiency of cardiac pumping (Hoffman and Ritman, 1987, Carlsson *et al*., 2004, Carlsson *et al*. 2005, Steding *et al*., 2007). Another technique often to detect the heart size enlargement is the cardiothoracic ratio (Hammermeister *et al*. 1979, Cohn *et al*. 1993, Hemingway *et al*. 1998, Philbin *et al*. 1998, Browne *et al*. 2004), defined as the transverse diameter of the heart and is usually calculated with the help of an X-ray. Several cardiac imaging techniques exist today; Ultrasound (US), single-photon emission computed tomography (SPECT), computed tomography (CT) and magnetic resonance imaging (MRI) being the most popular and established ones. However, most of these techniques are expensive, complex in operation and are often invasive in nature.

This chapter presents an oppositional biogeography-based optimization algorithm (OBBO) (Du *et al*. 2009) to determine the overall size and the shape of human heart using 2D EIT, while simultaneously estimating the lung boundaries as well with an objective to reduce the estimation errors introduced due to the inaccurate *a priori* knowledge of the latter boundaries (Rashid *et al*. 2011). The estimation scenario depicts the situation in which a patient holds his/her breathe therefore the boundary of the lungs as well as that of the chest remain stationary. The organ boundaries are expressed as coefficients of truncated Fourier series and the conductivity distribution inside the thorax region is assumed to be known *a priori*. The proposed method is tested by doing numerical simulations using a realistic chest shape mesh structure, and with the help of an experimental phantom resembling human chest.

Collection @ jeju

4.1 Biogeography-based optimization applied to EIT

The basic idea behind the application of BBO to the EIT image reconstruction is that one can start from an initial set of perspective solutions and then refine them iteratively until the calculated voltages match the measured voltages with an acceptable error margin. The initial set of candidate solutions is usually referred to as the initial population and the subsequent iteration steps in the BBO algorithm are called generations. Within each BBO generation, a series of operations are performed on the candidate solutions, which include

- an emigration/immigration step for each of the candidate solutions,
- a mutation step for a small set of selected solutions,
- a feasibility check for each of the solutions,
- a cost functional evaluation step for each of the candidate solutions, and
- a rank evaluation step.

The detailed explanation of the BBO algorithm and its application to the EIT boundary estimation can be formulated as follows.

The first and foremost step in the BBO algorithm is the generation of an effective initial population, i.e., H^{N_P} with N_P individuals, each of them represented by m number of characteristic features SIV. In the current EIT boundary estimation problem, an SIV represents a Fourier coefficient γ which can assume any real value. The initial population in BBO is usually generated by incorporating the *a priori* information for the given problem. The ability of the BBO algorithm to incorporate the *a priori* information into the algorithm is one of its most important characteristics, particularly useful for EIT boundary estimation, and is often necessary to achieve satisfactory performance. The *a priori* information in the EIT image reconstruction can be the knowledge of the general size and shape of the internal organs and the conductivity values of the constituent tissues. This *a priori* information can easily be obtained from other measurement/imaging sources such as X-ray, ultrasound images and etc.

The migration step in BBO can be implemented in several ways. This paper retains the concept prescribed in the original BBO paper, known as the partial immigration-based BBO (Simon 2008, 2009, Simon *et al*. 2009). In this approach,

Collection @ jeju

the migration is based on the immigration rate of each island, and it is probabilistically decided whether or not to immigrate each SIV independently. In the BBO-EIT implementation, this step consists in randomly selecting a subset of the Fourier coefficients from the solution selected as the donor (i.e., emigrating island), and then replacing them in the recipient solution (i.e., immigrating island).

As the BBO algorithm proceeds, the solutions with a high probability of success, i.e., the best fit solutions, tend to dominate the least fit solutions. This would be unfair in the sense that the solutions with a lower fitness (consequently of higher cost) value will not get much chance to improve even if they have more potential than the other solutions. In BBO, there is a remedy available for this in the form of mutation. The mutation step aims to keep the search space open to new solutions, thus maximizing the chance to reach at the best solution. This is particularly beneficial for the EIT boundary estimation due to the fact that the EIT measurement noise might suppress the feasibility of the solutions which, otherwise, would have been better suited. Another reason for this is that the Fourier representation of the boundary is a complex notation and even a small change in the coefficients may result in the significant improvement of a relatively weaker solution. (The mutation step in the current study is implemented by simply replacing the solution, which is selected based upon a mutation probability, with a new randomly generated solution).

The fitness of each solution in EIT is measured by evaluating the cost functional (2.22), which serves as the HSI in the BBO algorithm. The sensitivity of the cost functional to the variations in the inverse parameters i.e., the Fourier coefficients γ is key to the success of any optimization algorithm and is presented in the beginning of the results section.

The feasibility step ensures that each individual solution conforms to any constraints imposed by the given problem. In the current organ boundary estimation problem, it is also known *a priori* that the organs do not intersect each other and, of course, they always stay within the domain (i.e., the human chest) boundary. The incorporation of the prior information regarding the intersection of organs has been integrated in the feasibility-check step of the algorithm and will be explained later.

Collection @ jeju

Finally, the population is ranked based upon the cost of each of the candidate solutions. This step is used to calculate the migration rates for each individual in the next step.

4.2 OBBO applied to EIT boundary estimation

The key steps of the OBBO algorithm for EIT boundary estimation are as follows

1) Initialize the BBO parameters i.e., S_{max}, E, I and etc. The SIVs are mapped to the Fourier coefficients $\gamma_k \in \Re^{2MN_\theta}$, while the EIT cost functional $\Phi(\gamma_k)$ is chosen as the HSI.
2) Initialize a set of N_P potential solutions (habitats) for the problem. Also, compute the cost $\Phi(\gamma_k)$ for each of the habitat in the initial population set.
3) Compute the immigration rate λ and emigration rate μ for each candidate solution.
4) Probabilistically perform immigration and emigration to modify non-elite habitats.
5) Perform mutation based upon the mutation probability.
6) Calculate the cost $\Phi(\gamma_k)$ of each new solution.
7) Generate a quasi-reflected opposition population and calculate the cost $\Phi(\gamma_k)$ of each opposite solution.
8) Compare the BBO generated solutions (steps 3-6) with their quasi-reflected solutions and retain the N_P most feasible solutions for the next generation. Keep the elite habitats in the new population by replacing the least feasible solutions.
9) Go to step 3 for the next iteration, if needed.

The migration/HSI modification (step 4) can be elaborated in the pseudo-algorithmic way as follows

```
for i = 1 to NP (for each habitat)
    repeatCount=0
    feasibilityFlag = false
    repeat while feasibilityFlag = false and repeatCount <= NP/2
```


Collection @ jeju

for c = 1 to m (for each of the $m = 2MN_\theta$ Fourier coefficients)

Use the probability λ_i to decide whether to immigrate to habitat H_i

if habitat H_i selected for immigration

Randomly pick an habitat H_j with emigration probability μ_i

$H_i(c) = H_j(c)$ (replace the coefficient c in H_i with the coefficient c in H_j)

end if

end for

Check the feasibility of the solution H_i

if H_i is feasible

Set feasibilityFlag = true

end if

repeatCount = repeatCount+1

end repeat

end for

while the step 7 i.e., the generation of a quasi-reflected population can be elaborated in the algorithmic form as follows

1) Decide with a (randomly generate) jumping probability, J_r, whether to skip the quasi-reflection step.

if $J_r >$ rand

skip the quasi-reflection step

end if

2) Calculate the minimum, maximum and the median of the current population.

3) Generate a reflection weight w_i based upon the fitness of each candidate solution

4) Now execute the quasi-reflection step

for i = 1 to N_P (for each habitat)

repeatCount=0

feasibilityFlag = false

dCollection @ jeju

repeat while feasibilityFlag = false **and** repeatCount <= $N_P/2$

for c = 1 to m (for each of the $m = 2MN_\theta$ Fourier coefficients)

if $H_i(c)$ < Median(c)

$OH_i(c) = H_i(c)$ + (Median(c) - $H_i(c)$)w_i

else

$OH_i(c)$ = Median(c) + ($H_i(c)$ - Median(c))w_i

end if

end for

Check the feasibility of the solution OH_i

if OH_i is feasible

Set feasibilityFlag = true

end if

repeatCount = repeatCount+1

end repeat

end for

The migration and opposition jumping steps have already been discussed in the chapter 3. Notice the inclusion of repeat statement inside the outermost loops, for both the migration and the opposition population jumping steps, respectively. This statement has been incorporated in order to ensure the feasibility of the OBBO-generated solutions. (A solution is assumed to be feasible if the organs do not intersect each other and they stay within the domain.) This statement implies that the immigration/opposition population jumping step is attempted repetitively until the new solution is found to be feasible. However, in order to avoid an infinite loop, the step is only repeated for $N_P/2$, times, i.e., half of the population size (chosen arbitrarily). In the case of migration step, if a solution is still infeasible after $N_P/2$ attempts, it is left up to the next stage i.e., the opposite population jumping step, to resolve this issue. If the individual solution is still infeasible after $N_P/2$ opposite population jumping attempts, the OBBO-generated solution OH_i is then replaced with a new randomly generated feasible OH_i. This last step, however, is expected to take place very infrequently. Although the feasibility step is very effective in enforcing the *a priori* information, its premature introduction (i.e., avoiding the

Collection @ jeju

organ crossing scenarios) in the case of organ boundary estimation may result in losing the diversity of the population at an early stage of the BBO algorithm. More specifically there may be one or more candidate solutions which offer excellent estimation of the lung boundaries but the estimated heart boundary may be dislocated to intersect with one of the lungs. These solutions will inherit from other solutions in the due course of OBBO generations and can potentially become the best solution in the end. In order to avert this scenario, the feasibility enforcement step in the current implementation of the OBBO algorithm has been postponed until the second last generation. Since the last two iteration steps are deemed enough to enforce the feasibility of the solutions, the possibility of an unexpected infeasible final solution has been effectively eliminated. Moreover, a 25% penalty has been added to the cost of the infeasible solutions in the early generations before they are subsequently discarded or replaced by the feasible solutions.

An alternative approach to enforce the feasibility of the solution could have been reverting the infeasible solution to the original solution and consequently attempting the migration and the quasi-reflection for that particular solution in the next generation, if any. However, the latter approach is bound to slow down the convergence process.

An important characteristic of OBBO is the addition of dynamic domain scaling to accelerate the estimation process. The dynamic domain scaling means that the quasi-reflected population is generated in the same solution space as the current (BBO generated) population. This has the obvious advantage of shrinking the solution space with each iteration step, thus leading to a quicker convergence. The disadvantage, however, is the possibility of a premature convergence to the wrong local minimum. The remedy for this is already available in the form of mutation step. It should be reminded that the mutation step had been skipped in the original version of OBBO (Ergezer *et al*. 2009), however, the authors have included it for in order to keep the population diversity intact. It should also be noted that the introduction of the opposite population inevitably leads to extra computational burden within each iteration step. However, since OBBO converges much faster than BBO, the former requires substantially lesser number of generation steps to reach the best solution as compared to the later.

Collection @ jeju

Even with all the tools available in OBBO to accelerate the convergence process, one would like to keep the best solutions at hand, always with an option to revert back to them in case the migration/mutation/opposition jumping steps malign the original solution beyond repair. This step has been incorporated into the OBBO algorithm in the form of elitism (in steps 4 and 8). In this step, a predefined number of the best fit solutions (referred to as the elitism count) are retained at the end of each generation step and replace the worst fit solutions before the next generation step. The mutation and elitism schemes have been explained well in the literature (Simon 2008, Simon *et al*. 2009).

4.3 Results and discussions

4.3.1 Numerical results

This section presents a detailed analysis of the proposed OBBO-based EIT boundary estimation scheme using numerical simulations. In order to carry out the numerical simulations, we have chosen two test cases. In the first test case, a big sized heart surrounded by two lungs has been considered, while in the second case a small heart along with the two lungs is considered. The estimation scenario portrays the situation in which a patient holds his/her breathe so that the chest and the lung boundaries are fixed while we concentrate on the correct estimation of the size and the location of the heart. A chest-shaped mesh structure resembling the cross section of actual human torso is considered to verify the performance of the proposed method. The radius of the chest mesh structure is 16 cm in the x-direction and 13 cm in the y-direction. In order to simulate the true voltage measurements, a forward finite element mesh with true boundaries of the heart and the lungs embedded in the mesh structure has been used. Next, to solve the inverse problem, an inhomogeneous mesh structure, concentrated in the regions of the heart and lung boundaries has been used. The inhomogeneous forward mesh structure minimizes the errors introduced in the calculated voltages due to the boundary crossing elements, for which an area averaging technique has to be used. On the other hand, the inhomogeneous inverse mesh structure is solely introduced to speed up the calculation time, using a coarse mesh of elements in the regions where an organ boundary is unlikely to be found.

Collection @ jeju

This is justifiable since the region of interest, i.e., the region in which the lungs and the heart are located, is assumed to be well known. Such a speedup is also very important since the time spent on the cost functional calculation in EIT (which in turn depends upon the size of the FEM mesh structure) accounts for the major portion of the running time of this optimization algorithm. The mesh used to solve the forward problem consists of 4372 triangular elements with 2315 nodes. The mesh used for the inverse problem is composed of 3610 triangular elements with 1934 nodes. The mesh structures are shown in figure 4.1. Even though the shape of the forward and inverse inhomogeneous mesh structures resemble each other, a close look into the mesh structure makes it clear that the constituent triangular elements in the two mesh structures are totally different from each other. The different mesh structure for the forward and the inverse solvers was used to avoid the so called inverse crime (Wirgin 2004). The authors have also analyzed the performance of the OBBO algorithm with the use of a homogenous inverse mesh structure, and the results have been summarized at the end of this section. The simulations have been carried out on an AMD Athlon Core 2 Duo machine. Open source libraries providing the basic framework of the BBO algorithm (Simon 2009) and the FEM-based EIT forward solver EIDORS-2D (Vauhkonen *et al*. 2001) have been used in this work. MATLAB random number generators are used to generate the uniforms distributions used as the initial population for OBBO.

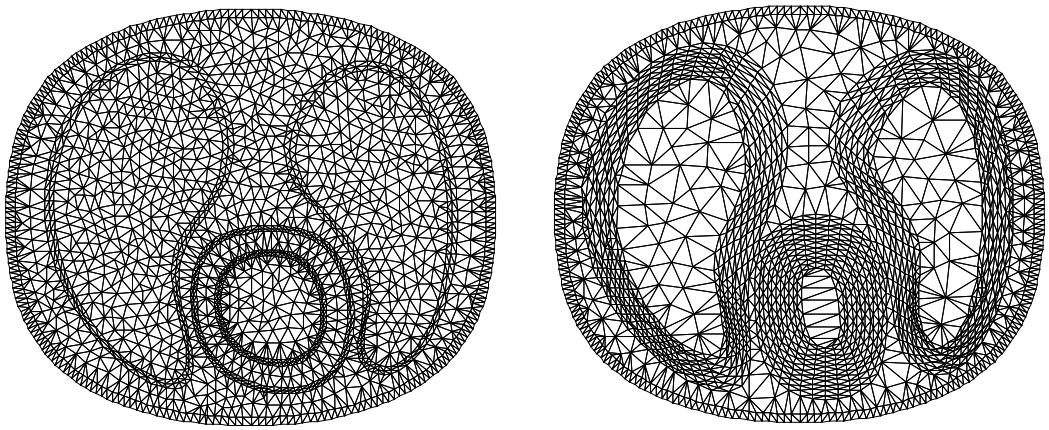

Figure 4.1. Forward FEM mesh (left) and inverse FEM mesh (right) structures. The forward mesh structure has the boundaries of the heart, the lungs and the backbone embedded into it, while the inverse mesh structure is inhomogeneous concentrated in the regions of interest.

Collection @ jeju

It should be further noted that the number of Fourier coefficients required to express the organ boundaries is not exactly known. Therefore, a different number of the Fourier coefficients are used in the inverse problem than the number used while generating the true data. In this thesis, we use $N_\theta = 7$ to express the true heart as well as the true lung boundaries. For the inverse problem, the heart is assumed to have an elliptic boundary ($N_\theta = 3$) while the two lungs have non-elliptic boundaries ($N_\theta = 5$). Clinically correct conductivities are assigned to the region, i.e., the conductivities of the heart, lungs and the background are 0.65 S/m, 0.12 S/m and 0.18 S/m respectively (Faes *et al*. 1999, Witsoe and Kinnen 1967).

An effective current injection protocol is vital to achieve good convergence in the EIT image reconstruction. Kim *et al*. (2005) have presented a comparison of various current injection schemes in EIT. They concluded that the trigonometric current pattern with lower modes performs better than other types of current patterns. In this study, the trigonometric current injection patterns are injected into 32 electrodes attached to the chest mesh structure. The complete electrode model with effective contact impedance of 0.005 Ωcm^2 has been used to enforce the boundary conditions for the EIT problem. In EIT, the voltage measurements are often noisy in nature. Therefore, zero-mean Gaussian noise with a standard deviation of one percent relative to the corresponding measured voltages has been added to the observed voltage data to simulate realistic measurements.

As explained before, the OBBO algorithm attempts to reconstruct the boundaries of the organs by minimization the cost functional (2.22). The performance of the algorithm thus depends upon the sensitivity of the cost functional to the variations in the conductivity distribution (or more specifically the variations in the geometry of the organs, in the current case) inside the domain with the given current injection mechanism. Therefore, as a first step, the sensitivity of the cost functional has been analyzed by performing series of translations and scaling of the organ boundaries, and then calculating the $RMSE_{Voltage}$ for each of the variations.

Collection @ jeju

$$RMSE_{Voltage} = \sqrt{\frac{(V_{calculated} - V_{measured})^{T}(V_{calculated} - V_{measured})}{V_{calculated}.V_{calculated}}} = \sqrt{\frac{[V(\gamma) - U]^{T}[V(\gamma) - U]}{[V(\gamma).U]}} \quad (4.1)$$

The response of the cost functional to these variations is then plotted in the graphical format in figure 4.2 and figure 4.3. A similar approach has been considered in other related studies (de Munck *et al.* 2000, Rolnik Seleghim Jr P 2006). The global minimum in the case of scaling errors in all the organs is reasonable prominent, and is generally located near the true boundary locations. However, in the case of translation errors, global minimum sometimes resides quite away from the true boundary location, and may not be easily distinguishable from the local minima. Also, most of the RMSE values in this case stay low, making it more difficult for a location search algorithm to detect the true boundary location. This problem is more critical in the case of the heart boundary location. This seems to suggest that the sensitivity of the EIT measurements is relatively low to the variations in the location of the organs, especially in the case of heart. The heart is located located relatively away from the outside boundary to which the electrodes have been attached. Moreover, heart is more conductive compared to the background and is surrounded by the lungs which are even more resistive than the background. All these factors make the sensitivity of the EIT boundary measurements low with respect to the variations in the heart boundary. The problem becomes even more critical for the smaller heart which is also further away from the boundary electrodes.

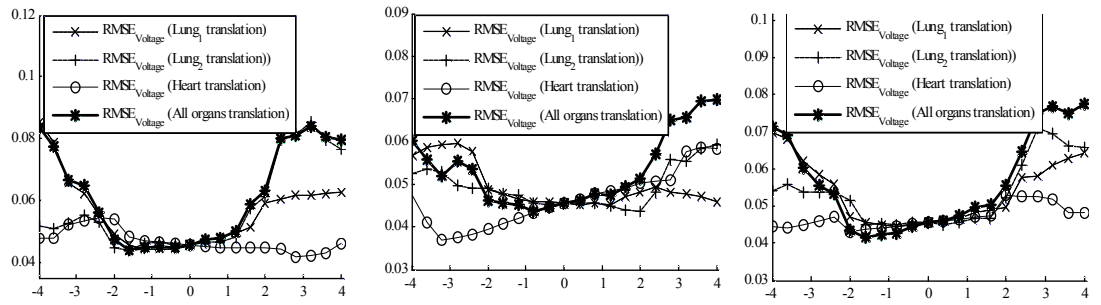

Figure 4.2. Voltage RMSE for different location errors in the organ boundaries. (a) Voltage RMSE plotted against *x*-translation errors. (b) Voltage RMSE plotted against *y*-translation errors. (c) Voltage RMSE plotted against *x* & *y*- translation errors.

Collection @ jeju

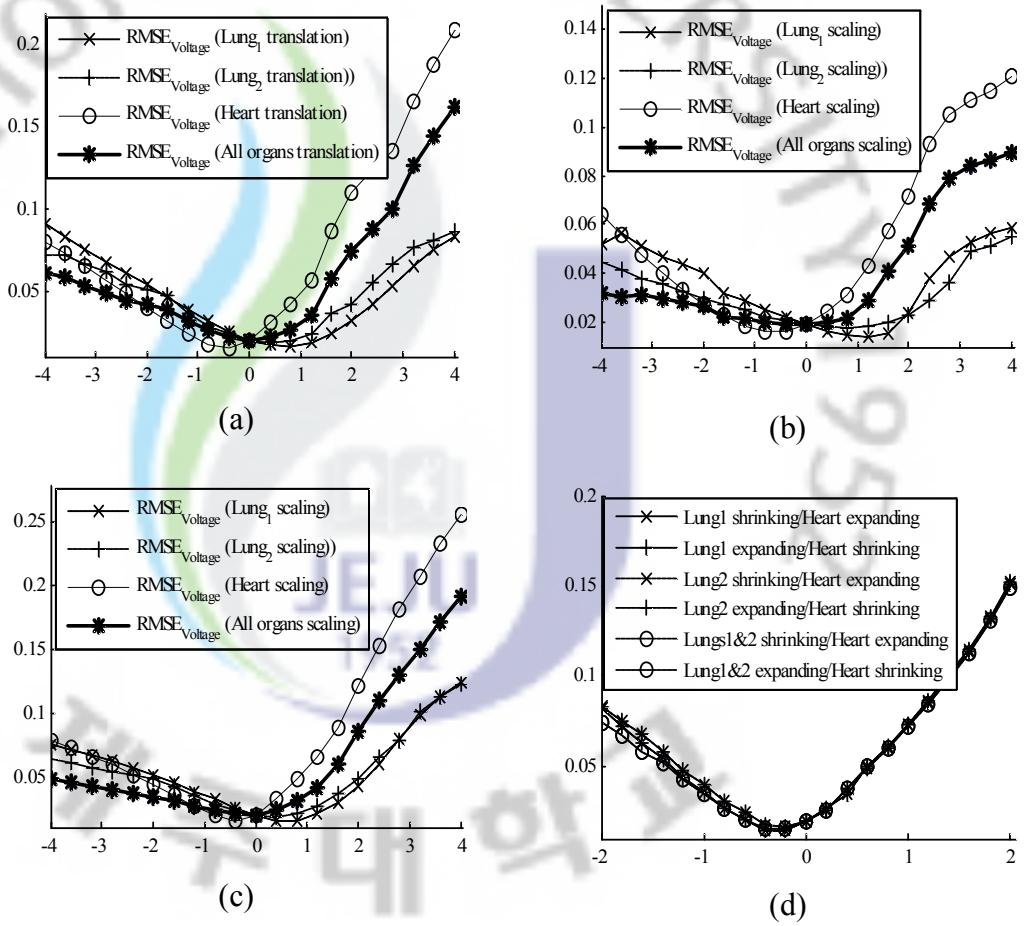

Figure 4.3. Voltage RMSE for different scaling errors in the organ boundaries. (a) Voltage RMSE plotted against *x*-scaling errors. (b) Voltage RMSE plotted against *y*-scaling errors. (c) Voltage RMSE plotted against *x* & *y*- translation errors. (d) Voltage RMSE plotted against due to simultaneous expansion/shrinking of different organs.

An important consideration in the OBBO algorithm is the selection of the initial population. The size and the range of the initial population are problem dependent and strongly affect the performance of the algorithm. In the EIT boundary estimation, this is one of the most critical decisions in order to achieve an effective solution due to the high computational requirements of the underlying algorithm. The initial population size and the range of the Fourier coefficients to generate the initial set of feasible solutions should be chosen wisely in order to achieve a fast convergence. For the first set of simulations, it is assumed that the approximate shape and location of the true organs are known *a priori*. This information can easily be obtained from the statistical data gathered from readily available chest images such as the MRI scans and etc. It can then be utilized to identify a region of interest (ROI) and an initial set

Collection @ jeju

of population concentrated in the ROI can be generated. Such an approach significantly reduces the search space required by the OBBO algorithm to reach the final solution, requiring a much smaller population size, thus reducing the running time and improving the performance of the algorithm.

A uniformly distributed initial population comprising of 50 habitats has been chosen for this study. The uniform distribution has been generated such that the Fourier coefficients representing the radii and the locations (x- and y-coordinates) of the organs are distributed with a maximum deviation of 2 cm from their respective mean values. The mean values, as in the case of the lungs, are at an absolute distance of 0.5 cm from their respective best true values. In the case of the heart, the mean of the uniformly distributed initial population (for location and size parameters) is chosen as near the near average of the respective Fourier coefficients for the two heart sizes. The rest of the Fourier coefficients, which express the shape and orientation of the organ boundaries, have a maximum deviation of 1 cm from the respective mean values. The initial population has been selected based upon the assumption that a good prior knowledge of the general shape of the organs is available, with a relatively poor knowledge of their size and the location. Another important parameter affecting the performance of the OBBO algorithm is the generation count, i.e., the maximum number iterations for the main algorithm. The selection of the generation count is problem dependent and also depends upon the size and the range of initial set of population. The statistical nature of OBBO is such that the initial population transforms towards a flat population (with all individual solutions having the same value) with each iteration step. In general, as the population size increases, a higher number of iterations are needed to reach a uniform population (Simon 2009). However, we are interested in only one good solution and a uniform population is not our final goal at all. Therefore, considering the high computational requirement, we have chosen an absolute generation count of 10 to reach the final solution. Although better performance can be achieved for a higher generation count, the algorithm exhibits satisfactory performance with this generation count for a carefully selected population. The value of the OBBO jumping probability, J_r, has been fixed as 0.6 throughout the simulations, while an elitism count of two has been used. In order to verify the robustness of the proposed

Collection @ jeju

algorithm Monte Carlo type simulations of η = 20 runs (each run with a different noise seed, and a different set of initial population) was performed. Five statistical parameters, namely the mean $\overline{\hat{\gamma}}$, mean absolute error $\overline{MAE}_\gamma$, the error standard deviation s_e, the mean error squared $\overline{MES}_\gamma$, and the mean root mean square error $\overline{RMSE}_\gamma$ of the estimated Fourier coefficients for the numerical scenario have been reported in Tables 4.1-4.4. $\overline{MAE}_\gamma$ and $\overline{RMSE}_\gamma$ give provide a measure of the estimation error with respect to the corresponding true values. The error standard deviation s_e calculates the dispersion of the error e_i in the estimated parameters, whereas $\overline{MES}_\gamma$ is the square of the bias of the error (Bendat and Piersol 1971). The statistical formulae for each of these parameters are given as follows

$$\overline{\hat{\gamma}} = \frac{1}{\eta}\sum_{i=1}^{\eta}\gamma_i \tag{4.2}$$

$$\overline{MAE}_\gamma = \frac{1}{\eta}\sum_{i=1}^{\eta}\left|\gamma_{true}-\hat{\gamma}_i\right| = \frac{1}{\eta}\sum_{i=1}^{\eta}\left|e_i\right| = E\left[\left|e_i\right|\right] \tag{4.3}$$

$$\overline{MES}_\gamma = \left(\frac{1}{\eta}\sum_{i=1}^{\eta}\left(\gamma_{true}-\hat{\gamma}_i\right)\right)^2 = \left(\frac{1}{\eta}\sum_{i=1}^{\eta}e_i\right)^2 = \left(E\left[e_i\right]\right)^2 = (\bar{e})^2 \tag{4.4}$$

$$\overline{MSE}_\gamma = \frac{1}{\eta}\sum_{i=1}^{\eta}\left(\gamma_{true}-\hat{\gamma}_i\right)^2 = \frac{1}{\eta}\sum_{i=1}^{\eta}e_i^2 = E\left[e_i^2\right] \tag{4.5}$$

$$s_e = \sqrt{\frac{1}{\eta}\sum_{i=1}^{\eta}\left(e_i-\bar{e}\right)^2} = \sqrt{E\left[e_i^2\right]-\left(E\left[e_i\right]\right)^2} = \sqrt{\overline{MSE}_\gamma-\overline{MES}_\gamma} \tag{4.6}$$

$$RMSE_\gamma = \sqrt{\frac{(\overline{\hat{\gamma}}-\gamma_{true})^{\mathrm{T}}(\gamma-\gamma_{true})}{\gamma_{true}^{\mathrm{T}}\gamma_{true}}} \tag{4.7}$$

$$\overline{RMSE}_\gamma = \frac{1}{\eta}\sum_{i=1}^{\eta}RMSE_{\gamma_i} \tag{4.8}$$

where $\hat{\gamma}$ is the estimated values, while γ_{true} is the true value of the respective Fourier coefficient and. A comprehensive analysis of the OBBO algorithm with the help of aforementioned statistical parameters follows here.

Collection @ jeju

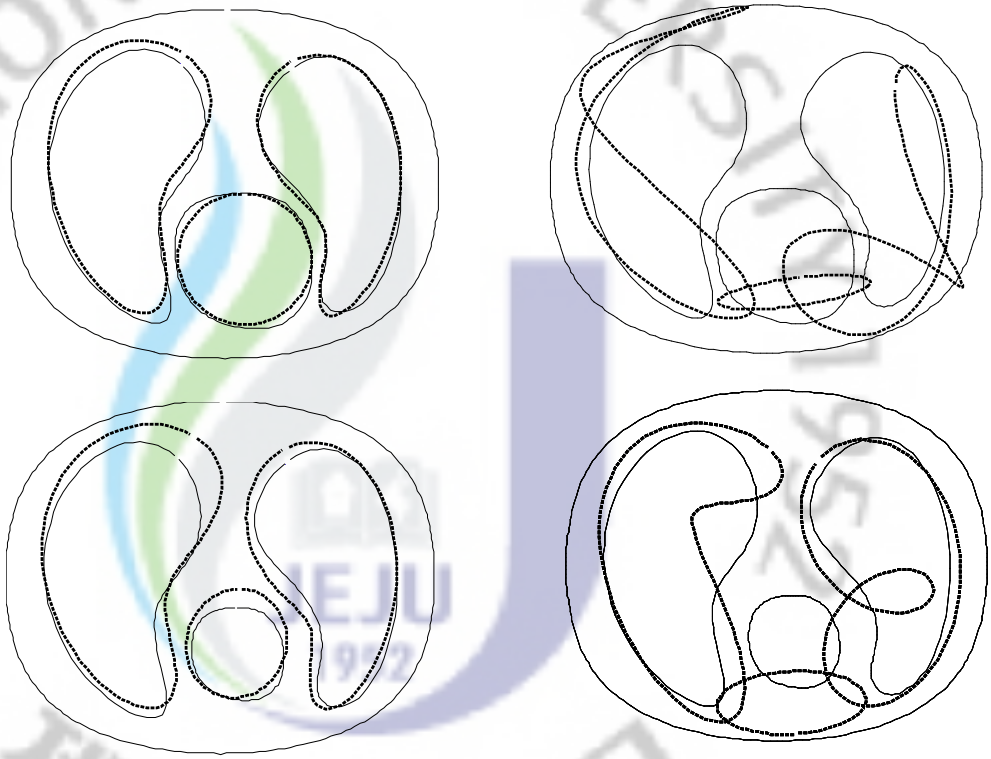

Figure 4.4. Estimated organ boundaries in a simulated human chest cross section using OBBO and mNR. The solid line is used to draw the true organ boundaries while the broken line is used to show the (mean) estimated boundaries using OBBO (left) and mNR (right). The results in the top row are for the big heart case while the bottom results are for small heart.

The statistical parameters reported in the Tables 4.1-4.4 provide useful information regarding the stability and accuracy of the algorithm. Especially, the performance of the algorithm with respect to the Fourier coefficients accounting for the size and the location of the organs should be analyzed very carefully. (The coefficients $\gamma_1^{x_1}, \gamma_1^{y_1}, \gamma_1^{x_2}, \gamma_1^{y_2}, \gamma_1^{x_3}$ and $\gamma_1^{y_3}$ correspond to the x- and y-coordinates of the $Lung_1$, $Lung_2$ and $Heart$ respectively, while the coefficients $\gamma_2^{x_1}, \gamma_3^{y_1}, \gamma_2^{x_2}, \gamma_3^{y_2}, \gamma_2^{x_3}$ and $\gamma_3^{y_3}$ correspond to the radii in the x- and y- directions, respectively, of these organs.) The statistical parameters $\bar{\hat{\gamma}}$, $\overline{MAE}_\gamma$, $\overline{MES}_\gamma$ and s_e have thus only been calculated for the location and size estimates while the $\overline{RMSE}_\gamma$ has been calculated for the aggregated Fourier coefficients for each of the organ. As reported in Tables 4.2 and 4.4, $\overline{RMSE}_{Lung_1}$, $\overline{RMSE}_{Lung_2}$ and $\overline{RMSE}_{Heart}$ are the aggregated $\overline{RMSE}_\gamma$ values, calculated for $Lung_1$, $Lung_2$ and $Heart$, respectively, while the $\overline{RMSE}_{Overall}$

Collection @ jeju

corresponds to the mean *RMSE* of all the coefficients for the three organs, aggregated together. The mean Fourier boundaries are plotted in the graphical format in figure 4.4.

Table 4.1. Simulation scenario 1 (big heart case): mean $\bar{\hat{\gamma}}$, error standard deviation s_e, mean error squared $\overline{MES}_\gamma$ and the mean absolute deviation $\overline{MAE}_\gamma$ of the Fourier coefficients estimated using OBBO and mNR.

Fourier coeff.	True value	Estimated mean, standard deviation and mean absolute deviation							
		OBBO				mNR			
		$\bar{\hat{\gamma}}$	$\overline{MAE}_\gamma$	$\overline{MES}_\gamma$	s_e	$\bar{\hat{\gamma}}$	$\overline{MAE}_\gamma$	$\overline{MES}_\gamma$	s_e
$\gamma_1^{x_1}$	-6.00	-6.2017	0.3407	0.0407	0.3535	- 7.5546	3.2535	2.4167	3.8112
$\gamma_2^{x_1}$	4.40	4.5711	0.2828	0.0293	0.3254	0.1793	4.3844	17.8141	4.2363
$\gamma_1^{y_1}$	-0.50	0.2049	0.7645	0.4969	0.4395	2.4766	5.3897	8.8600	6.6539
$\gamma_3^{y_1}$	9.20	9.2249	0.2357	0.0006	0.2943	11.1994	6.8828	3.9977	8.9175
$\gamma_1^{x_2}$	7.70	7.6448	0.1405	0.0030	0.1733	9.5220	0.7800	3.3197	3.9325
$\gamma_2^{x_2}$	3.60	3.6301	0.1979	0.0009	0.2528	-0.6465	4.4758	18.0325	4.1793
$\gamma_1^{y_2}$	-1.20	-0.9609	0.3817	0.0572	0.4074	-3.6869	4.2339	6.1848	4.8577
$\gamma_3^{y_2}$	8.60	8.7598	0.4213	0.0256	0.5538	6.3621	6.4916	5.0081	8.1106
$\gamma_1^{x_3}$	1.20	1.5079	0.3577	0.0948	0.2881	2.0442	1.6979	0.7127	1.7829
$\gamma_2^{x_3}$	5.20	4.9927	0.2234	0.0430	0.2385	5.6400	1.6490	0.1936	1.9407
$\gamma_1^{y_3}$	-5.80	-5.9049	0.1800	0.0110	0.2224	-8.7596	3.1838	8.7591	3.3121
$\gamma_3^{y_3}$	5.20	4.8659	0.3584	0.1116	0.2685	1.0969	4.4203	16.8357	4.4177

Table 4.2. Simulation scenario 1 (big heart case): mean RMSE of the aggregated Fourier coefficients for the *Lung*$_1$, Lung$_2$ and Heart, respectively, estimated using OBBO and mNR.

	Mean RMSE values of the aggregated Fourier coefficients	
	OBBO	mNR
$\overline{RMSE}_{Lung_1}$	0.0959	1.4502
$\overline{RMSE}_{Lung_2}$	0.0757	1.5309
$\overline{RMSE}_{Heart}$	0.0865	0.7361
$\overline{RMSE}_{Overall}$	0.0882	1.4296

Collection @ jeju

Table 4.3. Simulation scenario 2 (small heart case): mean $\overline{\hat{\gamma}}$, error standard deviation s_e, mean error squared $\overline{MES}_\gamma$ and the mean absolute deviation $\overline{MAE}_\gamma$ of the Fourier coefficients estimated using OBBO and mNR.

Fourier coeff.	True value	Estimated mean, standard deviation and mean absolute deviation							
		OBBO				mNR			
		$\overline{\hat{\gamma}}$	$\overline{MAE}_\gamma$	$\overline{MES}_\gamma$	s_e	$\overline{\hat{\gamma}}$	$\overline{MAE}_\gamma$	$\overline{MES}_\gamma$	s_e
$\gamma_1^{x_1}$	-6.00	-5.5043	0.4957	0.2457	0.1918	-5.6139	1.8902	0.1491	2.4314
$\gamma_2^{x_1}$	4.40	4.9875	0.5875	0.3451	0.1624	3.7160	1.8566	0.4679	2.6065
$\gamma_1^{y_1}$	-0.50	0.3703	0.8703	0.7575	0.3754	0.8105	2.8396	1.7175	3.3287
$\gamma_3^{y_1}$	9.20	9.5993	0.5044	0.1594	0.3855	9.2064	3.5929	0	4.4820
$\gamma_1^{x_2}$	7.70	7.2773	0.4227	0.1787	0.2099	7.8412	2.8949	0.0199	3.6862
$\gamma_2^{x_2}$	3.60	4.0498	0.4604	0.2024	0.2493	1.2483	5.2611	5.5304	6.0190
$\gamma_1^{y_2}$	-1.20	-0.8913	0.4120	0.0953	0.3923	-1.3666	5.0833	0.0278	5.8828
$\gamma_3^{y_2}$	8.60	8.7594	0.2853	0.0254	0.3074	5.9963	4.4964	6.7793	4.5839
$\gamma_1^{x_3}$	1.20	1.2287	0.2771	0.0008	0.3591	1.1320	3.6216	0.0046	4.7901
$\gamma_2^{x_3}$	3.50	3.7496	0.3074	0.0623	0.2484	5.6548	2.7577	4.6430	2.9905
$\gamma_1^{y_3}$	-5.80	-5.1661	0.6339	0.4019	0.3504	-10.468	4.8197	21.7914	4.5548
$\gamma_3^{y_3}$	3.50	3.9980	0.5205	0.2480	0.3694	-2.3314	6.3733	34.0053	5.0113

Table 4.4. Simulation scenario 2 (small heart case): mean RMSE of the aggregated Fourier coefficients for the *Lung*$_1$, *Lung*$_2$ and *Heart*, respectively, estimated using OBBO and mNR.

	Mean RMSE values of the aggregated Fourier coefficients	
	OBBO	mNR
$\overline{RMSE}_{Lung_1}$	0.1134	0.8487
$\overline{RMSE}_{Lung_2}$	0.1017	1.2192
$\overline{RMSE}_{Heart}$	0.1508	1.4140
$\overline{RMSE}_{Overall}$	0.1180	1.1670

In order to do a comparative analysis, mNR, which is a conventional algorithm used for the static imaging, was also used to solve the same problem. The mNR has also been repeated for η = 20 runs and the same statistical parameters, as for OBBO,

Collection @ jeju

have been gathered. In contrast to the OBBO algorithm, mNR requires a single initial guess for each run. However, the initial guess for the mNR method is different for each subsequent run, by randomly choosing a value for the Fourier coefficients representing the radii and the locations (x- and y-coordinates) of the organs from a uniform distribution with a standard deviation of 1.0 centred at its respective true value, while the rest of the Fourier coefficients have a maximum deviation of 0.5 cm from the respective mean values. Note that this initial guess is chosen from a distribution which is closer to the true value as compared to that of OBBO. Even with a relatively closer initial guess the estimated results for mNR have been very poor (see figure 4.4). The $\overline{RMSE}_\gamma$, s_e, and $\overline{MAE}_\gamma$ values for mNR are very high compared to those of OBBO. The major reason behind the poor performance of the mNR algorithm is that it requires the calculation of the Jacobian for all the coefficients. The Jacobian for the higher order coefficients is extremely sensitive to the initial guess, and even a small deviation from the respective true value leads to large deviations in the results. It should be further noted that when using mNR for this case, the estimation goes out of bound when the solution is iterated, consequently leading to a meaningless reconstructed results. Therefore, for comparison purposes, all the reconstructed results shown in the paper are using one-step mNR.

The mean estimated boundaries using OBBO are much closer to the true boundaries. It can easily be observed from the results that the proposed estimation algorithm can clearly distinguish between the two heart sizes, besides the same initial population chosen for both the cases. The values of the error calculated in terms of $\overline{MAE}_\gamma$, $\overline{MES}_\gamma$ and s_e is very low for OBBO as compared to that of mNR. Also, for OBBO the relative magnitude of error for most of the Fourier coefficients compared to their original values is reasonably low. The relative magnitude of the error compared to the respective true values in the case of some of the Fourier coefficients, for example the coefficient corresponding to a few location parameters, is a bit high.

Collection @ jeju

Table 4.5. Big heart case: different sets of uniformly-distributed initial populations to verify the robustness of OBBO algorithm to a varying range of initial guess.

No.	Range of Fourier coefficients for the uniformly distributed initial population		
	Location parameters $\gamma_1^{x_1}, \gamma_1^{y_1}, \gamma_1^{x_2}, \gamma_1^{y_2}, \gamma_1^{x_3}, \gamma_1^{y_3}$	Radius Parameters $\gamma_2^{x_1}, \gamma_3^{y_1}, \gamma_2^{x_2}, \gamma_3^{y_2}, \gamma_2^{x_3}, \gamma_3^{y_3}$	All other parameters $\gamma_3^{x_1}, \gamma_4^{x_1}, \gamma_5^{x_1}, \gamma_2^{y_1}, \gamma_4^{y_1}, \gamma_5^{y_1}, \gamma_3^{x_2}, \gamma_4^{x_2}, \gamma_5^{x_2}, \gamma_2^{y_2}, \gamma_4^{y_2}, \gamma_5^{y_2}\ \gamma_3^{x_3}, \gamma_2^{y_3}$
1	$\gamma_{true}-1.5 \le \gamma \le \gamma_{true}+2.5$	$\gamma_{true}-1.5 \le \gamma \le \gamma_{true}+2.5$	$\gamma_{true}-0.9 \le \gamma \le \gamma_{true}+1.1$
2	$\gamma_{true}-2 \le \gamma \le \gamma_{true}+3$	$\gamma_{true}-2 \le \gamma \le \gamma_{true}+3$	$\gamma_{true}-1 \le \gamma \le \gamma_{true}+1.5$
3	$\gamma_{true}-2.5 \le \gamma \le \gamma_{true}+3.5$	$\gamma_{true}-2.5 \le \gamma \le \gamma_{true}+3.5$	$\gamma_{true}-1.25 \le \gamma \le \gamma_{true}+1.75$
4	$\gamma_{true}-3 \le \gamma \le \gamma_{true}+4$	$\gamma_{true}-3 \le \gamma \le \gamma_{true}+4$	$\gamma_{true}-1.5 \le \gamma \le \gamma_{true}+2$
5	$\gamma_{true}-3.5 \le \gamma \le \gamma_{true}+4.5$	$\gamma_{true}-3.5 \le \gamma \le \gamma_{true}+4.5$	$\gamma_{true}-1.75 \le \gamma \le \gamma_{true}+2.25$
6	$\gamma_{true}-4 \le \gamma \le \gamma_{true}+5$	$\gamma_{true}-4 \le \gamma \le \gamma_{true}+5$	$\gamma_{true}-2 \le \gamma \le \gamma_{true}+2.5$
7	$\gamma_{true}-4.5 \le \gamma \le \gamma_{true}+5.5$	$\gamma_{true}-4.5 \le \gamma \le \gamma_{true}+5.5$	$\gamma_{true}-2.25 \le \gamma \le \gamma_{true}+2.75$

This fact is also reflected in the aggregated $\overline{RMSE}_\gamma$ values, which provides a popular measure of the relative error with respect to the true value. This is not entirely unexpected. In fact, the comparison of the magnitude of the error with respect to the respective true values does not truly reflect the performance of the algorithm, especially in the case of location parameters in which the true value depends upon the choice of the origin of the coordinates. It would be more meaningful to compare the magnitude of the error with respect to the size of the respective organ or the size of the domain. For instance, it has been calculated that the magnitude of the calculated error ($\overline{MAE}_\gamma$, $\overline{MES}_\gamma$ and s_e) for all of the coefficients estimated by OBBO normalized with respect to the chest radius stays within 0.05; in fact, most of the normalized values are within 0.03. On the other hand, the deviations for the parameters estimated by mNR are significantly higher. In fact, the results demonstrate that the mNR algorithm is not a suitable reconstruction algorithm in the case of multiple non-elliptic boundaries, very close to each other. The shortcoming of the OBBO algorithm as compared to mNR is its computational complexity. With the current selection of OBBO population, the average running

Collection @ jeju

time of an OBBO generation is approximately ten times of that of a single iteration in mNR. Although the order of running time is quite high, the OBBO algorithm is robust to initial guess and outperforms OBBO algorithm, which justifies its use here. Moreover, the nature of OBBO is such that the migration/mutation/opposition jumping steps for each candidate solution can be executed independent of each other. This flexibility makes it a perfect algorithm to be run in parallel mode. The availability of computers with high computational power and offering parallelism, both at the hardware and the software levels, reduces the significance of high computational complexity of the OBBO algorithm.

The plotted results and the respective statistical analysis verify the performance of OBBO for the scenario when a good *a priori* knowledge of the size, location and shape of the organs is available and thus the initial population has been generated relatively close to the true values. In order to verify the robustness of the algorithm further analysis of the algorithm needs to be done, when the initial population has been generated with more flexibility, depicting the scenario when the *prior* knowledge of size, location and shape is not so correct. More specifically, the performance of the OBBO algorithm has been tested in the case of big heart for seven different types of initial population distribution. The first population is the same for which a detailed statistical analysis has already been presented, and it is only included here in for its comparative purposes. The range of the Fourier coefficients chosen for each of the uniformly distributed initial population has been given in Table 6.5 and the results have been plotted in figure 4.5. Notice the mean of the uniform distributions for all the initial populations has been chosen away from the respective true values. This measure has been taken in order to generate an unbiased initial population distribution, considering the fact that exact knowledge of the true values is not available. Another thing to consider here is that the limiting values given in Table 6.5 do not give the absolute range of the initial populations; instead these are the ranges from which the initial population distributions are chosen. The actual ranges of the initial sets of Fourier coefficients, especially for the widely distributed populations, may be smaller given the fact that the each candidate solution in the initial population is subject to a well known *a priori* constraint that all the organs should stay within the domain.

Collection @ jeju

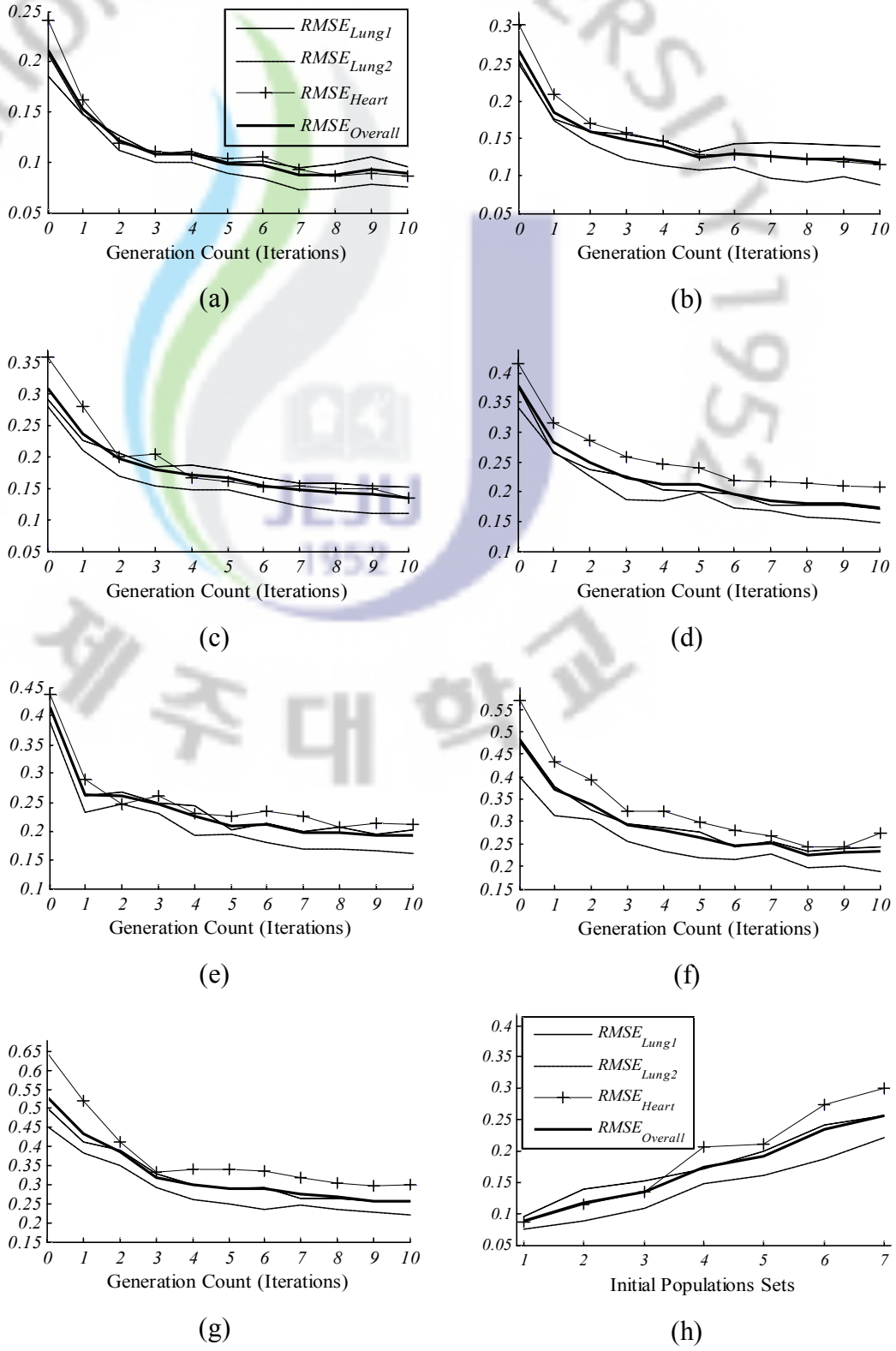

Figure 4.5. $\overline{RMSE}_{\gamma}$ for different sets of initial populations. (a) – (g) show the $\overline{RMSE}_{\gamma}$ values calculated for all three organs, plotted iteratively for each OBBO generation. (h) summarizes the best $\overline{RMSE}_{\gamma}$ values, as obtained at the end of the 10*th* OBBO generation, plotted against each set of the initial population.

Collection @ jeju

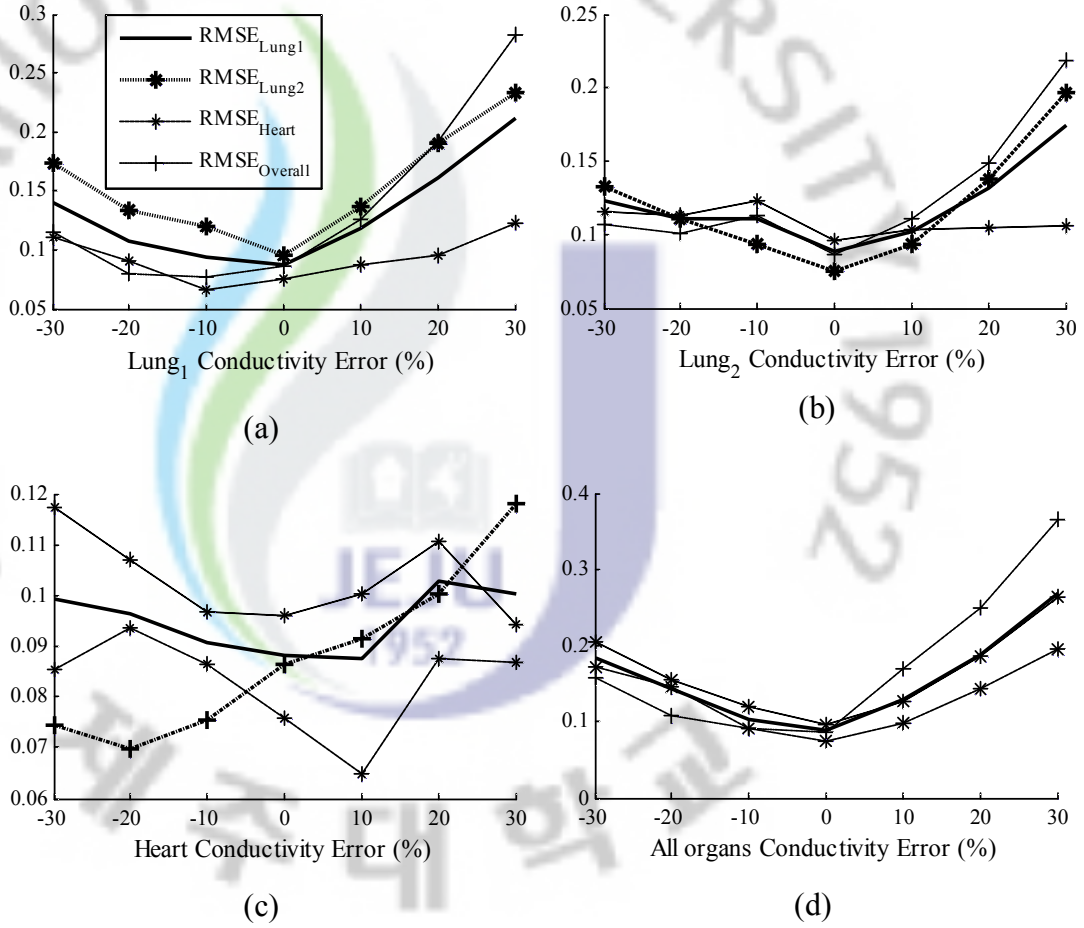

Figure 4.6. $\overline{RMSE}_\gamma$ for different conductivity errors. (a)-(d) plot the best $\overline{RMSE}_\gamma$ values, as obtained at the end of OBBO generations, for different (percentage) errors in the conductivity of $Lung_1$, $Lung_2$, *Heart*, and all the three organs, respectively.

The plots in figure 4.5(a)–(g) show the iterative progress of $\overline{RMSE}_\gamma$ values calculated for all three organs, throughout the OBBO generations for seven different kinds of initial population distributions. $\overline{RMSE}_\gamma$ values for all these cases have been calculated by repeating the execution of the algorithm for 20 times, and then calculating and plotting the average values for each iteration step individually. The final $\overline{RMSE}_\gamma$ values, calculated at the end of OBBO generations, have been summarized for all the initial population sets in figure 4.5(h). As expected, the estimation performance of OBBO deteriorates as the range of initial population distribution increases with respect to the true values. It has been emphasized time and again that the EIT boundary estimation problem (especially the non-elliptic boundaries so close to each other) is extremely hard to be solved and the lack of a

Collection @ jeju

good *a priori* knowledge significantly affects the performance of any optimization algorithm selected in this case. In fact, the conventional gradient-based inverse algorithms, such as mNR, fail to solve this problem if the initial guess is not very close to the true target. OBBO, on the other hand, still offers a solution (though a weak one) even for a quite far away initial population distribution. The progressive decline of $\overline{RMSE_\gamma}$ values for all the population distributions clearly shows the effectiveness of the OBBO in reaching the global minimum.

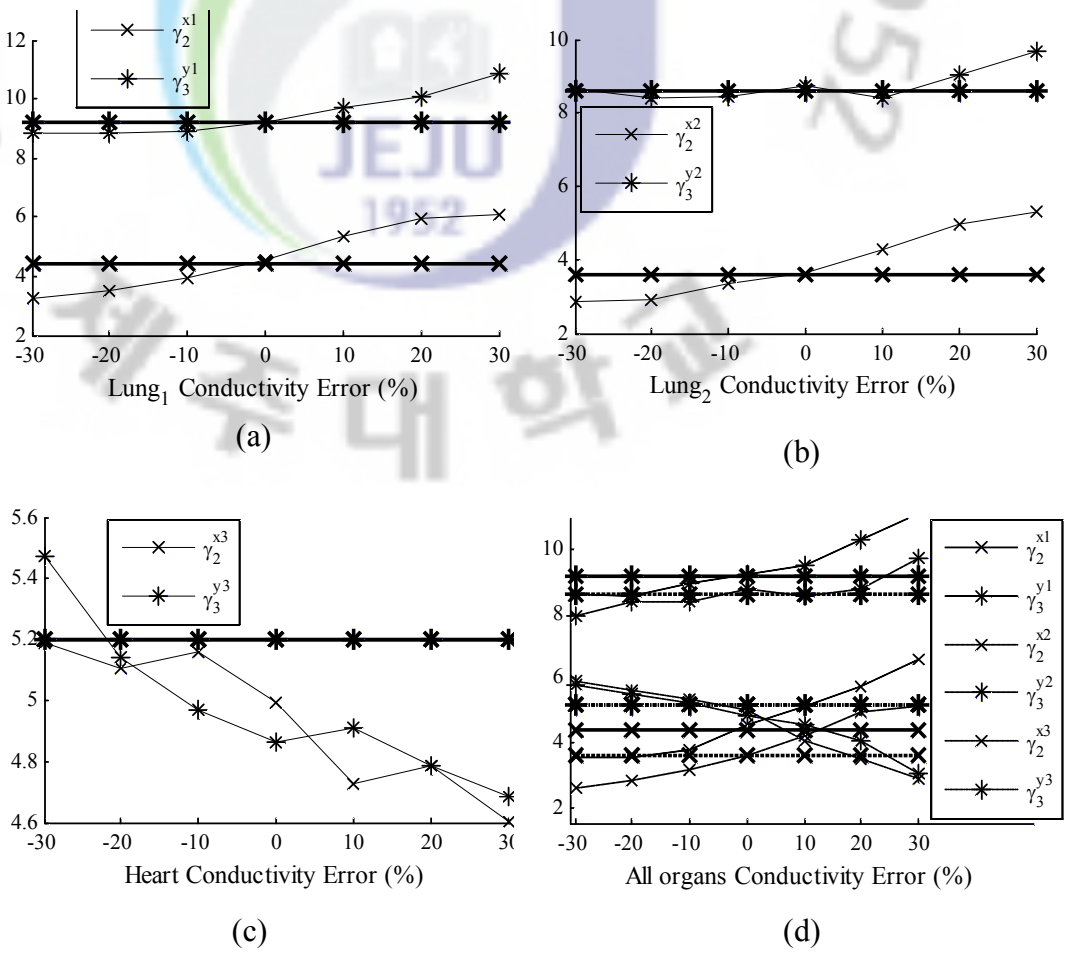

Figure 4.7. Estimated size of the organs for different conductivity errors, expressed as Fourier coefficients corresponding to their radii. (a) plots the radii $\gamma_2^{x_1}$ and $\gamma_3^{y_1}$ of *Lung*$_1$, (b) plots the radii $\gamma_2^{x_2}$ and $\gamma_3^{y_2}$ of *Lung*$_2$, (c) plots the radii $\gamma_2^{x_3}$ and $\gamma_3^{y_3}$ of *Heart* and (d) plots the radii of all the organs, against different (percentage) errors in the conductivity of the respective organs.

Another test to verify the performance of OBBO is to check its robustness against the conductivity errors, i.e., when the *a priori* knowledge of the conductivity of the

Collection @ jeju

organs is inaccurate. $\overline{RMSE}_\gamma$ values have been plotted for different conductivity errors, calculated as percentage errors with respect to the true conductivity values (see figure 4.6). The $\overline{RMSE}_\gamma$ values for each of these cases have been obtained by repeating the execution of the algorithm for 10 times, and then plotting the mean of the final $RMSE_\gamma$ values obtained so. It can clearly be observed that the $\overline{RMSE}_\gamma$ values increase with the increase in the conductivity error. This is not unexpected at all. It is to be reminded that the conductivity of the lungs is less than that of the background, while the reverse is true for the conductivity of the heart. Therefore, if the given conductivity of a lung is larger than the respective true value, it results in the overestimation of its size due the presence of a more conductive region around it, whereas a smaller given conductivity value results in the underestimation its size (de Munck *et al*. 2000). Conversely, a larger *a priori* conductivity of the heart results in the underestimation of its size and a smaller given conductivity value, in turn, results in the overestimation of the heart size due to the presence of a less conductive region around it. The effect of the conductivity errors on the size of the organs, expressed as Fourier coefficients corresponding to their radii in the *x* and *y* directions respectively, has been plotted in figure 4.7. In general, the error (expressed, either as $\overline{RMSE}_\gamma$, or in terms of the size of the organ) is reasonably small if the *a priori* conductivity error is within 20% of the respective true value. The smaller $\overline{RMSE}_{Heart}$ values for the smaller *a priori* conductivity of the heart seem to suggest that the estimation performance OBBO increases for the heart shape. However, incidentally the mean estimated size of the heart for the correct conductivity is slightly smaller than its true size. Therefore an overestimation of the heart size, due to the reasons explained before, happens to match closely with the true size.

Finally, all the simulations results presented so far have been obtained using an inhomogeneous inverse mesh structure, shown in figure 4.1. In order to further verify the robustness of the OBBO-EIT algorithm against different mesh structures, the authors have also performed a set of simulations when a homogeneous inverse mesh structures is used instead. The homogeneous mesh is composed of 4864 triangular elements with 2561 nodes. These simulations were performed for the big-heart numerical scenario and the uniform distribution marked as population 1 in

Collection @ jeju

Table 6.5 is used as the initial population distribution. The performance of OBBO was found to be independent of the type of mesh structure. However, it was noted that the density of the finite elements in the regions of interest, where the boundaries are located, significantly affects the performance of the algorithm. In the current selection of the homogenous mesh structure, a higher number of total mesh elements is selected in order to keep the density of the elements in the regions of interest, close to the inhomogeneous mesh structure (in which case the density of the finite elements was more in the region of interest as compared to the other regions). However, a 20% rise in the mean running time of the algorithm in this case, as compared to the case when an inhomogeneous mesh structure was used, has been noticed.

4.3.2 Experimental results

This section analyses the performance of the proposed EIT boundary estimation scheme using 2D EIT measurement data obtained from a chest-type experimental setup with two lungs and a heart. The experiments have been performed using the ACT3 system at Electrical Impedance Imaging lab, RPI, USA. The radius of the chest phantom is 15 cm with 32 electrodes, each of 2.54 cm width, attached around the surface of the phantom. The saline level in the phantom is 2.3 cm and the amplitude of the injected current is 0.5 mA. Note that EIT is essentially a 3D phenomenon, whereas the current results have been obtained using a 2D EIT measurement setup in which the problem domain is assumed to be a single measurement plane. 3D EIT is a complex problem and is computationally expensive (Chateaux and Nadi 2000). Since the physical electrodes are 3-dimensional, the current injected into the electrodes is not limited to a single measurement plane and is subject to variable measurement noise arising due to the inhomogeneities present around the measurement plane. In the 2D formulation, the magnitude of the current is adjusted by dividing it with the electrode height (or more specifically the saline level in the phantom) resulting in further measurement error. The quality of the 2D EIT image can be improved by increasing the number of measurement electrodes, introducing several layers of electrode planes (Gadd 1992), or by using the 3D

Collection @ jeju

measurements and then correcting them with the 2D and 3D calculated measurements (Ider 1990).

Similar to the simulation scenarios, trigonometric current pattern has been used and two different heart sizes have been considered. The big heart is 9.4 cm wide and 10 cm long, while the small heart has a width of 5.5 cm and a length of 6.1 cm (see figure 4.8). The background in chest phantom is composed of saline solution with a conductivity of 0.64 S/m while the lungs and the heart are constructed using agar with a conductivity of 0.40 S/m and 1.51 S/m respectively. Only the real components of the measured admittivity have been considered because the imaginary part of the admittivity of the agar is negligible and can be considered as part of measurement noise.

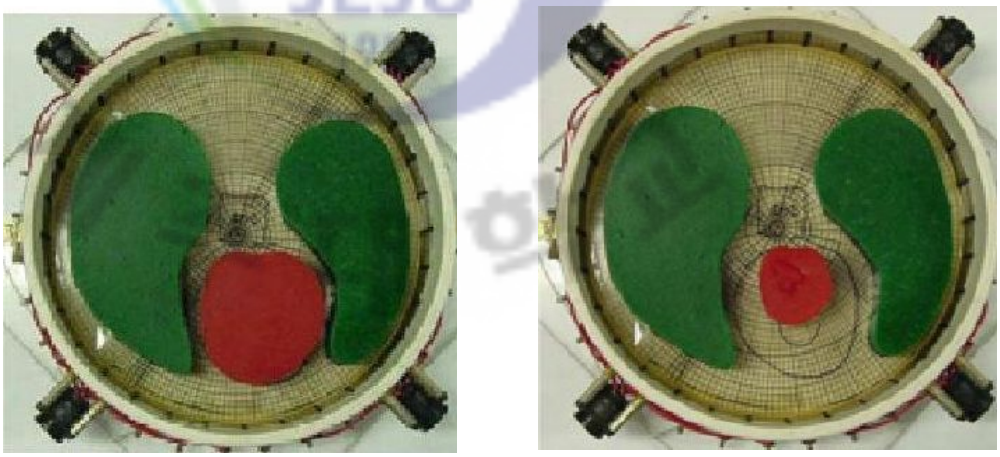

a b

Figure 4.8. Chest-like EIT experimental setup: (a) Two lungs and a big heart. (b) Two lungs and a small heart. The experiments have been performed using the ACT3 system at Electrical Impedance Imaging lab, RPI, USA.

Note that the conductivity values of the experimental setup are different from the clinically true values considered for the numerical scenarios. This is because of the difficulty of constructing exactly same conductivity values using the experimental setup. However, the contrast ratio of the organs and the background resembles closely to that of clinically true values. It should be reminded that in EIT reconstruction, the contrast ratio, rather than the actual conductivity values, determines the performance of the reconstruction algorithm.

Collection @ jeju

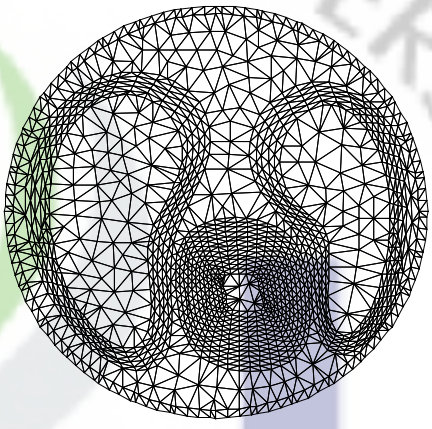

Figure 4.9. The inverse mesh structure used with the experimental setup. It is inhomogeneous concentrated in the regions of interest.

The mesh structure used to solve the inverse problem for the experimental scenarios, and all the OBBO related parameters, such as the initial population selection and the generation counts, have been chosen in the same way as in the case of the numerical scenarios. The only difference is that there is no forward mesh structure this time, since the true voltage data has been obtained through experimental measurements. The mesh used for the inverse problem is composed of 2894 triangular elements with 1512 nodes and is shown in figure 4.9. The performance of OBBO in the case of experimental scenarios is also compared with that of mNR and the results have been plotted in figure 4.10, while the statistical analysis of the results has been presented in Tables 4.6 – 4.9. Note that the true values of the Fourier coefficients to express the organ boundaries in the experimental scenario are not exactly known. Therefore, prior to the application of OBBO on the experimental data, best approximate of the true values is calculated using a trial-and-error approach, and then the statistical parameters, namely, $\overline{\hat{\gamma}}$, $\overline{MAE_\gamma}$, $\overline{MES_\gamma}$ s_e, and $\overline{RMSE_\gamma}$ are calculated with respect to the best true values. Clearly, the experimental results confirm the robustness of the proposed estimation scheme to estimate the organ boundaries inside a human chest-like structure.

Similar to the numerical scenario, the performance of the OBBO algorithm for the first experimental scenario (big heart case) has been tested for seven different types of initial population distribution, summarized in Table 5, and the progress of $\overline{RMSE_\gamma}$ throughout the OBBO generations has been plotted (in figure 4.11) for each

Collection @ jeju

type of the population. Furthermore, the $\overline{RMSE}_\gamma$ values for this experimental scenario have also been plotted for different conductivity errors (see figure 4.12) and the effect of the conductivity errors on the size of the organs has been plotted in figure 4.13. $\overline{RMSE}_\gamma$ values for all these cases have been calculated by repeating the execution of the algorithm, similar to the numerical scenario. These results demonstrate the robustness of the OBBO algorithm to varying initial guess, sometimes subject to incorrect *a priori* knowledge of the conductivities of the organs, in the experimental conditions.

Figure 4.10. OBBO and mNR estimated organ boundaries using EIT measurement data obtained from an experimental setup with two lungs and a big heart. The broken line is used to show the (mean) estimated boundaries using OBBO (left) and mNR (right). The results in the top row are for the big heart case while the bottom results are for small heart.

Collection @ jeju

Table 4.6. Experimental Scenario 1 (big heart case): mean $\overline{\hat{\gamma}}$, error standard deviation s_e, mean error squared $\overline{MES}_\gamma$ and the mean absolute deviation $\overline{MAE}_\gamma$ of the Fourier coefficients estimated using OBBO and mNR.

Fourier coeff.	True value	Estimated mean, standard deviation and mean absolute deviation							
		OBBO				mNR			
		$\overline{\hat{\gamma}}$	$\overline{MAE}_\gamma$	$\overline{MES}_\gamma$	s_e	$\overline{\hat{\gamma}}$	$\overline{MAE}_\gamma$	$\overline{MES}_\gamma$	s_e
$\gamma_1^{x_1}$	-6.00	-6.1665	0.2662	0.0277	0.2957	-5.7895	0.7648	0.0443	0.8979
$\gamma_2^{x_1}$	4.40	4.2027	0.2118	0.0389	0.2042	2.3651	2.1559	4.1406	1.3170
$\gamma_1^{y_1}$	-0.50	0.0990	0.5990	0.3588	0.2776	1.9661	2.4661	6.0814	0.5291
$\gamma_3^{y_1}$	9.20	9.1714	0.3224	0.0008	0.3727	7.4177	1.7823	3.1768	0.8381
$\gamma_1^{x_2}$	8.00	7.4484	0.5628	0.3042	0.2622	7.7035	0.7099	0.0879	0.8585
$\gamma_2^{x_2}$	3.60	3.0358	0.5642	0.3183	0.1770	2.6048	1.4592	0.9905	1.2940
$\gamma_1^{y_2}$	-1.20	-0.3555	0.8550	0.7131	0.4301	2.1492	3.3492	11.2174	0.9863
$\gamma_3^{y_2}$	8.60	9.1042	0.5424	0.2542	0.4289	8.5028	1.9381	0.0162	2.3764
$\gamma_1^{x_3}$	2.00	1.7092	0.3609	0.0846	0.3157	1.6015	1.2468	0.1588	1.4958
$\gamma_2^{x_3}$	4.70	4.8247	0.2642	0.0155	0.2724	5.1470	1.2659	0.1998	1.5174
$\gamma_1^{y_3}$	-6.40	-5.7161	0.6839	0.4678	0.3664	-6.4337	0.5774	0.0011	0.7654
$\gamma_3^{y_3}$	5.00	5.1327	0.2370	0.0176	0.2593	3.7509	1.3925	1.5603	1.1949

Table 4.7. Experimental Scenario 1 (big heart case): mean RMSE of the aggregated Fourier coefficients for the *Lung*$_1$, *Lung*$_2$ and *Heart*, respectively, estimated using OBBO and mNR.

	Mean RMSE values of the aggregated Fourier coefficients	
	OBBO	mNR
$\overline{RMSE}_{Lung_1}$	0.0956	0.5347
$\overline{RMSE}_{Lung_2}$	0.1217	0.5219
$\overline{RMSE}_{Heart}$	0.1121	0.3158
$\overline{RMSE}_{Overall}$	0.1116	0.4951

Collection @ jeju

Table 4.8. Experimental Scenario 2 (small heart case): mean $\overline{\hat{\gamma}}$, error standard deviation s_e, mean error squared $\overline{MES_\gamma}$ and the mean absolute deviation $\overline{MAE_\gamma}$ of the Fourier coefficients estimated using OBBO and mNR.

Fourier coeff.	True value	Estimated mean, standard deviation and mean absolute deviation							
		OBBO				mNR			
		$\overline{\hat{\gamma}}$	$\overline{MAE_\gamma}$	$\overline{MES_\gamma}$	s_e	$\overline{\hat{\gamma}}$	$\overline{MAE_\gamma}$	$\overline{MES_\gamma}$	s_e
$\gamma_1^{x_1}$	-6.00	-5.4676	0.6301	0.2834	0.4422	-5.9392	0.5704	0.0037	0.7777
$\gamma_2^{x_1}$	4.40	4.8350	0.4504	0.1892	0.3406	1.7288	2.6712	7.1352	0.8473
$\gamma_1^{y_1}$	-0.50	-0.3414	0.3265	0.0252	0.3898	1.3586	1.8586	3.4545	0.7234
$\gamma_3^{y_1}$	9.20	9.7761	0.6451	0.3319	0.3893	8.2709	1.1631	0.8633	0.9456
$\gamma_1^{x_2}$	8.00	6.8391	1.1609	1.3478	0.4640	8.0873	0.5661	0.0076	0.6664
$\gamma_2^{x_2}$	3.60	3.6264	0.1435	0.0007	0.1763	0.9362	2.6638	7.0959	0.8116
$\gamma_1^{y_2}$	-1.20	-0.5896	0.6112	0.3726	0.3107	1.3753	2.5753	6.6323	1.1649
$\gamma_3^{y_2}$	8.60	9.5169	0.9385	0.8407	0.5600	9.9841	1.8212	1.8336	1.9224
$\gamma_1^{x_3}$	1.60	1.8987	0.4793	0.0892	0.4907	-0.6167	2.3625	4.9138	1.8393
$\gamma_2^{x_3}$	2.80	3.4242	0.6414	0.3896	0.3861	1.3945	1.9387	1.9753	1.8575
$\gamma_1^{y_3}$	-4.00	-3.9693	0.4763	0.0009	0.5942	1.6747	5.6747	32.2023	1.1758
$\gamma_3^{y_3}$	3.00	3.3928	0.4750	0.1543	0.3917	1.8540	1.3686	1.3134	1.1707

Table 4.9. Experimental Scenario 2 (small heart case): mean RMSE of the aggregated Fourier coefficients for the $Lung_1$, $Lung_2$ and *Heart*, respectively, estimated using OBBO and mNR.

	Mean RMSE values of the aggregated Fourier coefficients	
	OBBO	mNR
$\overline{RMSE}_{Lung_1}$	0.1185	0.5381
$\overline{RMSE}_{Lung_2}$	0.1483	0.5089
$\overline{RMSE}_{Heart}$	0.2164	1.2190
$\overline{RMSE}_{Overall}$	0.1473	0.6327

Collection @ jeju

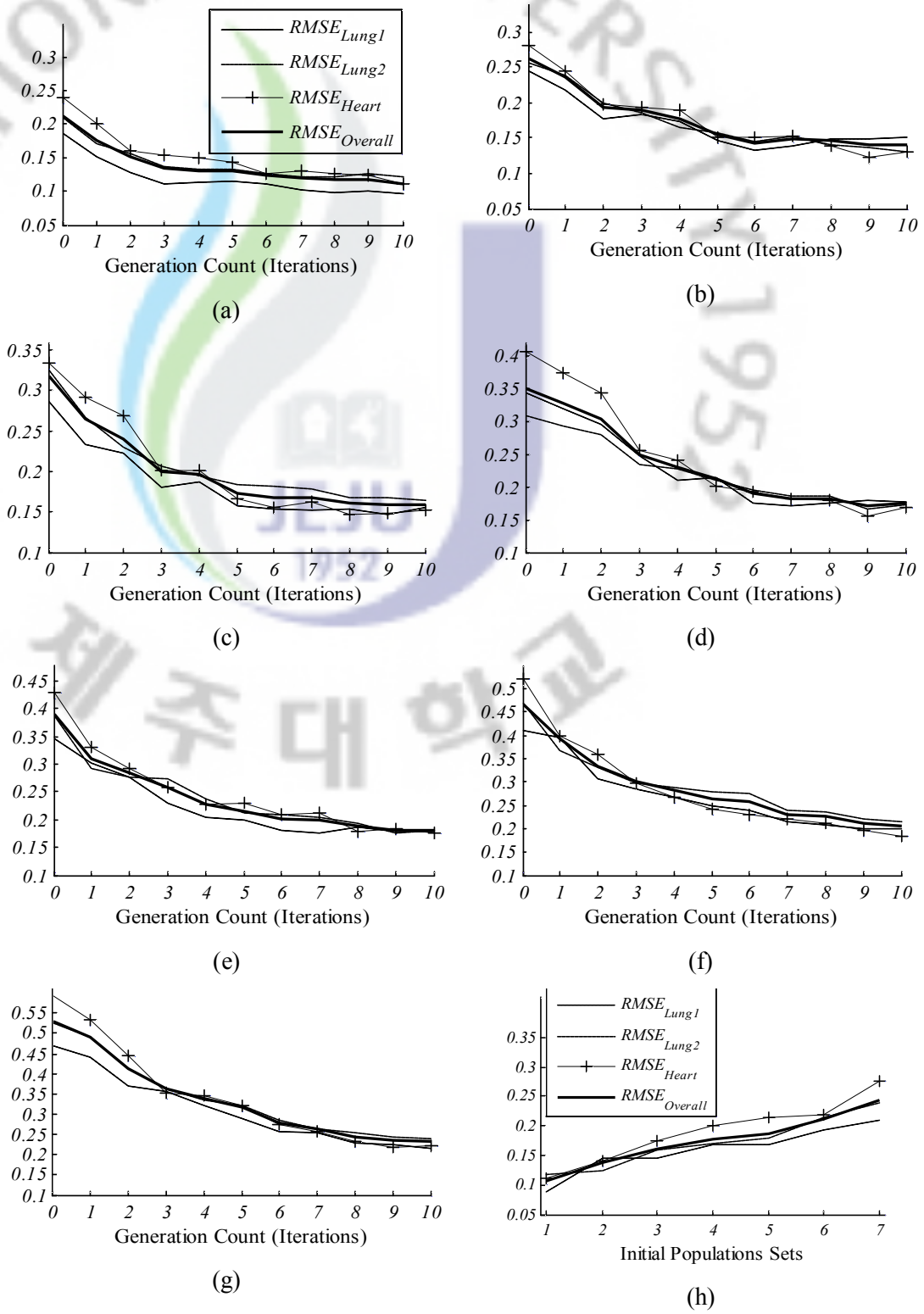

Figure 4.11. Experimental Scenario 1 (big heart case): $\overline{RMSE}_{\gamma}$ for different sets of initial populations. (a) – (g) show the $\overline{RMSE}_{\gamma}$ values calculated for all three organs, plotted iteratively for each OBBO generation. (h) summarizes the best $\overline{RMSE}_{\gamma}$ values, as obtained at the end of the 10*th* OBBO generation, plotted against each set of the initial population.

Collection @ jeju

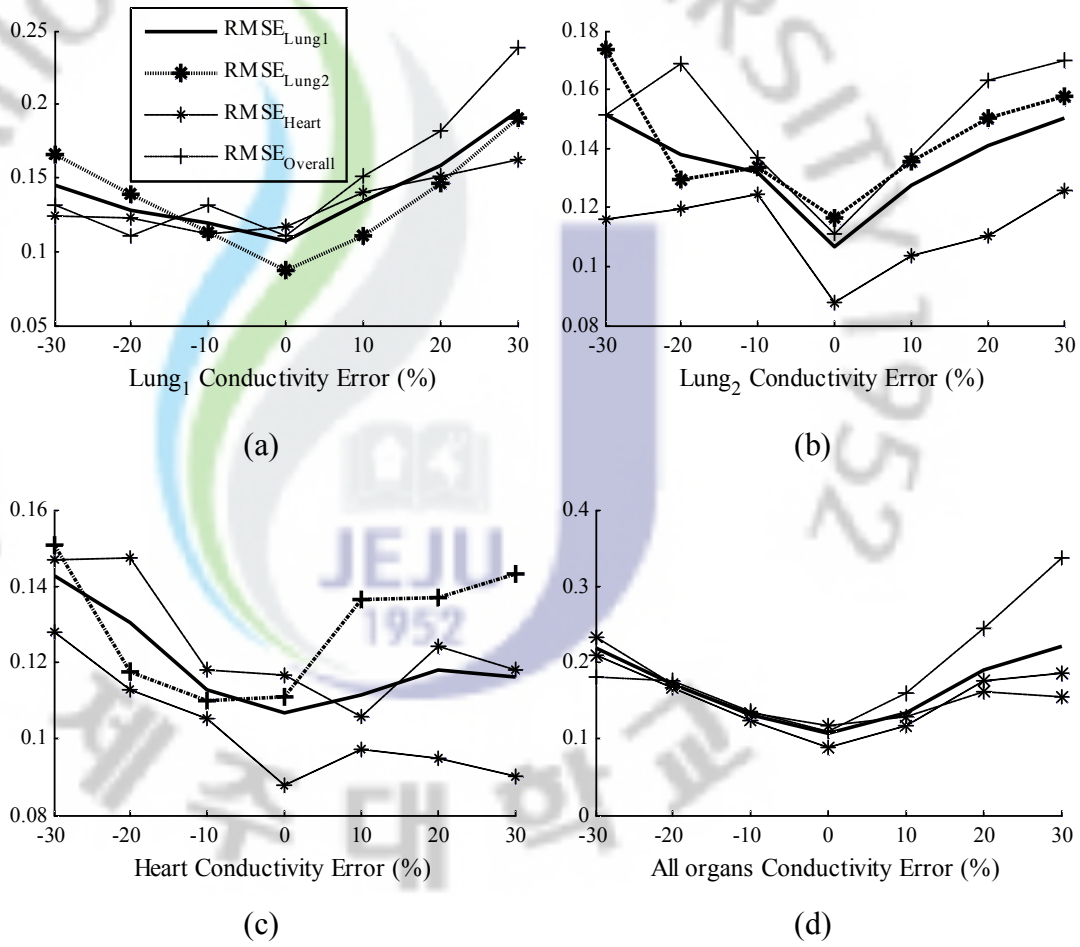

Figure 4.12. $\overline{RMSE}_\gamma$ for different conductivity errors. (a)-(d) plot the best $\overline{RMSE}_\gamma$ values, as obtained at the end of OBBO generations, for different (percentage) errors in the conductivity of *Lung*$_1$, *Lung*$_2$, *Heart*, and all the three organs, respectively.

The performance of the algorithm can be further improved by using a larger set of initial population and increasing the maximum number of iterations allowed by the algorithm to reach the final solution. Nevertheless, it will further increase the computational complexity of the algorithm. Another point to consider, while analyzing the performance of OBBO, is that the worst half of its total population is discarded at the end of each iteration step. The population disposal step is totally based upon the value of the cost functional, without any regard to the distribution of the population. A more intelligent population selection approach resulting in a more evenly distributed population at the start of each new iteration step should further increase the performance of the algorithm. Several population distribution schemes have been discussed in the literature (Simon 2009, Simon *et al*. 2009). Selection of

Collection @ jeju

the best suitable population is problem dependent and remains an open research problem.

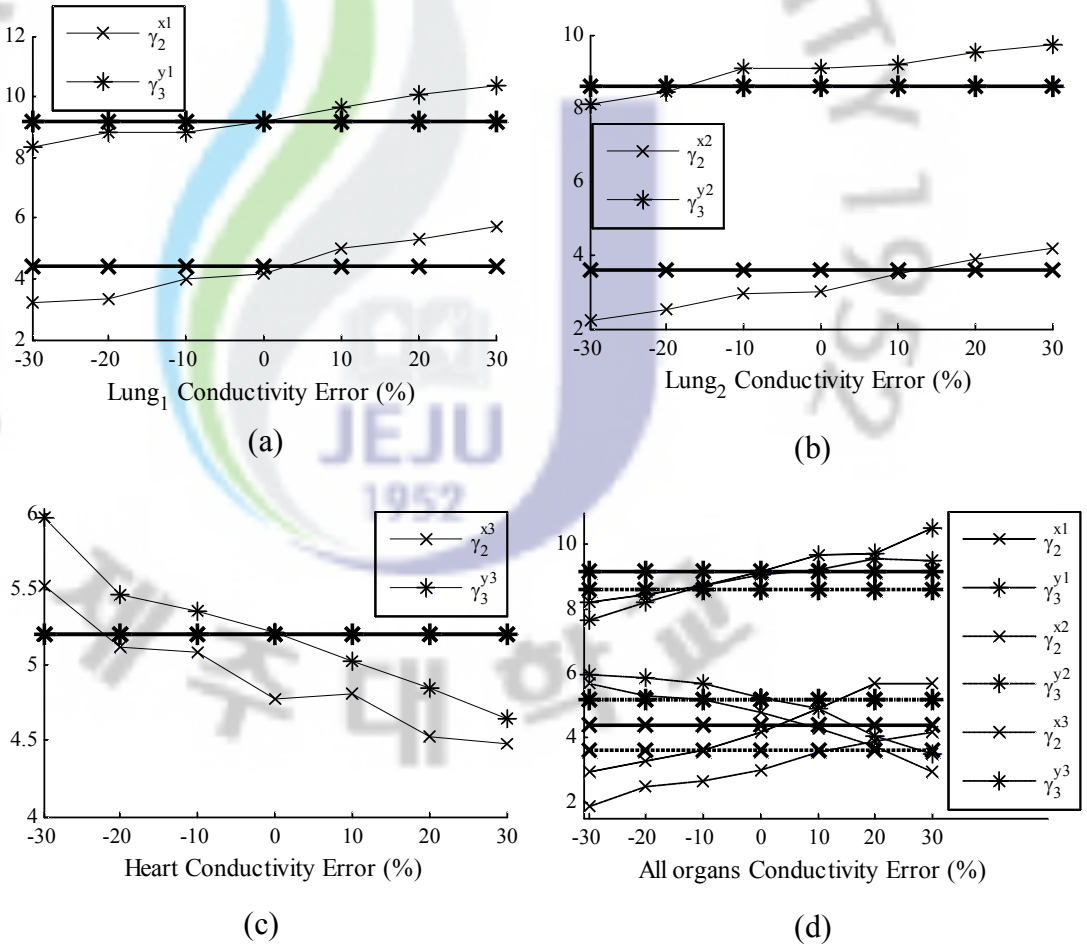

Figure 4.13. Experimental Scenario 1 (big heart case): Estimated size of the organs for different conductivity errors, expressed as Fourier coefficients corresponding to their radii. (a) plots the radii $\gamma_2^{x_1}$ and $\gamma_3^{y_1}$ of $Lung_1$, (b) plots the radii $\gamma_2^{x_2}$ and $\gamma_3^{y_2}$ of $Lung_2$, (c) plots the radii $\gamma_2^{x_3}$ and $\gamma_3^{y_3}$ of *Heart* and (d) plots the radii of all the organs, against different (percentage) errors in the conductivity of the respective organs.

5. Dynamic optimization

Collection @ jeju

When the optimum solution of a problem varies through time, such a problem is called a dynamic optimization problem (DOP). The dynamic change in the optimum solution may occur either due to an uncertainty in the decision space or uncertainty in the fitness/objective function of the problem. If the gravity of change is small the standard optimization algorithms, such as the standard evolutionary algorithms, should be able to find the optimal solution with reasonable accuracy. However, if the change is significant, a static search and optimization technique to solve such a problem would result in suboptimum solution and may completely fail to solve the problem if the frequency or severity of the dynamic change is too severe. Under such circumstances, the need of a dynamic optimization technique, such as a dynamic evolutionary algorithm (DEA) is imminent. This section summarizes the important features of DOPs, the desired characteristics of a DEA suitable to solve DOPs and, finally, presents the most common evolutionary approaches to solve them.

5.1 The uncertainties in DOPs

In general, there are four major categories of uncertainties in dynamic optimization problems (DOPs) (Jin and Branke 2005, Woldesenbet *et al*. (2009)

1) uncertainty in the decision space due to perturbations in the design variables,
2) uncertainty in the fitness/objective function caused by the noise in the fitness function and the approximation in the fitness function,
3) uncertainty in the fitness/objective function caused by the approximation in the fitness function, and
4) uncertainty in the location, height, and shape of the optimal solutions through time due to the dynamism in optimal solutions. Such changes often result in global optima becoming local optima and vice versa. The dynamic changes in the height, shape and location of the optimal solution, are graphically shown in figures 5.1, 5.2 and 5.3, respectively. The left side of each of these pictures shows the peaks before the dynamic change whereas the right hand side shows the peaks after change. The convergence to the optimal solution becomes even more difficult if the peaks move independent of each other.

Collection @ jeju

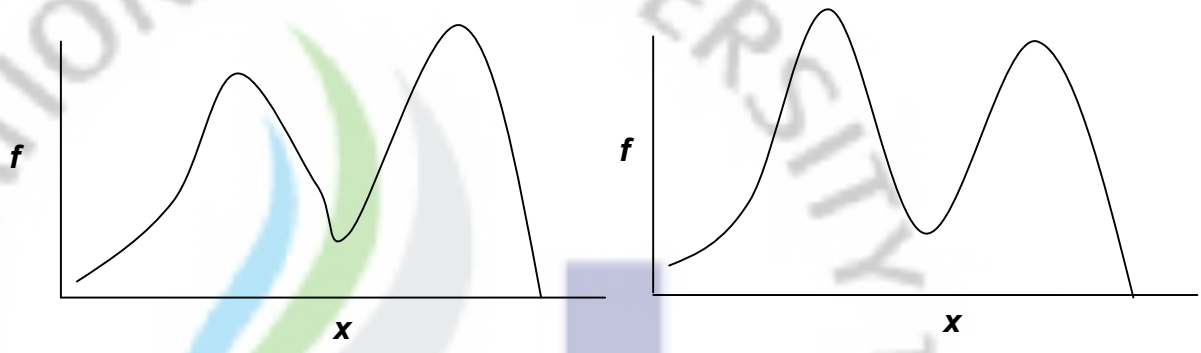

Figure 5.1. Changing fitness peak heights. The left side shows the peaks before the dynamic change whereas the right hand side shows the peaks after change.

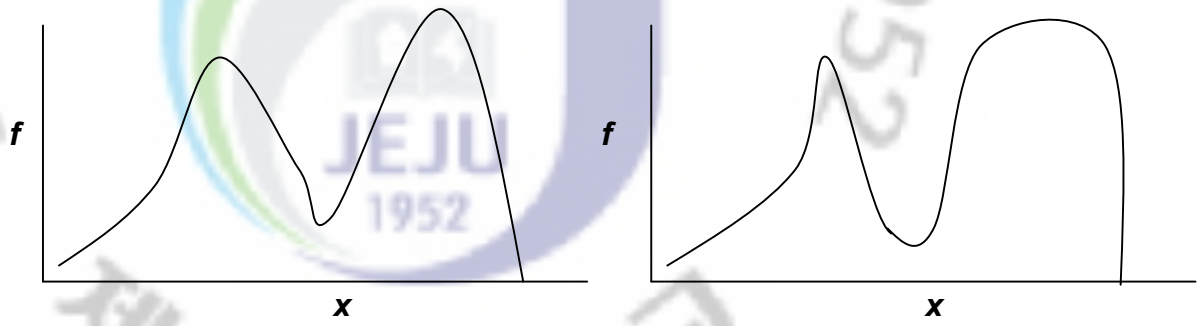

Figure 5.2. Changing fitness peak shapes. The left side shows the peaks before the dynamic change whereas the right hand side shows the peaks after change.

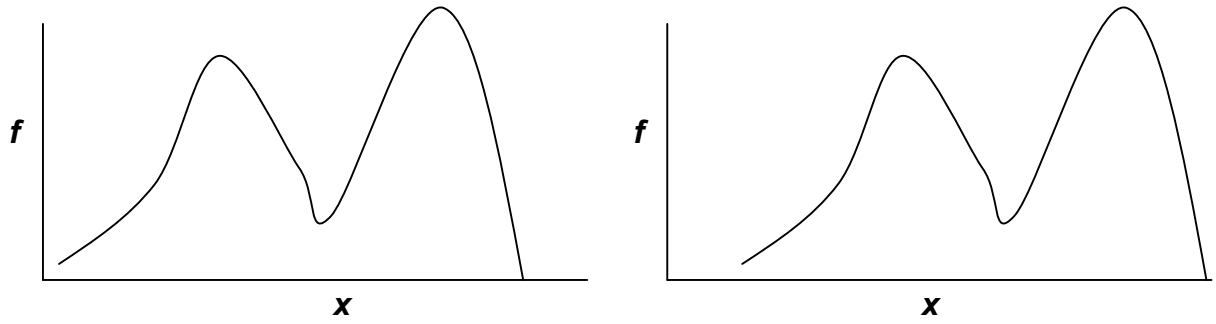

Figure 5.3. Changing fitness peak locations. The left side shows the peaks before the dynamic change whereas the right hand side shows the peaks after change.

5.3 Important features of DOPs

The dynamic optimization problems can be classified based upon the following features/aspects (Branke 2001, Weicker 2003)

- severity of change
- frequency of change
- observability of change

dCollection @ jeju

- detectability of change
- dynamics of change

A brief description of the aforementioned DOP classifications and their effect on the ability of dynamic optimization algorithms (namely the DEAs) to find an optimal solution follows.

5.3.1 Severity of change

Severity of change requires DEAs to increase the diversity of population in order to improve its ability to explore the solution space. If the change is too severe for the DEA to handle it properly, it may get trapped in a local optimum or may not be able to track the change at all.

5.3.2 Frequency of change

If the optimum solution is changing very frequently with time, the convergence speed of the DEA needs to be adjusted accordingly. Otherwise, the DEA may trail behind the changing optimal solution and will potentially lose the track of the solution if preemptive steps are not taken in time.

5.3.3 Observability and detectability of change

Assuming that the change is observable, the detection of the change can be done explicitly or implicitly. The detection is implicit if, for example, it is observed that the average performance of the DEA worsens over a period of time. On the other hand, the detection is explicit if the DEA is implemented using fixed-interval time steps assuming that the environment changes noticeably after each time step. The explicit approach is often preferred over the implicit approach since it separates the problem to handle the uncertainty of change from its detection, effectively handling the core issue, i.e., the uncertainty handling (Branke 2001).

5.3.4 Dynamics of change

The behavior of the dynamic change in the environment can be distinguished as variable or constant, linear or nonlinear, random or systematic, cyclic (circular, revolving, periodic or etc) or non-cyclic, and etc (Branke 2001). A good DEA is

Collection @ jeju

expected to adapt to the dynamic environment without having an explicit knowledge of the nature of change (Woldesenbet *et al*. 2009). However, certain DEAs have been proposed to work better in certain environments. For example, memory based DEAs, to be discussed later, are expected to perform better in cyclically changing environments.

5.4 Desired characteristics of a DEA suitable to solve a DOP

In the case of DOPs, when an evolutionary algorithm converges to an optimum solution of the problem at any time instant, the diversity of population vanishes, severely affecting its ability to further explore the solution space after the change in the environment. Unless and until an adaptation scheme is introduced, the EA will be unable to offer a reasonable solution in the dynamic environment and may get stuck in a local optimum. The standard EAs thus need to be modified so that their populations are automatically adapted according to the changing environment. The desired characteristics of a DEA suitable to solve dynamic optimization problems are as follows (Woldesenbet *et al*. 2009)

- reusability
- better adaptation
- faster convergence
- higher accuracy
- improved performance
- easier implementation

Reusability refers to the ability of DEA to utilize the current population to find the optimal solution in the changing environment, while the adaptation means modifying the current set of solutions to make them fit in the new environment. Effective reuse of the old population accelerates the speed of convergence and consequently leads to better adaptation. However, if the change is too severe, the reusability of current population reduces drastically, requiring a new population which can explore the solution space more efficiently. Similarly, if the change is occurring very frequently, the ability of DEA to detect and observe the changes diminishes and the faster convergence and the adaptation ability of the algorithm becomes more relevant. Adaptation can be achieved either through specifically introduced evolutionary

Collection @ jeju

operators, such as hyper-mutation and etc., or by incorporating the historical evolutionary data into the evolutionary process.

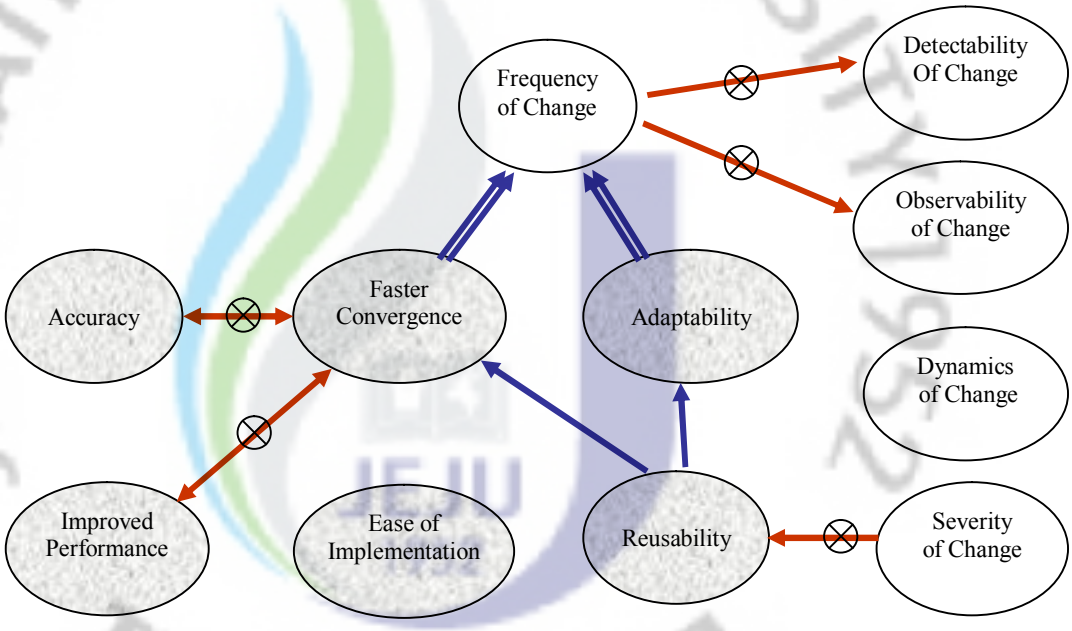

Figure 5.4. The desired characteristics of the DEAs and their effect on the different features of the DOPs, as well as, on each other The DEAs' desired characteristics have been shaded to distinguish them from the DOP features.

Accuracy of the optimal solution is usually measured based on some error measure, calculated as the difference between the true solution and the best found solution, using DEA. The need for an improved accuracy may have a negative effect on the convergence speed of the algorithm; therefore, DEA should be designed and implemented with caution, finding a balance between the computational complexity and the expected performance of the algorithm. Figure 5.4 provides a schematic perspective of the desired characteristics of the DEAs and their effect on the other characteristics as well as different features of the DOPs. In this figure, the single arrow is drawn to show that a given characteristic, if present in the DEA, automatically leads to the existence of the other characteristic pointed out by the arrow. The double arrows towards a certain feature of DEA (i.e., frequency of change) are used to link them to the characteristics which are necessary to be present in the DEA in order to achieve a reasonable performance. The arrows with a cross mounted on them means that the existence of a certain DOP feature has a negative impact on other important features of the DOP or on some desired characteristic of the DEA. The double-sided arrow with a cross means those characteristics which are

Collection @ jeju

difficult to coexist at the same time, i.e., the presence of one characteristic is very likely to compromise the other characteristic. The unconnected feature(s)/characteristic(s) do not mean that they are isolate from each other; it only means that a direct relation with other features /characteristics of DOP/DEA may not be available.

5.5 Evolutionary approaches to solve DOPs

This subsection summarizes the evolutionary approaches developed to solve the DOPs. These approaches can be broadly categorized into six different types of strategies to cope up with the dynamic changes occurring in the system (Weicker 2003)

1. reinitialization
2. memory-based approaches
3. multiple population approaches
4. mutation and self-adaptation
5. local variation
6. other diversity preserving techniques

5.5.1 Reinitialization

It is the simplest approach to solve the DOPs. In this approach, the evolutionary process is reinitialized whenever a change occurs. However, the major shortcoming of this approach is that all of the evolutionary progress so far is lost and, therefore, it may significantly affect the speed of convergence.

5.5.2 Memory-based approaches

The memory based approaches can be further categorized into

- explicit memory approaches, and
- implicit memory approaches

In the implicit memory approaches there is no external memory, rather the system contains some form of implicit memory. One such form of memory is the redundant representation, which is usually used to slower the convergence rate, thus keeping the population diversity intact. The most common redundant representation approach is

Collection @ jeju

the diploid scheme, which is used by many researchers (Ng and Wong 1995, Dasgupta and McGregor 1992, Lewis *et al*. 1998, Ryan 1997). In the diploid scheme, each individual contains multiple times of information as compared to the haploid, which contains only one set of information, i.e., a single set of values or characteristic features of each individual in the population.

The explicit memory approaches make use of the external memory to store the historical evolutionary data, potentially useful in the upcoming evolutionary steps. One particular benefit of the explicit memory-based approach is that it allows the population to jump to a solution space which may not be achievable within an iteration using other evolutionary approaches such as hyper-mutation. The explicit memory-based approach results in a more directed population jumping step as compared to the hyper-mutation which may require several iterations to reach to that point in the solution space. The explicit memory can be a local memory or it can be a shared memory.

Trojanowski and Michalewicz (1999) applied a short-term local memory. Their main idea was to remember and recall some of the solutions of an individual's ancestors. In the case of a dynamic change in the environment, each solution is compared with its stored ancestor solutions, thus incorporating the best solution into the current populations, while keeping the others in the memory. The size of the memory is fixed and the individuals from the first generation start with an empty memory buffer. For each of the following generations the parent solution is stored in memory and if the memory is already full the oldest memory solution is replaced with the newest parent.

In one of the simplest shared memory-based approaches, whenever a change occurs the population is re-initialized with a seed from the previous populations, rather than starting from the scratch. The same approach had been considered by Louis and XU (1996). The memory in this approach is not a permanent memory; instead, it is only temporarily filled with a few solutions from the old population and is discarded and refilled with a new seed after each dynamic change.

Alternatively, the shared memory can be permanently filled with historical data obtained over a period of time. For example, in a DEA approach considered by Ramsey and Greffenstette (1993) a few good candidate solutions for a robot

Collection @ jeju

controller are stored in a permanent memory along with the information about the robot environment. The relevant memory sections can be incorporated into the population of the EA if the robot environment resembles the corresponding stored environment. The disadvantage, however, is that it is assumed that one can measure the similarity of the robot environment.

In the real-world problems, an old solution stored in the memory rarely receives the identical fitness in the future. However, the optimal solution may be in the vicinity of an old solution after the dynamic change in the environment. Therefore, under the realistic conditions the static memory may be redundant and of little or no use at all. Bendtsen and Krink (2002) introduced a dynamic memory model in which the memory is frequently updated during the evolutionary process. The best individuals during the time between dynamic changes are stored in the memory, while allowing the stored individuals to evolve by small amounts of Gaussian mutation in the direction of the current best individual. In this approach the best individual in the current population is selected and is matched with the nearest stored solution in the memory. The closest stored solution then gradually moves in the direction of the current best solution in the evolutionary population. The result is that the stored candidate solutions trace optimal solution in the dynamic environment, by creating colonies of solutions in different locations. If the optimal solution returns to one of these colonies in future, the memory automatically adjusts accordingly and results in much faster convergence.

5.5.3 Multiple population approaches

The fundamental idea behind this approach is to divide the total population into a number of subsets such that each subpopulation explores a different region in the solution space, thus simultaneously tracking multiple optima at a time. Such an approach was proposed by Branke *et al*. (2000) in which a small portion of the total population, termed as the child population, tracks the most promising peaks found so far, whereas the remaining population searches for other peaks. The motivation was to simultaneously track different regions of the solution space having a strong potential to converge to the optimal solution in the dynamic environment. In a similar approach known as the shifting balance genetic algorithm (Oppacher and Wineberg

Collection @ jeju

1999) a core population is used to further optimize the current best solution while other portions of the population, termed as colonies, explore the search space. The fitness of the colonies is evaluated using a diversity measure, namely the distance to the core population. Ursem (2000) proposed a multinationals genetic algorithm using a hill valley detection procedure. A hill valley describes the boundaries of the subpopulations and is detected if the fitness of a sample point is less than that of the end points.

The major challenge faced by the multiple population approaches is their ability to communicate between the subpopulations. Higher communication means improved performance, however, it inevitably results in significant increase in the computational cost of the algorithm.

5.5.4 Mutation and self-adaptation

These are among the most popular and successful techniques used in the case of static optimization problems. Therefore, a straightforward extension and application of these techniques to the dynamic optimization problems makes a lot of sense. Weicker and Weicker (2000) compared a number of self adaptation techniques, namely, the uniform self-adaptation, different mutation level for each dimension, mutation with covariance matrix adaptation and sphere mutation. Brest *et al.* (2009) proposed the dynamic optimization using self-adaptive differential evolution in which the DE control parameters F and CR were self-adapted. Bäck (1997) and (Salomon and Eggenberger, 1997) also studied self-adaptive evolutionary strategies with the lognormal update rule.

In a related technique, termed as the hypermutation (Cobb and Grefenstette 1993) a higher mutation probability is used whenever a dynamic change in the environment occurs. A drastic raise in the mutation rate increases the population diversity, thus making it more suitable for the dynamic environment. Similarly Angeline (1997) introduced the multiplicative update rule to adapt the mutation level in the case of the change in environment.

Collection @ jeju

5.5.5 Local variation

If the magnitude of the change in environment is relatively small, a localized change in the characteristic variables of the current set of individual solutions may give a better performance to other approaches. The local variation can be introduced with the help of certain mutation operators, such as some Gaussian update rule (Saleem and Reynolds 2000) or a lognormal update rule (Bäck 1997, Salomon & Eggenberger, 1997) or special variable local search operator (Vavak *et al*. 1996). Weicker (2003) presented a detail analysis of an exemplary local operator using a theoretical model, leading to ten qualitative design rules for the application of local variation to dynamic tracking problems. He proposed using certain local parameters such as directed mutations, small mutation penalizing steps and etc. In a fairly recent study, Woldesenbet *et al*. (2009) proposed to use the evolutionary progress history to relocate and adapt the current set of individual solutions to the new environment. The details of this particular technique will be covered in the next chapter.

5.5.6 Diversity preserving techniques

The objective of all the dynamic evolution techniques introduced so far is to preserve the diversity of the evolutionary population in order to avoid its premature convergence. This subsection enlists a few of those diversity enhancing techniques which have not been covered before.

Andersen (1991) used fitness sharing to favor less populated areas. The fitness of the individuals lying in the densely populated areas is shared by a larger number of individuals as compared to the individuals lying in the sparsely populated areas, in which case the fitness is shared by a smaller number of individuals. The result is that the solutions lying in the less congested areas of the solution space will have a relatively higher chance of selection as compared to the solutions lying in the densely populated areas, thus preserving the diversity of the population.

Weicker (2003) categorized the diversity preserving techniques into three broad categories namely, diversity increasing techniques which introduce random immigrants in population at each generation, niching techniques which prevent premature convergence and restricted mating which divide the population into

Collection @ jeju

several subpopulations, limiting the recombination operator to the individuals belonging to the same subpopulation.

Grefenstette (1992) introduced random immigrants in population at each generation, in order to keep its diversity intact. Although it is a very straight forward algorithm, it unable to quickly adapt the population to dynamic changes in the environment due to its unpredictable randomness. Moreover, the number of random immigrates required to track severe changes in the environment are quite high, thus leading to an inferior performance of the algorithm.

Other diversity preserving techniques include favoring the middle aged individuals over other individuals (Ghosh *et al*. 1998) and adding an artificial objective function to transform a single objective optimization problem into a multi-objective optimization (Bui *et al*. 2005).

Collection @ jeju

6. Dynamic OBBO with variable relocation

This chapter presents an evolutionary approach to estimate the shape, size and location of non-stationary region boundaries inside an object domain using 2D EIT. The evolutionary algorithm selected for this purpose is the oppositional biogeography-based optimization (OBBO) and the dynamic optimization is achieved by incorporating the concept of variable relocation, proposed by Woldesenbet *et al*. (2009), to OBBO. The proposed algorithm uses the evolutionary progress history to relocate and adapt the current set of individual solutions to the new environment. The relocation of decision variables introduces some sort of uncertainty in the decision space and aims to account for the estimated change in the objective space. The ultimate effect is the introduction of a diversified population and an accelerated exploration of the solution space and faster convergence to the optimal solution under dynamic and uncertain environments. It should be noted that the selected dynamic evolutionary technique falls under the category of location variation and may also be considered to belong to the general category of mutation and self adaptation. It is computationally less expensive as compared to many other DEAs.

In this algorithm, each of the decision variables is relocated on the basis of a special parameter known as the relocation radius. The distinctive feature of this technique is that the scope of the relocation radius used in the algorithm is local to each individual solution in the populations which results in a population which is more adaptable to the new dynamic environment as compared to those adaptive techniques which use global relocation/adaptation. The relocated population is specifically far more superior and more adaptive compared to randomly-generated new population.

6.1 Variable relocation

Let Δx_c denote the evolutionary progress in cth decision variable of a newly generated solution with respect to its parents, measured as the difference between the cth decision variable of the new solution and that of the centroid of its parents (Woldesenbet *et al*. 2009)

Collection @ jeju

$$\Delta x_c(child) = x_c(child) - \frac{x_c(parent_1) + x_c(parent_2)}{2} \tag{6.1}$$

The evolutionary progress Δf in the fitness function of the new solution is calculated as the difference of the fitness of the new solution and the interpolated fitness of its parents

$$\Delta f(child) = f(child) - \frac{\Delta X_{C-P_2} . f(parent_1) + \Delta X_{C-P_1} . f(parent_2)}{\Delta X_{C-P_1} + \Delta X_{C-P_2}} \tag{6.2}$$

where

$$\begin{aligned} \Delta X_{C-P_i} &= \left\| X(child) - X(parent_i) \right\|, \qquad i = 1, 2 \\ &= \sqrt{\sum_{c=1}^{m} (x_c(child) - x_c(parent_i))^2} \end{aligned} \tag{6.3}$$

The cumulative average evolutionary progress in the cth decision variable and fitness of the newly generated solution are calculated as the weighted sum of the child's evolutionary progress and the average evolutionary progress in the parents' cth decision variable/fitness values, denoted as $\overline{\Delta x_c}$ and $\overline{\Delta f}$, respectively, can be computed as

$$\overline{\Delta x_c}(child) = \frac{\Delta x_c(child) + w.nGen. \dfrac{\overline{\Delta x_c}(parent_1) + \overline{\Delta x_c}(parent_2)}{2}}{w.nGen + 1} \tag{6.4}$$

$$\overline{\Delta f}(child) = \frac{\Delta f(child) + w.nGen. \dfrac{\Delta X_{C-P_2} . \overline{\Delta f}(parent_1) + \Delta X_{C-P_1} . \overline{\Delta f}(parent_2)}{\Delta X_{C-P_1} + \Delta X_{C-P_2}}}{w.nGen + 1} \tag{6.5}$$

where $nGen$ is the total number of generations so far, starting from the beginning of the evolutionary process or since the last dynamic change in the environment, if any. w is the relative weight given to the past evolutionary progress compared to the most recent one. It is not difficult to note that a value of w less than one gives more importance to the most recent evolutionary progress as compared to the previously computed progress.

Collection @ jeju

The average evolutionary progress $\overline{\Delta X}$ in the decision space of an individual can be calculated as

$$\overline{\Delta X} = \sqrt{\sum_{c=1}^{m} (\overline{\Delta x_c})^2} \tag{6.6}$$

Average sensitivity $\overline{S^X}$ of the decision space to change in the objective space is defined as

$$\overline{S^X} = \frac{\overline{\Delta f}}{\overline{\Delta X}} \tag{6.7}$$

The average $\overline{s_c^x}$ sensitivity of the cth decision variable to change in the objective space, in turn, can be calculated as follows

$$\overline{s_c^x} = \overline{S^X} \frac{\overline{\Delta x_c}}{\overline{\Delta X}} = \overline{\Delta x_c} . \frac{\overline{\Delta f}}{\sum_{c=1}^{m} (\overline{\Delta x_c})^2} \tag{6.8}$$

Now we are ready to calculate the relocation radius which is the anticipated uncertainty in the decision space of an individual and is used to estimate the required offsets in the decision variables matching the fitness changes caused by the environment

$$\Delta R = \begin{cases} -\dfrac{f^{e_2} - f^{e_1}}{\overline{S^X}} & if\ f^{e_2} \le f^{e_1} \\ \min\left\{ \dfrac{f_{best}^{e_2} - f^{e_1}}{\overline{S^X}}, \dfrac{f^{e_2} - f^{e_1}}{\overline{S^X}} \right\} & if\ f^{e_2} > f^{e_1} \end{cases} \tag{6.9}$$

Where, f^{e_1} and f^{e_2} are the fitness values of an individual solution in the old environment e_1 and new environment e_2, respectively. $f_{best}^{e_2}$ is the fitness value of the least cost/best fit individual solution in the new environment. The relocation radius for the cth decision variable is then calculated as

$$\Delta r_c = \Delta R \frac{\overline{s_c^x}}{\overline{S^X}} = \Delta R . \frac{\overline{\Delta x_c}}{\overline{\Delta X}} \tag{6.10}$$

where

$$\Delta r_c = \begin{cases} \text{sign}(\Delta r_c).(\Delta r_c^{\max} - \Delta r_c^{\min}) & if\ \left|\Delta r_c\right| > \Delta r_c^{\max} - \Delta r_c^{\min} \\ \Delta r_c^{\min} & if\ \Delta r_c < \Delta r_c^{\min} \end{cases} \tag{6.11}$$

Collection @ jeju

where $\Delta r_c^{\max}$ and $\Delta r_c^{\min}$ are the maximum and minimum values of the relocation radius allowed in the cth decision variable. The new offspring is then generated as follows

$$x_c^{new} = x_c^{old} + rand.\Delta r_c \tag{6.12}$$

where the random number $rand \in [0,1]$. The last step (6.12) will be repeated for each of the decision variables.

The above technique to generate the new set of initial population in the case of a dynamic environmental change has been developed for the general evolutionary algorithms for which the new offspring is generated using exactly two parents. In the case of OBBO, however, this is not true and the above algorithm has to be modified accordingly. In fact OBBO, which has been derived from BBO, does not include the reproduction or the generation of children in the classical sense, rather, it maintains and evolves a set of candidate solutions from one iteration to the next, relying on migration as well as opposition jumping to probabilistically adapt those solutions (Simon 2008, Ergezer *et al.* 2009). Therefore, in order to apply the concept of variable location introduced by Woldesenbet *et al.* (2009) to OBBO, some simplistic assumptions have to be made. To be more specific, the dynamic variable relocation step has to be adjusted to cater for two different kinds of offspring generations in the OBBO, i.e.,

- the migration step involves more than two parents, and
- the opposite jumping step involves only one parent.

The calculations for evolutionary progresses in the cost functional, defined as (6.2) and (6.5), have to reformulated in for each of the above two cases. Moreover, in the case of opposite jumping step, the evolutionary progress of the decision variables, defined as (6.1) and (6.4), have to be modified as well.

In the case of migration step, the $parent_1$ is the probabilistically selected solution for the immigration, while the $parent_2$ corresponds to a set of probabilistically selected characteristic variables belonging to more than one solutions selected as emigrating islands. It means that the values of $f(parent_2)$ and $\overline{\Delta f}(parent_2)$ depend upon the cost functional calculated for each of the individual

Collection @ jeju

solutions selected as emigrants. For simplistic reasons, this step is implemented by taking the average of the cost functional of all the donors, respectively, i.e.

$$f(parent_2) = \frac{\sum_{i=1}^{N_{em}} f(parent_i)}{N_{em}}, \text{ and} \tag{6.13}$$

$$\overline{\Delta f}(parent_2) = \frac{\sum_{i=1}^{N_{em}} \overline{\Delta f}(parent_i)}{N_{em}} \tag{6.14}$$

where N_{em} is the number of individuals participating in the emigration process for a particular immigrating individual solution. Since each of decision variable, in the case of migration, is evolved separately involving two parents at a time, their evolutionary progress, given in (6.1) and (6.4), does not need to be modified.

In the case of opposite jumping, the evolutionary progress in the decision space and the fitness values is modified as follows

$$\Delta x_c(child) = x_c(opposite) - x_c(child) \tag{6.15}$$

$$\Delta f(child) = f(opposite) - f(child) \tag{6.16}$$

$$\overline{\Delta x_c}(child) = \frac{\Delta x_c(child) + w.nGen.\overline{\Delta x_c}(opposite)}{w.nGen + 1} \tag{6.17}$$

$$\overline{\Delta f}(child) = \frac{\Delta f(child) + w.nGen.\overline{\Delta f}(opposite)}{w.nGen + 1} \tag{6.18}$$

6.2 Dynamic OBBO algorithm

The key steps of the Dynamic OBBO algorithm for EIT boundary estimation with variable relocation are as follows

1) Initialize the BBO parameters i.e., S_{max}, **E**, **I** and etc. The SIVs are mapped to the Fourier coefficients $\gamma_k \in \Re^{2MN_\theta}$, while the EIT cost functional $\Phi(\gamma_k)$ is chosen as the HSI.
2) Initialize a set of N_P potential solutions (habitats) for the problem. Also, compute the cost $\Phi(\gamma_k)$ for each of the habitat in the initial population set.
3) Repeat the following until the end of criteria is met
   While in steady state:

Collection @ jeju

a. Compute the immigration rate λ and emigration rate μ for each candidate solution.
b. Probabilistically perform immigration and emigration to modify non-elite habitats.
c. Calculate mean evolutionary progresses $\overline{\Delta X}$ in the decision space and $\overline{\Delta f}$ as in the fitness values of the newly created solutions.
d. Perform mutation based upon the mutation probability.
e. Calculate the cost $\Phi(\gamma_k)$ of each new solution.
f. Generate a quasi-reflected opposition population and calculate the cost $\Phi(\gamma_k)$ of each opposite solution.
g. Calculate mean evolutionary progresses $\overline{\Delta X}$ in the decision space and $\overline{\Delta f}$ in the fitness values of the quasi-reflected opposition solutions.
h. Compare the BBO generated solutions with their quasi-reflected solutions and retain the N_P most feasible solutions for the next generation. Keep the elite habitats in the new population by replacing the least feasible solutions.

While in the transient state:

a. Calculate the average sensitivity $\overline{s_c^x}$ of the decision variables to the change in the objective space
b. Calculate the relocation radius Δr_c for each individual solution.
c. Relocate the individual solutions using Δr_c a number of times.
d. Calculate the cost $\Phi(\gamma_k)$ for each of the relocated individual in the new environment.
e. Generate a set of new solutions.
f. Select the best N_P solutions to be used as OBBO initial population for the new dynamic environment.

Note that the steps 'e' and 'f' in the transient state provide an additional measure to add fresh blood to the OBBO population. This step is aimed at establishing a hybrid dynamic evolutionary approach which is based upon the self-adaptation as well as new population generation in case of a change in the environment. Such an approach is expected to perform better than a raw variable

Collection @ jeju

relocation approach in which case all the individuals may be relocated potentially leading to a population of infeasible solutions, if the relocation step goes wrong. Note that this step is in contrast to the original scheme by Woldesenbet *et al*. (2009) for this kind of situation, which retained the least-cost individual from an OBBO-generated solution and its relocated solution. The currently proposed measure is specifically suitable for the case in which the sensitivity $\overline{s_c^x}$ of the decision variables to the change in the objective space is very low.

Collection @ jeju

7. Dynamic OBBO applied to dynamic heart boundary estimation using EIT

The fourth chapter focused on the estimation of organ boundaries inside the human chest while assuming that a full frame of independent EIT measurements can be obtained while the boundaries remain stationary. This assumption may hold true for the case of lung boundaries if the subject is told to hold breathe while the current is injected to the electrodes attached to the chest boundary and voltages across the electrodes are measured. However, this assumption may not be accurate in the case of heart boundary estimation since the heart of a living human being cannot be stopped. When the full target inside an object moves before the full frame of independent measurements is available, the EIT imaging problem transforms into a dynamic image reconstruction problem. In order to solve such a problem, a dynamic optimization algorithm is needed. This chapter presents a study of dynamic OBBO applied to dynamic heart boundary estimation using EIT.

7.1 Results and discussions

7.1.1 Numerical results

This section presents a detailed analysis of the dynamic OBBO-based EIT boundary estimation scheme using numerical simulations. In order to carry out the numerical simulations, a scenario depicting a full heart cycle, i.e., a heart contraction followed by an expansion, has been chosen. The boundaries of the lungs are fixed, depicting the situation in which a patient holds his/her breathe so that we concentrate on the dynamic estimation of the size and the location of the heart. The number of Fourier coefficients to represent the organ boundaries, both for the forward and the inverse problems, as well as the conductivity of the organs is the same as given in the last section. The size and the shape of the simulated chest phantom is also the same as considered before. However, the number of elements in the region where heart is likely to be found is increased. This change has been done in order to accommodate

Collection @ jeju

different shapes and sizes of the heart. The simulation scenario considers a total of nine iterations, five for the heart expansion and four for the contraction, respectively.

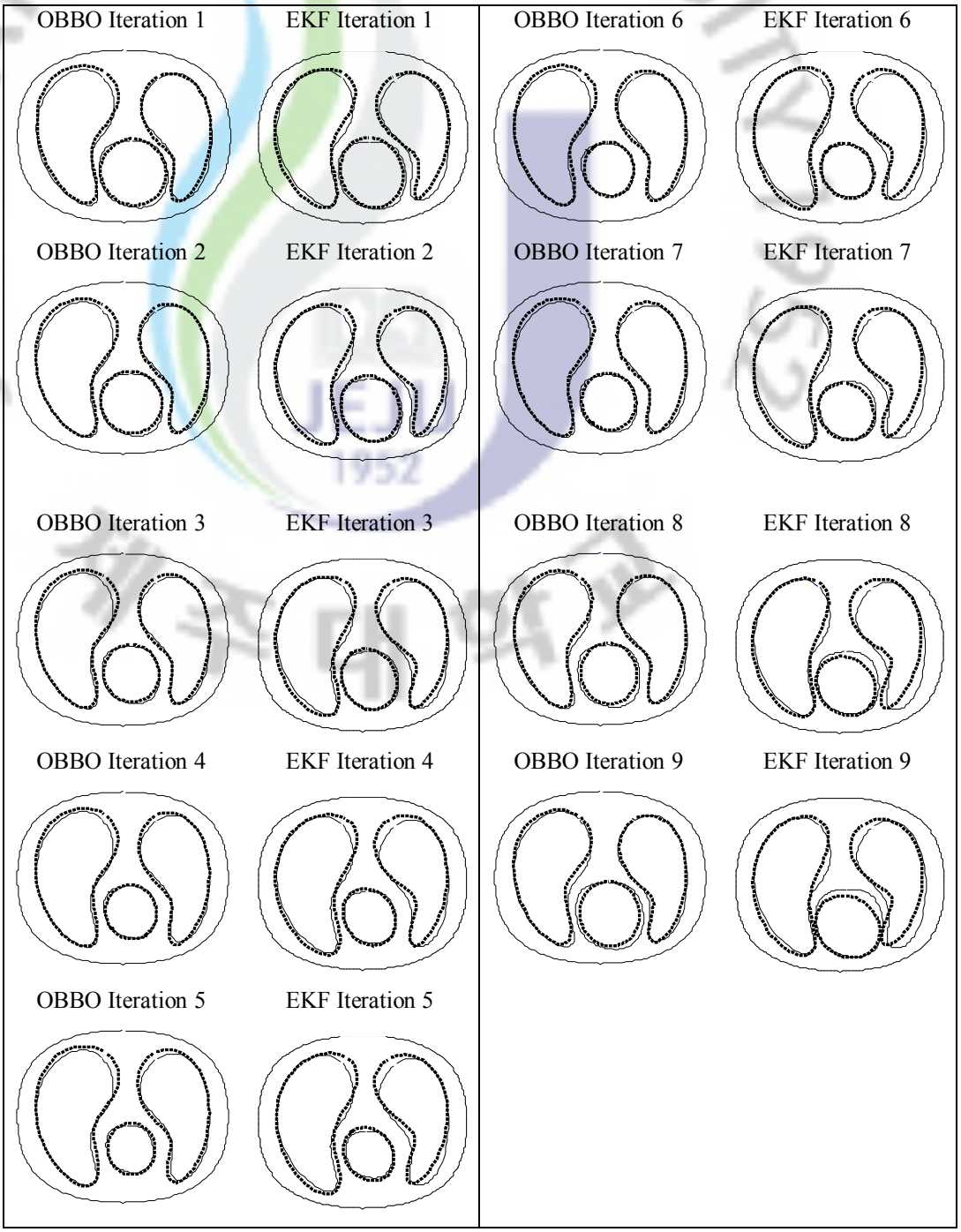

Figure 7.1. Result with 1% measurement noise. Estimated organ boundaries in a simulated human chest cross section using dynamic OBBO and EKF. The solid line is used to draw the true organ boundaries while the broken line is used to show the (mean) estimated boundaries, estimated at each iteration, using dynamic OBBO (left) and EKF (right).

Collection @ jeju

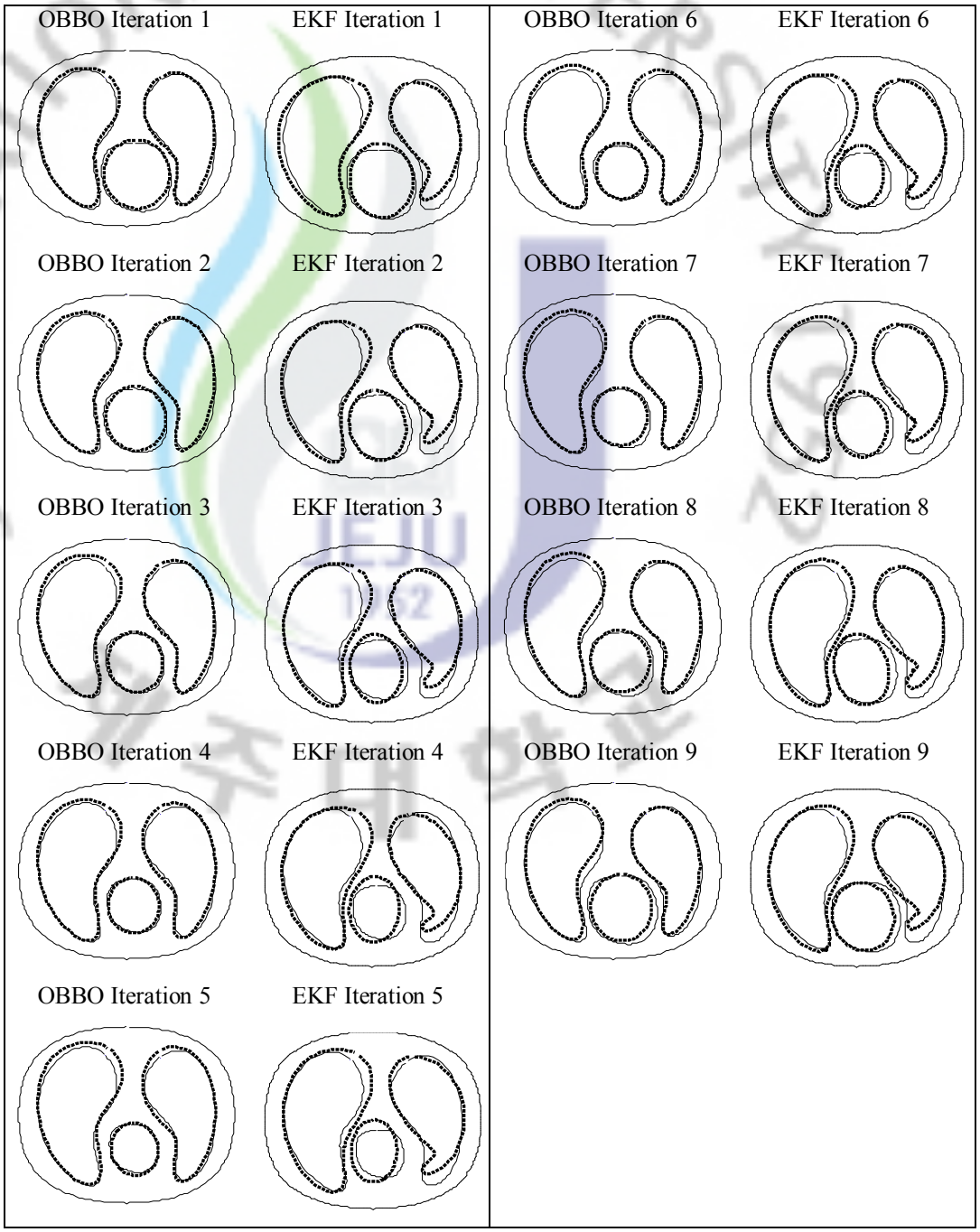

Figure 7.2. Result with 2% measurement noise. Estimated organ boundaries in a simulated human chest cross section using dynamic OBBO and EKF. The solid line is used to draw the true organ boundaries while the broken line is used to show the (mean) estimated boundaries, estimated at each iteration, using dynamic OBBO (left) and EKF (right).

The mesh used to solve the forward problem consists of 4580 triangular elements with 2419 nodes. The mesh used for the inverse problem is composed of 3994 triangular elements with 2126 nodes. Once again, the trigonometric current injection protocol has been used for the simulated dynamic heart boundary estimation. With

Collection @ jeju

32 electrodes, sixteen cosine and fifteen sine current patterns are possible. However, in order to simulate a dynamic environment, out of all the possible trigonometric current patterns, only the first two modes of cosine and sine current patterns were used at each iteration considering that they are more sensitive compared to the other modes (Kim *et al*. 2007). Furthermore, to simulate the noisy EIT measurements, zero-mean Gaussian noise with 1% and 2% standard deviations, respectively, relative to the corresponding measured voltage has been added to the simulated voltage data.

In order to compare the performance of the dynamic scenario, the organ boundaries have also been reconstructed using the extended Kalman filter (EKF) which is one of the most popular dynamic estimation algorithms. The EKF has also been repeated for η = 20 runs and the same statistical parameters, as for OBBO, have been gathered. Similar to mNR, and in contrast to OBBO, EKF also requires a single initial guess for each run. Thus, for EKF a different initial guess is chosen for each subsequent run, by randomly choosing a value for the Fourier coefficients representing the radii and the locations (x- and y-coordinates) of the organs from a uniform distribution which is similar to that of the initial population chosen for the dynamic OBBO. A uniformly-distributed initial population comprising of 30 habitats has been chosen for this study. The uniform distribution has been generated such that the Fourier coefficients representing the radii and the locations (x- and y-coordinates) of the organs are distributed with a maximum deviation of 1.75 cm from their respective mean values. The mean values, as in the case of the lungs, are at an absolute distance of 0.25 cm from their respective best true values. In the case of the heart, the mean of the uniformly-distributed initial population (for location and size parameters) is chosen as an average of the respective Fourier coefficients for the two extreme cases, i.e., when the heart size is full and when it is of the smallest size. The rest of the Fourier coefficients, which express the shape and orientation of the organ boundaries, have a maximum deviation of 0.5 cm from the respective mean values. The initial population for the dynamic case has been selected based upon the same assumption as that of the static case, i.e., a good prior knowledge of the general shape of the organs is available, with a relatively poor knowledge of their size and the location. The number of generations for the first iteration is five while three OBBO generations are used for the rest of the iterations. A higher number of generation

Collection @ jeju

count is used for the first iteration in order to get a better solution since the initial population for this iteration step is randomly generated, given the fact that the variable relocation step is not available at this time due to the absence of any evolutionary data so far. The variable relocation step introduces a better adapted and closely located population for the later iterations, thus requiring relatively lesser number of iterations to reach to the optimal solution. It should, however, be remembered that a larger population with a higher number of generation steps, in general, improves the performance of evolutionary algorithms, though at additional computational cost. The value of the OBBO jumping probability J_r has been set to 1.0 for the first two generations, while $J_r = 0$ after the second generation within each iteration. The idea is to adjust the jumping step according to the situation, i.e., jumping should be done more frequently during the early stages of evolution, when most of the individual solutions in the population are less optimal, and jump less frequently after the population starts to converge. Finally, an elitism count of two has been used again. In order to verify the robustness of the proposed algorithm Monte Carlo type simulations of η = 20 runs (each run with a different noise seed, and a different set of initial population) has been performed. A quantitative analysis of the algorithm has been carried by plotting the mean $\bar{\gamma}_i = \frac{1}{\eta}\sum_{i=1}^{\eta}\gamma_i$ and standard deviation $s_\gamma = \sqrt{\frac{1}{\eta-1}\sum_{i=1}^{\eta}(\gamma_i - \bar{\gamma})^2}$ of the estimated parameters in the graphical format. The mean is plotted with a broken line whereas the standard deviation is plotted using the error bars. In addition, the $RMSE_\gamma$ values (i.e., the *RMSE* of the Fourier coefficients, aggregated for each of the organs individually) have been calculated for each of the 20 runs of the algorithm. The mean *RMSE* of the aggregated coefficients, i.e., $\overline{RMSE}_\gamma$ values are then shown in a graphical format, by calculating and plotting the average for each iteration step individually.

The mean reconstructed boundaries, using dynamic OBBO (left side) as well as EKF (right side), for the 1% measurement noise are plotted in figure 7.1, while the figure 7.2 shows the reconstructed results for the 2% noise case. Figure 7.3 plots the mean and standard deviation of the estimated Fourier coefficients $\gamma_2^{x_3}$ and

Collection @ jeju

$\gamma_3^{y_3}$ corresponding to the heart radii in the *x*- and *y*- directions, respectively, for each iteration. Figure 7.4 plots the evolution of the mean and standard deviation of the estimated area of the heart, and figure 7.5 iteratively plots the mean and standard deviation of Fourier coefficients $\gamma_1^{x_3}$ and $\gamma_1^{y_3}$ corresponding to the *x*- and *y*- locations, respectively, of the heart estimated with 1 % measurement noise. The aggregated $\overline{RMSE}_\gamma$ values for the three individual organs as well the total aggregate of all the organs are plotted for each iteration in figure 7.6. Next, the figures 7.7 to 7.9 iteratively plot the mean and standard deviation of the radii, area and location of the heart, respectively, calculated for the 2% measurement noise case. The aggregated $\overline{RMSE}_\gamma$ values for the 2% noise case are then plotted in figure 7.10.

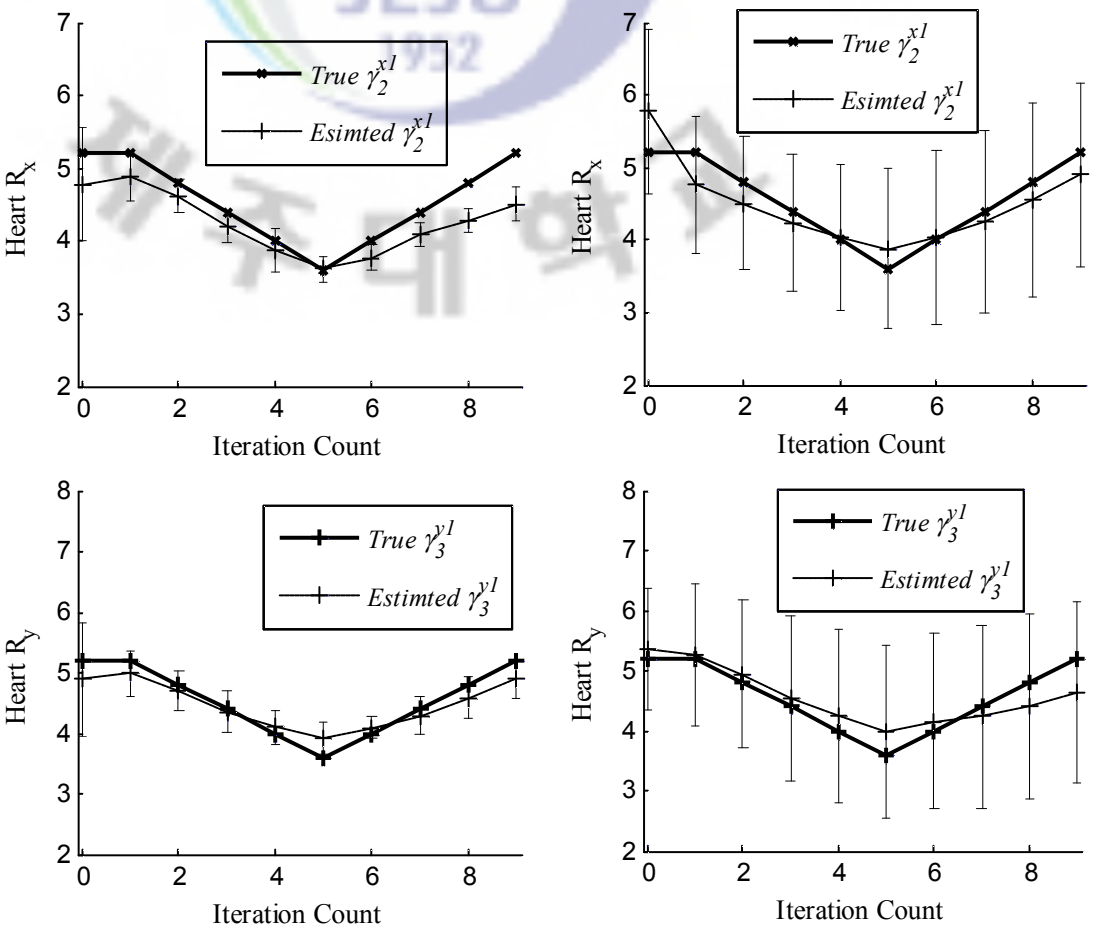

Figure 7.3. Dynamic heart estimation results with 1% measurement noise. The Fourier coefficients $\gamma_2^{x_3}$ and $\gamma_3^{y_3}$ corresponding to the radii in the *x*- and *y*- directions, respectively, of the heart plotted iteratively. The solid lines show the true evolution of these parameter while the broken lines are used to plot the mean estimates using dynamic OBBO (left) and EKF(right) respectively. The error bars show the standard deviation *s* of the estimated parameters at each measurement instance.

Collection @ jeju

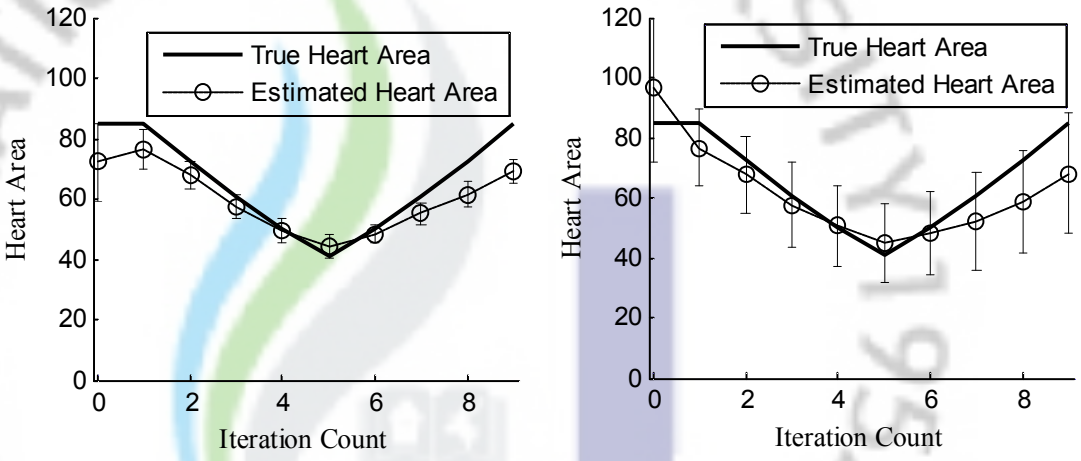

Figure 7.4. Heart area estimation results with 1% measurement noise. The solid line shows the true evolution of area of the heart while the broken line is used to plot the mean estimated area using dynamic OBBO (left) and EKF(right) respectively. The error bars show the standard deviation *s* of the estimated parameters at each measurement instance.

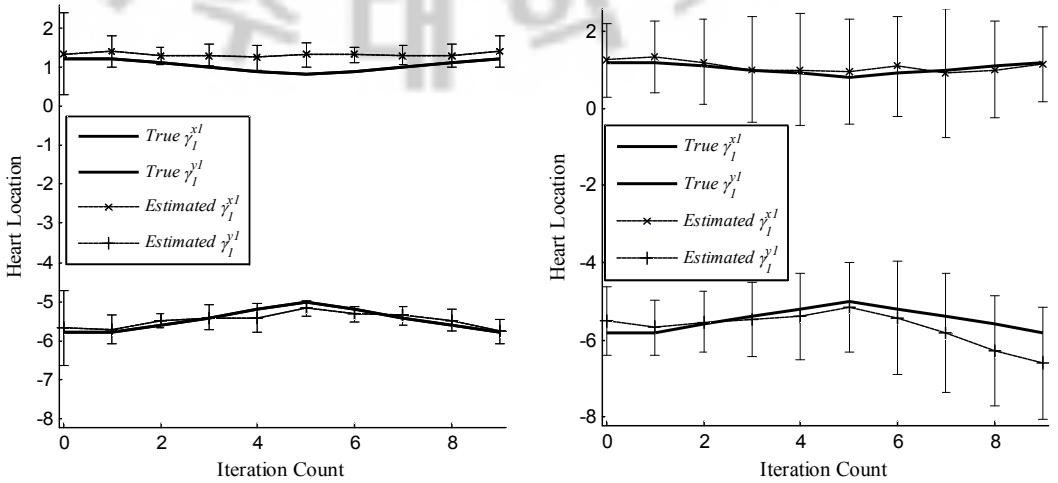

Figure 7.5. Dynamic heart estimation results with 1% measurement noise. The Fourier coefficients $\gamma_1^{x_3}$ and $\gamma_1^{y_3}$ corresponding to the *x*- and *y*- locations, respectively, of the heart plotted iteratively. The solid lines show the true evolution of these parameter while the broken lines are used to plot the mean estimates using dynamic OBBO (left) and EKF(right) respectively. The error bars show the standard deviation *s* of the estimated parameters at each measurement instance.

Collection @ jeju

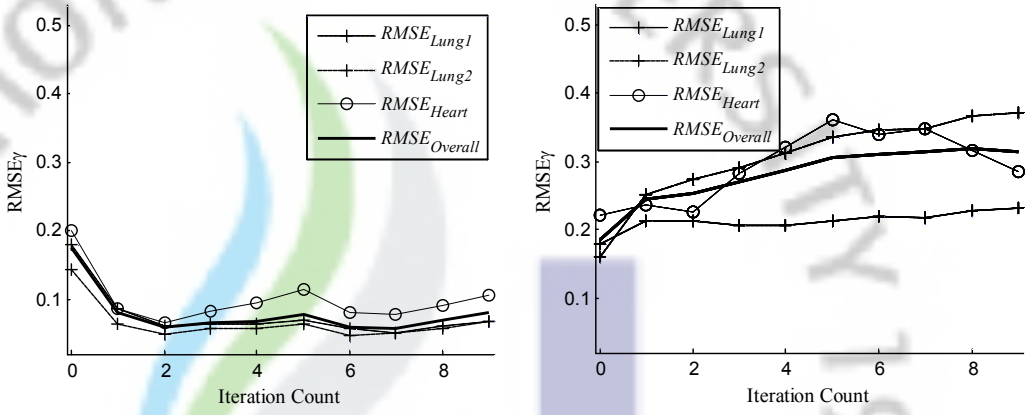

Figure 7.6. Error analysis with 1% measurement noise. $\overline{RMSE}_{\gamma}$ values calculated for all three organs, plotted iteratively for OBBO (left) and EKF (right) respectively.

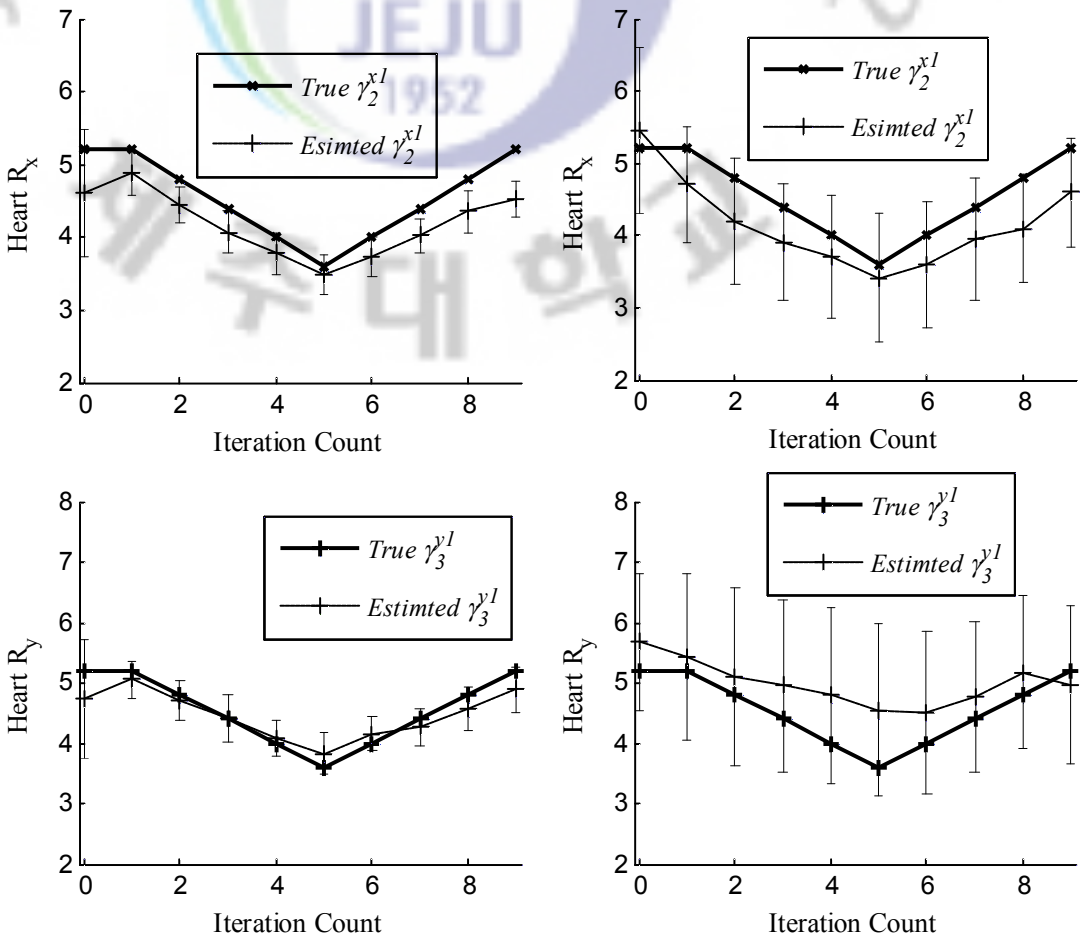

Figure 7.7. Dynamic heart estimation results with 2% measurement noise. The Fourier coefficients $\gamma_2^{x_3}$ and $\gamma_3^{y_3}$ corresponding to the radii in the *x*- and *y*- directions, respectively, of the heart plotted iteratively. The solid lines show the true evolution of these parameter while the broken lines are used to plot the mean estimates using dynamic OBBO (left) and EKF(right) respectively. The error bars show the standard deviation *s* of the estimated parameters at each measurement instance.

Collection @ jeju

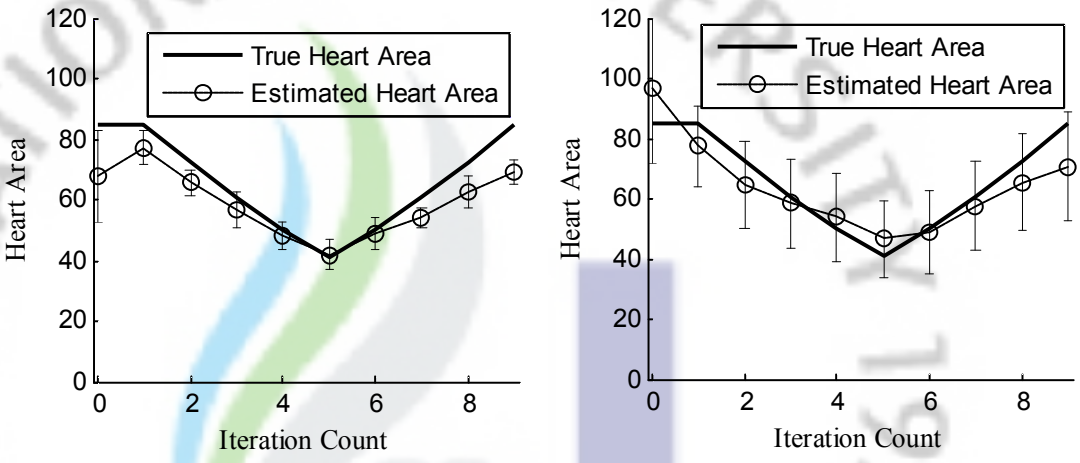

Figure 7.8. Heart area estimation results with 2% measurement noise. The solid line shows the true evolution of area of the heart while the broken lines is used to plot the mean estimated area using dynamic OBBO (left) and EKF(right) respectively. The error bars show the standard deviation *s* of the estimated parameters at each measurement instance.

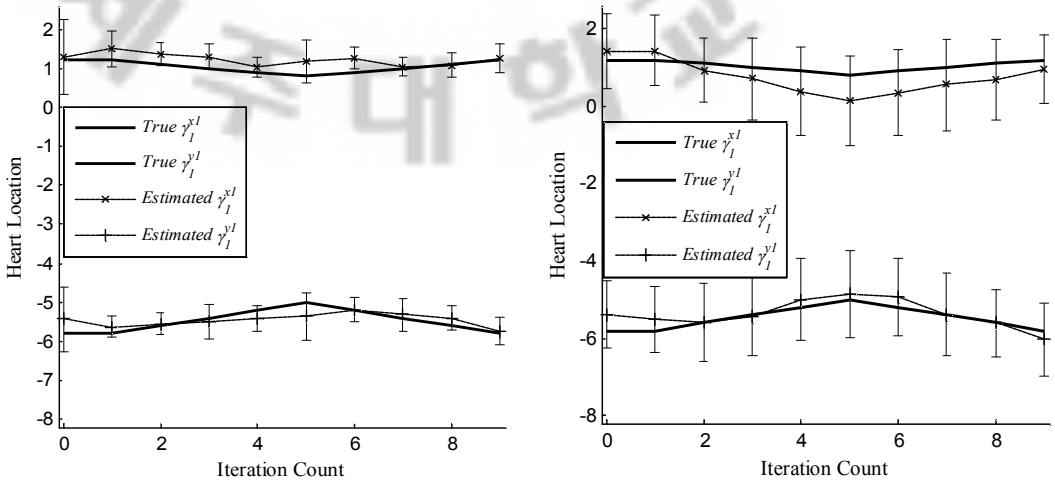

Figure 7.9. Dynamic heart estimation results with 2% measurement noise. The Fourier coefficients $\gamma_1^{x_3}$ and $\gamma_1^{y_3}$ corresponding to the *x*- and *y*- locations, respectively, of the heart plotted iteratively. The solid lines show the true evolution of these parameter while the broken lines are used to plot the mean estimates using dynamic OBBO (left) and EKF(right) respectively. The error bars show the standard deviation *s* of the estimated parameters at each measurement instance.

Collection @ jeju

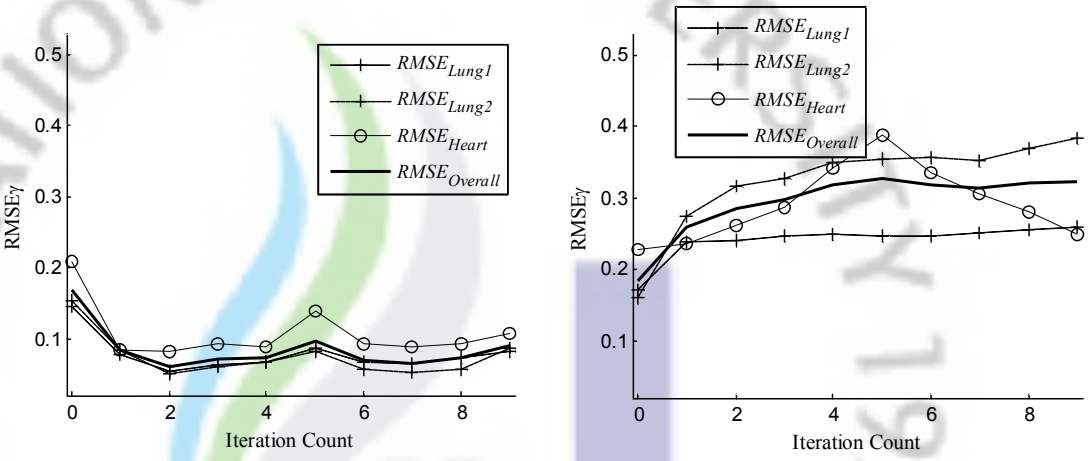

Figure 7.10. Error analysis with 2% measurement noise. $\overline{RMSE}_\gamma$ values calculated for all three organs, plotted iteratively for OBBO (left) and EKF (right) respectively.

It can be very easily noticed from the simulation results that the dynamic OBBO has been able to reconstruct the organ boundaries with far superior accuracy as compared to that of EKF. The mean estimates of EKF are comparable to those of the dynamic OBBO; however, the standard deviations in the case of EKF are very high. The reason for this is that EKF is extremely sensitive to initial guess. As mentioned before, a different initial guess has been chosen for each of the 20 EKF runs. If the initial guess is incidentally chosen close to the true boundaries, the EKF performance is quite reasonable; however, if the initial is not so close, the estimation performance of EKF is significantly affected, thus resulting in a higher standard deviation. It can thus be concluded that EKF is not a reliable algorithm to estimate the organ boundaries unless and until a very close initial guess at the start of simulation scenario is available. Dynamic OBBO, on the other hand, has been found robust enough to estimate almost all the heart parameters considered for the simulation. The $\overline{RMSE}_\gamma$ comparisons for the two algorithms reaffirm the aforementioned conclusion. Although the performance of dynamic OBBO is relatively poorer in the case of 2% measurement noise resulting in higher standard deviations of estimated parameters, the results are still reasonable and far superior to those of EKF. The deteriorated performance of the chosen DEA in the case of 2% noise is not unexpected at all, due to the extreme sensitivity of the EIT measurements to the presence of noise. It should also be noted that the standard deviation of the heart area estimates is quite low compared to the heart radii. It means than an

Collection @ jeju

overestimate in the radius of the heart in the *x*-direction is compensated by an underestimate in the y-direction, thus keeping the estimated area close to the true one. This is good news in the sense that the area of the heart, which in turn can be used to estimate to total size of the heart, has a greater physiological significance as compared to individual radii. (Ziegler *et al*., 1962, Cotes *et al*., 1980, Hoffman and Ritman, 1987, Carlsson *et al*., 2004, Carlsson *et al*. 2005, Steding *et al*., 2007). Another thing which may be noticed here is the evolution of the mean estimated heart location parameters, which show relatively weak reconstruction performance. This is not unexpected as well, due to a very low sensitivity of EIT voltage measurements to heart dislocations, explained in a previous chapter.

7.1.2 Experimental results

This section analyses the performance of the dynamic OBBO-EIT boundary estimation scheme using 2D EIT measurement data obtained from a chest-type experimental setup with two lungs and a heart. The experiments for the dynamic scenario have been performed in the EIT lab at Jeju National University. The radius of the chest phantom is 14 cm with 32 electrodes, each of 1 cm width, attached around the surface of the phantom. The saline level in the phantom is about 2 cm and the amplitude of the injected current is 0.5 mA. The EIT measurement setup is shown in figure 7.11.

For the experimental scenario, opposite current patterns has been used. The conventional opposite current injection system for a 32-elctrode EIT system is composed of 16 opposite current patterns. However, since the objective of this specific study is the dynamic heart estimation, it is assumed that a full set of independent measurements cannot be measured before the boundary of the heart is changed. The current study, therefore, only considers four opposite current patterns for each iteration. Similar to the numerical scenario, a full heart cycle with a total of nine iterations is considered to create the experimental scenario. The biggest heart is 10.4 cm wide and 10 cm long, while the smallest heart has a width of 6.2 cm and a length of 6 cm (see figure 7.12). The background in chest phantom is composed of saline solution with a conductivity of 0.19 S/m while the lungs and the heart are constructed using a mixture of agar and saline with a conductivity of 0.14 S/m and

Collection @ jeju

0.55 S/m respectively. The organ-like structures had been prepared by mixing appropriate proportions of agar and potassium chloride (NaCl) salt in hot water and then letting it cool down and solidify at room temperature. The conductivity, however, was measured using the conductivity meter when the organs were in the liquid form. The exact values of the conductivity of organs in the solid form cannot be measured using the conductivity meter and thus are not known accurately. That is why only approximate values are considered which inevitably leads to estimation errors.

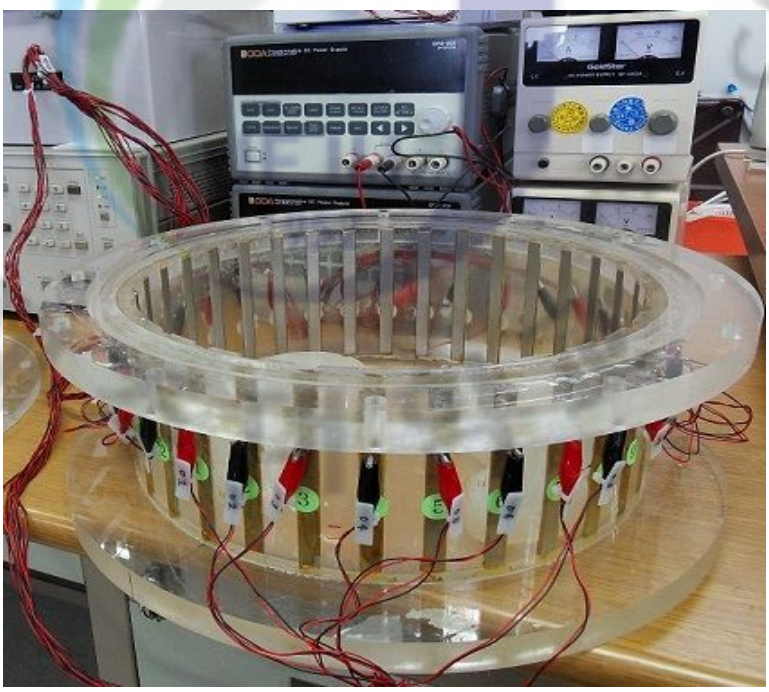

Figure 7.11. EIT experimental setup for dynamic heart estimation.

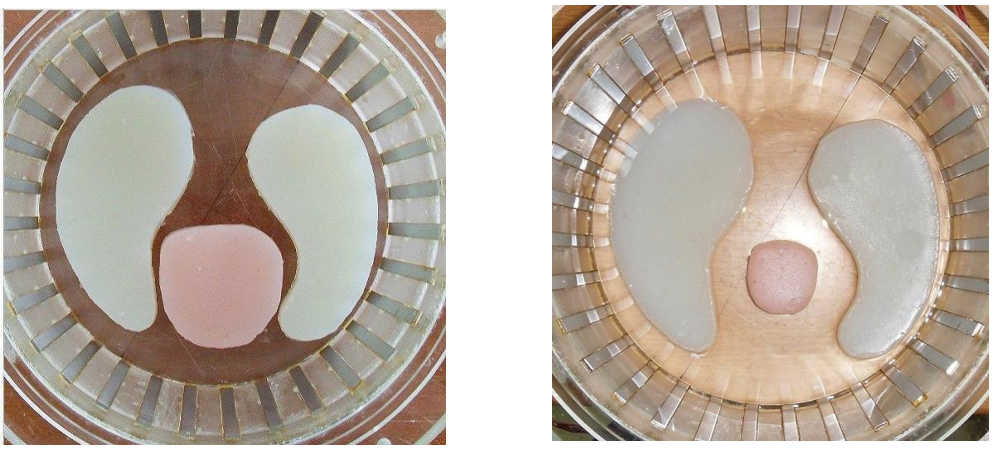

a b

Figure 7.12. (a) Two lungs with the biggest heart. (b) Two lungs with the smallest heart.

Collection @ jeju

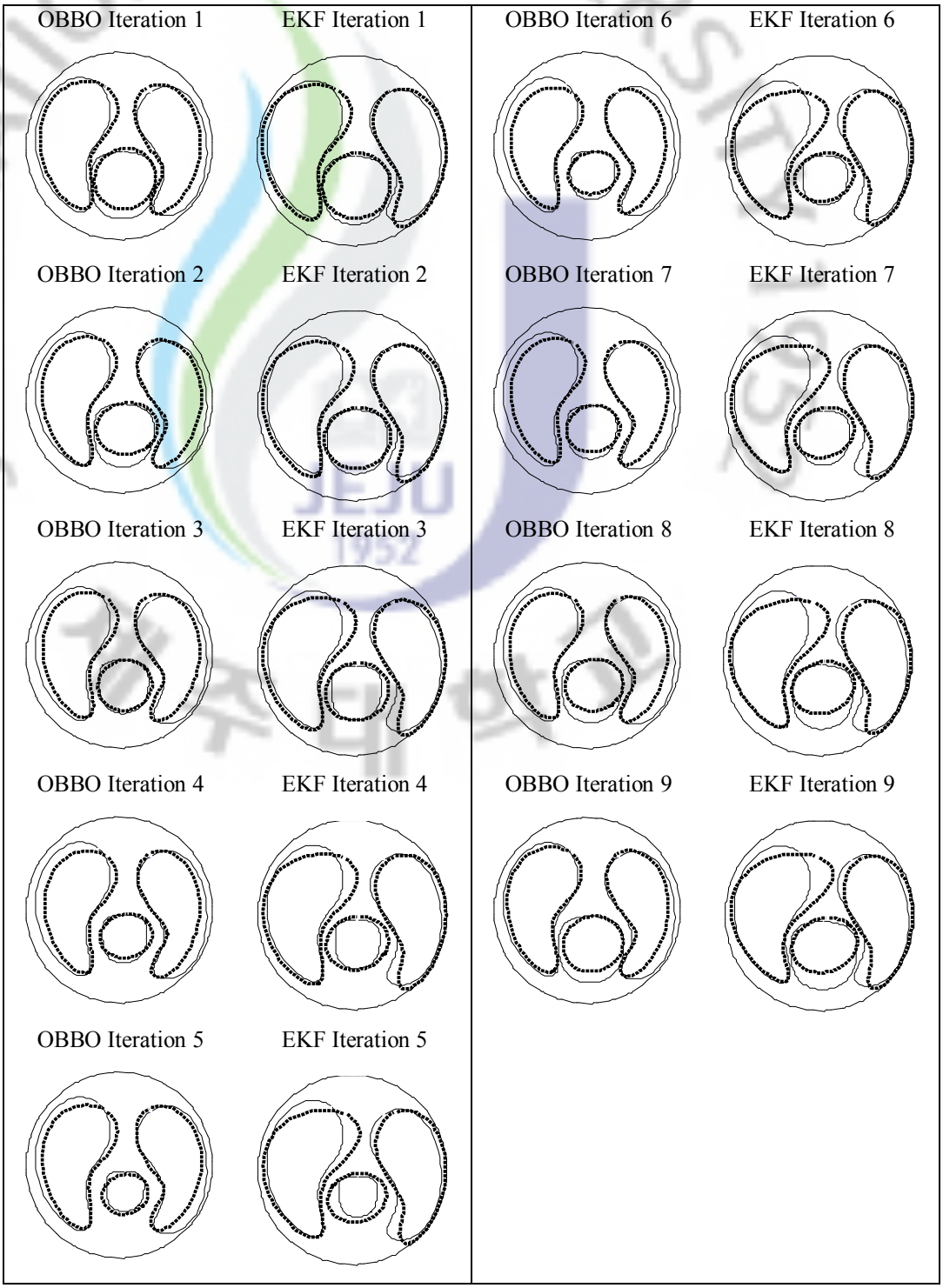

Figure 7.13. Experimental Results. Estimated organ boundaries in a simulated human chest cross section using dynamic OBBO and EKF. The solid line is used to draw the true organ boundaries while the broken line is used to show the (mean) estimated boundaries, estimated at each iteration, using dynamic OBBO (left) and EKF (right).

Collection @ jeju

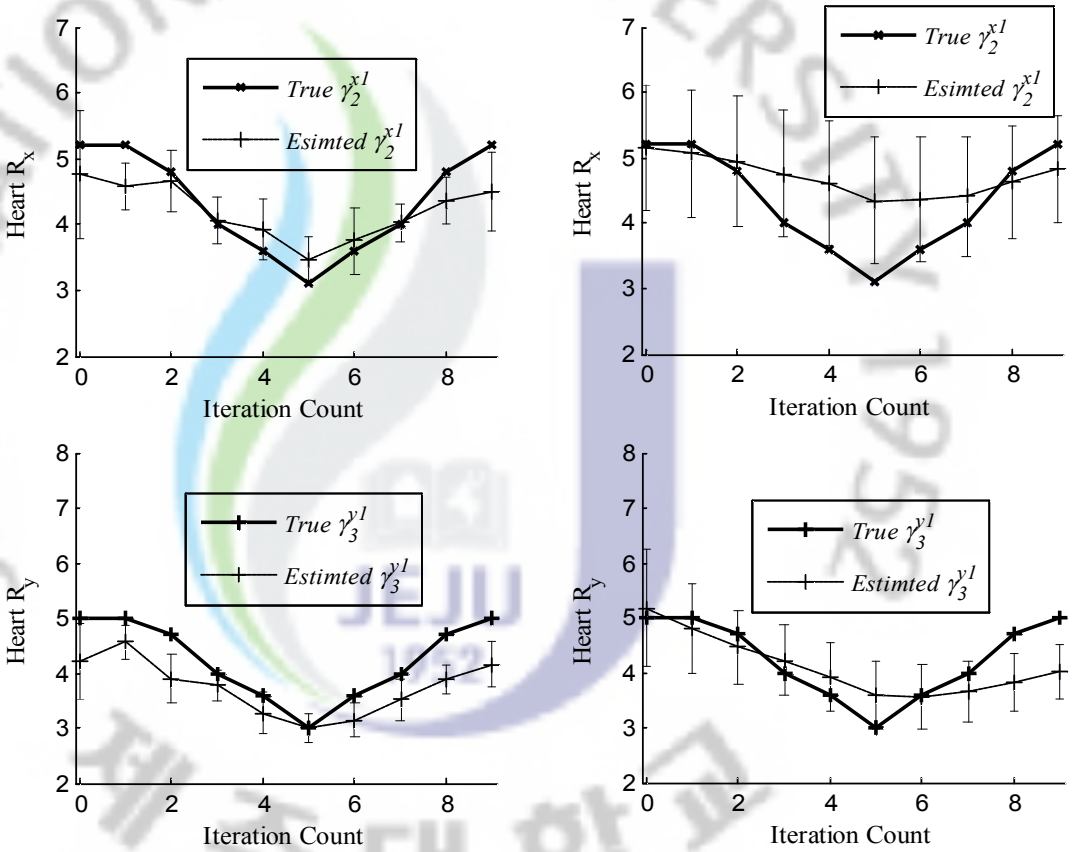

Figure 7.14. Dynamic heart estimation results for the experimental scenario. The Fourier coefficients $\gamma_2^{x_3}$ and $\gamma_3^{y_3}$ corresponding to the radii in the *x*- and *y*- directions, respectively, of the heart plotted iteratively. The solid lines show the true evolution of these parameter while the broken lines are used to plot the mean estimates using dynamic OBBO (left) and EKF(right) respectively. The error bars show the standard deviation *s* of the estimated parameters at each measurement instance.

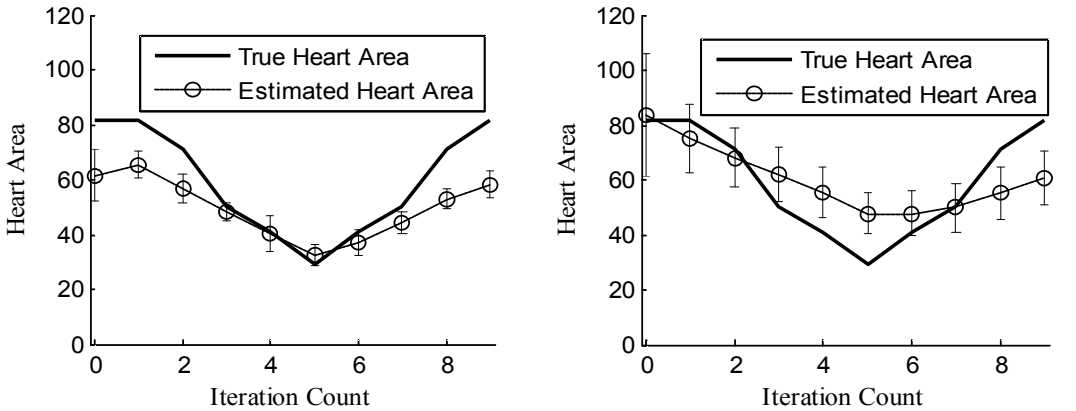

Figure 7.15. Heart area estimated for the experimental scenario. The solid line shows the true evolution of area of the heart while the broken lines is used to plot the mean estimated area using dynamic OBBO (left) and EKF(right) respectively. The error bars show the standard deviation *s* of the estimated parameters at each measurement instance.

dCollection @ jeju

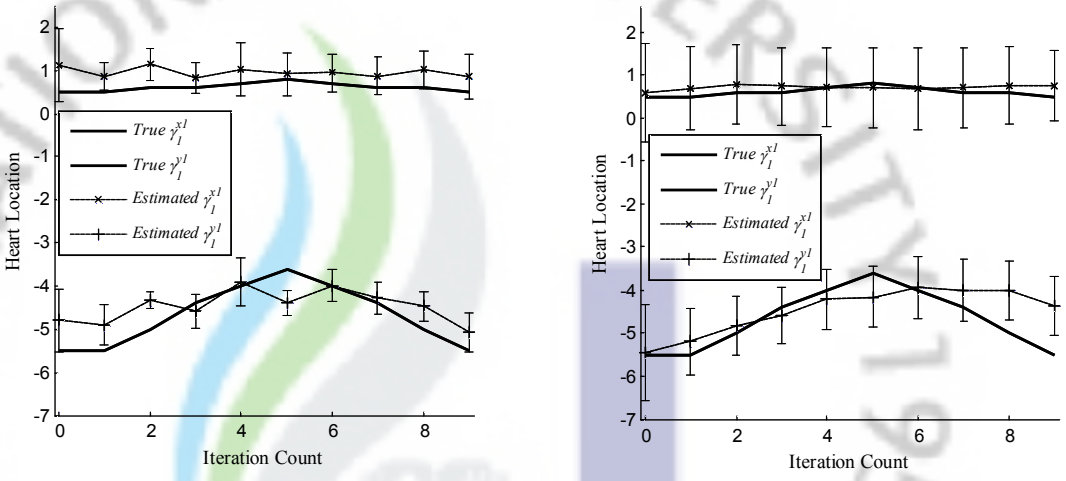

Figure 7.16. Dynamic heart estimation results for the experimental scenario. The Fourier coefficients $\gamma_1^{x_3}$ and $\gamma_1^{y_3}$ corresponding to the *x*- and *y*- locations, respectively, of the heart plotted iteratively. The solid lines show the true evolution of these parameter while the broken lines are used to plot the mean estimates using dynamic OBBO (left) and EKF(right) respectively. The error bars show the standard deviation *s* of the estimated parameters at each measurement instance.

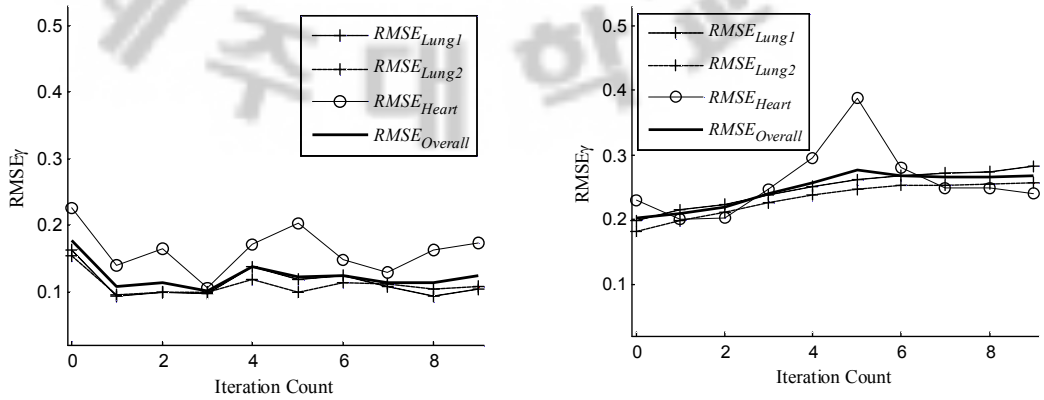

Figure 7.17. Error analysis for the experimental scenario. $\overline{RMSE}_\gamma$ values calculated for all three organs, plotted iteratively for OBBO (left) and EKF (right) respectively.

Similar to the simulations and experiments presented in previous sections, this experimental scenario has also been repeated for 20 times and the aforementioned statistical parameters have been gathered and plotted. The reconstructed boundaries using dynamic OBBO and EKF for the experimental case have been shown in figure 7.13. Figure 7.14 iteratively plots the mean and standard deviation of the heart radii in the *x*- and *y*- directions, respectively, while figure 7.15 plots the evolution of these statistical parameters for the area of the heart, estimated for the experimental scenario. Figure 7.16 plots, for each iteration, the mean and the standard deviation of

dCollection @ jeju

the heart location parameters. Finally, figure 7.17 plots the iterative evolution of the aggregated $\overline{RMSE}_\gamma$ values, calculated for all the three organs in the experimental scenario. These results demonstrate that dynamic OBBO is a robust algorithm in experimental conditions. Although the performance of OBBO is weaker for the experimental case, it is still significantly better than that of EKF. The relatively weak performance of OBBO in the experimental conditions can be attributed to several factors such as noise measurements, inaccurate knowledge of the conductivity values, using a 2D EIT measurement setup for an intrinsically 3D problem and etc.

Collection @ jeju

Conclusions

This paper presents a biogeography-based optimization technique to reconstruct the region boundaries inside an object, expressed as truncated Fourier series coefficients, using 2D EIT. The characteristic feature of this algorithm is its strong ability to exhaust the solution space, converging to the desired solution with reasonable accuracy. The stability and accuracy of the algorithm has been analyzed with the help of several statistical parameters gathered through repetitive execution of the algorithm using a realistic chest-shaped mesh structure, each time generating a different set of initial population and adding a zero-mean Gaussian-distributed measurement noise with a different seed. The accuracy of the algorithm has also been verified using chest-shape experimental setups. First of all, a static scenario has been considered such that all the organ boundaries are assumed be constant while a full frame of independent measurements is obtained. In the second situation, the boundaries of the lungs are fixed while a heart expansion/contraction cycle is considered, depicting the scenario in which a patient is told to hold his/her breathe while EIT measurements are taken. In this case, a partial subset of the full measurement frame is assumed to be available at each instance. A dynamic version of the OBBO is used to reconstruct the non-stationary organ boundaries in this case. An extensive statistical analysis of the estimated parameters using OBBO and its comparison with the traditional mNR and EKF algorithms is presented. The results demonstrate that OBBO has significantly better estimation performance as compared to the traditional algorithms, in the case of non-elliptic multiple boundaries located near to each other. The robustness of the algorithm has also been verified for several different types of initial population distributions, depicting the scenario when the prior knowledge of the size, location and shape is not so correct. Additionally, the accuracy of estimation has been tested for different conductivity errors, i.e., when the *a priori* knowledge of the conductivity of the organs is assumed to be inaccurate. The proposed algorithm has shown reasonable performance in situations when the *a priori* information is relatively poor.

One of the major challenges posed by the proposed technique is its high computational complexity due to the iterative nature of the underlying algorithm.

Collection @ jeju

However, the advent of high performance computing machines offering parallelism, both at the hardware and the software levels, has opened up the possibility of online deployment of evolutionary algorithms which at the moment has been prescribed for an offline use only. Currently, the conductivity values of regions are assumed to be known constants. Future work includes the simultaneous reconstruction of region boundaries and their conductivities, the extension of the method to 3D EIT for real time measurement, and the study and comparison of the best suitable population distribution and dynamic evolution schemes.

Collection @ jeju

Summary

Electrical impedance tomography (EIT) is a non-invasive imaging modality which has been actively studied for its industrial as well as medical applications. However, the performance of the inverse algorithms to reconstruct the conductivity images using EIT is often sub-optimal. Several factors contribute to this poor performance which includes high sensitivity of EIT to the measurement noise, the rounding-off errors, the inherent ill-posed nature of the problem and the convergence to a local minimum instead of the global minimum. Moreover, the performance of many of these inverse algorithms heavily relies on the selection of initial guess as well as the accurate calculation of a gradient matrix. Considering these facts the need of an efficient optimization algorithm to reach the correct solution cannot be overstated. This thesis presents an oppositional biogeography-based optimization (OBBO) technique to estimate the shape, size and location of the region boundaries inside an object domain using 2D EIT. The region boundaries are expressed as coefficients of truncated Fourier series while the conductivities of the regions are assumed to be known *a priori*. OBBO is first applied to reconstruct the static organ boundaries inside a chest like structure, when a full set of independent measurements is available at the measurement instance. A dynamic version of OBBO is then applied to estimate the non-stationary heart boundaries, assuming that only a partial subset of EIT measurement frame is available at a particular instance. The robustness of the algorithm, for static as well as dynamic cases, has been verified - first through repetitive numerical simulations by adding randomly generated measurement noise to the simulated voltage data, and then with the help of experimental setups. An extensive statistical analysis of the estimated parameters using OBBO and its comparison with the traditional mNR and EKF algorithms is presented. OBBO has shown far superior performance as compared to the traditional algorithms. Furthermore, it has been found that OBBO is robust to measurement noise and the initial guess of the size and location of the boundaries as well as it offers reasonable solution when the *a priori* knowledge of the conductivity is not very accurate.

Collection @ jeju

References

Ali M M and Törn A 2004 Population set-based global optimization algorithms: some modifications and numerical studies *Comput. Oper. Res.* **31** 1703-1725.

Andersen H C 1991 An investigation into genetic algorithms, and the relationship between speciation and the tracking of optima in dynamic functions *Honors thesis* Queensland University of Technology, Brisbane, Australia.

Angeline P J 1997 Tracking extrema in dynamic environments *Int. Conf. Evol. Program., Indianapolis IN* 1213-1219.

Bäck T 1997 Self-adaptation. In Bäck T Fogel D B, and Michalewicz Z *Handbook of Evolutionary Computation, Bristol, New York: Institute of Physics* (Publishing and Oxford University Press) pp **C7**:1-15.

Bäck T and Schwefel H-P 1993a An overview of evolutionary algorithms for parameter optimization *Evolut. Comput.* **1** 1-23.

Bäck T. Rudolph G and Schwefel H -P 1993 Evolutionary programming and evolution strategies: Similarities and differences *2nd Annual Conf. Evol. Prog. San Diego, CA* 11-22

Banzhaf W, Nordin P, Keller R E and Francone F D 1998 *Genetic Programming: An Introduction: On the Automatic Evolution of Computer Programs and Its Applications* (Morgan Kaufmann).

Barricelli Nils Aall 1954 Esempi numerici di processi di evoluzione *Methodos* 45–68.

Barricelli N A 1957 Symbiogenetic evolution process realized by artificial methods *Methodos* 143-182.

Beyer H and Schwefel H 2002 *Natural Computing* (Kluwer Academic Publishers).

Collection @ jeju

Bendat J S and Piersol A G 1971 *Random Data: Analysis and Measurement Procedures* (Wiley Interscience, NY).

Bendtsen C N and Krink T 2002 Dynamic memory model for non-stationary optimization *2002 Cong. on Evol. Comput.* 145-150.

Beyer H and Schwefel H 2002 *Natural Computing* (Kluwer Academic Publishers).

Branke J 2001 Evolutionary optimization in dynamic Environments *Norwell, MA: Kluwer*.

Branke J. Kaubler T Schmidt C and Schmeck H 2000 A multi-population approach to dynamic optimization problems *in Proc. Adaptive Comput. Conf. Design Manuf., Berlin, Germany* 96-101.

Brest J, Zamuda A, Boskovic B, Maucec M S and Zumer V 2009 Dynamic optimization using self-adaptive differential evolution *IEEE Cong. on Evol. Comput. CEC09* 415–422

Brest J. Boškovic B, Greiner S, Žumer V and Sepesy M M 2007 Performance comparison of self-adaptive and adaptive differential evolution algorithms *Soft Comput.* **11** 617-629.

Brest J, Greiner S, Boškovic B, Mernik M and Žumer V 2006 Selfadapting control parameters in differential evolution: a comparative study on numerical benchmark problems *IEEE Trans Evol Comput.* **10** 646-657.

Brown B H, Barber D C, Morica A H and Leathard A D 1994 Cardiac and respiratory related electric impedance changes in the human thorax *IEEE Trans. Biomed. Eng.* **41** 729-723.

Collection @ jeju

Barber D C and Brown B H 1984 Applied potential tomography *J phys. E: Sci Instrum* 17 723-733.

Browne R F J, Geraldine O R and David M 2004 Extraction of the two-dimensional cardiothoracic ratio from digital PA chest radiographs: correlation with cardiac function and the traditional cardiothoracic ratio. *J. Digit. Imaging* **17** 120-123.

Bui L T, Branke J and Abbass H A 2005 Multiobjective optimization for dynamic environments *Proc. Congr. Evol. Comput., Edinburgh, U.K.* 2349-2356.

Carlsson M, Cain P, Holmqvist C, Stahlberg F, Lundback S and Arheden H 2004 Total heart volume variation throughout the cardiac cycle in humans *Am. J. Physiol. Heart Circ. Physiol.* **287** H243-H250.

Carlsson M, Rosengren A, Ugander M, Ekelund U, Cain P A and Arheden H 2005 Centre of volume and total heart volume variation in healthy subjects and patients before and after coronary bypass surgery *Clin. Physiol. Funct. Imaging* **25** 226-33.

Chateaux J and Nadi M 2000 Comparison of performances of electrical impedance tomography evaluated with 2D and 3D models *IEEE Transactions on Microwave Theory and Techniques* **48** 1874-78.

Cheney M and Isaacson D 1992 Distinguishability in impedance imaging *IEEE Trans. Biomed. Eng.* 39 852-860

Cheng K S, Isaacson D, Newell J C and Gisser D G 1989 Electrode models for electric current computed tomography *IEEE Trans. Biomed. Eng.* **36** 918-24.

Cobb H G and Grefenstette J J 1993 Genetic algorithms for tracking changing environments *Fifth Int. Conf. on Genetic Algorithms, San Mateo, CA* 523-530.

Collection @ jeju

Cohn J N, Johnson G R, Shabetai R, Loeb H, Tristani F, Rector T, Smith R and Fletcher R 1993 Ejection fraction, peak exercise oxygen consumption, cardiothoracic ratio, ventricular arrhythmias, and plasma norepinephrine as determinants of prognosis in heart failure *Circulation* **87** VI5-16.

Cotes J E, Evans D L, Johnson G R, Macintyre I M and Saunders M J 1980 Radiographic heart volume, stroke volume and exercise cardiac frequency: relationship to body composition and other factors in healthy adult males *Q. J. Exp. Physiol. Cogn. Med. Sci.* **65** 9-17.

Dasgupta D and McGregor D R 1992 Non-stationary function optimization using the structured genetic algorithm *Parallel Prob. Solv. From Nature, Brussels, Belgium* 145-154.

Deibele J M, Luepschen H and Leonhardt S 2008 Dynamic separation of pulmonary and cardiac changes in electrical impedance tomography *Physiol. Meas.* **29** S1-14.

Dempster A P, Laird N M, Rubin D B 1977 Maximum Likelihood from incomplete data via the EM algorithm *J. Royal Stat. Soc.* B **39** 1-38.

de Munck J C, Faes T J C, and Heethaar R M 2000 The boundary element method in the forward and inverse problem of electrical impedance tomography *IEEE Trans. On Biomed. Eng.* **47** 792 -800**.**

Du D, Simon D and Ergezer M 2009 Biogeography-based optimization combined with evolutionary strategy and immigration refusal *IEEE Conf. Systems, Man, and Cybernetics*, San Antonio, TX, 1023-28.

Duraiswami R, Chahine G L and Sarkar K 1997 Boundary element techniques for efficient 2-D and 3-D electrical impedance tomography *Chem. Eng. Sci.* 13 2185–96.

Ergezer M, Simon D and Du D 2009 Oppositional biogeography-based optimization, *IEEE Conf. Systems, Man, and Cybernetics*, San Antonio, TX, 1035-40 .

Collection @ jeju

Faes T J C, van der Meij H A, Munck J C and Heethaar R M 1999 The electric resistivity of human tissues (100 Hz–10 MHz): A meta-analysis of review studies *Physiol. Meas.* **20** R1-10.

Fraser A S 1957 Simulation of genetic systems by automatic digital computers. I. Introduction *Aus. J. Biol. Sc.* **10** 484-491.

Gadd R, Vinther F, Record P M and Rolfe P 1992 Reconstruction of three-dimensional data for electrical impedance tomography *Electron. Lett.* **28** 974-76.

Ghosh A, Tsutsui S and Tanaka H 1998 Function optimization in non-stationary environment using steady state genetic algorithms with aging of individuals *in Proc. Congr. Evol. Comput. Anchorage, AK* 666-671.

Goldberg D 1989 Genetic algorithms in search, optimization and machine learning (Addison-Wesley Publishing Company).

Gong W Cai Z and Ling C X 2010 DE/BBO: a hybrid differential evolution with biogeography-based optimization for global numerical optimization *Soft Comput.* 1-21.

Grefenstette J J 1992 Genetic algorithms for changing environments *Proc. Parallel Prob. Solv. From Nature, Brussels, Belgium* 137-144.

Grosan C, Abraham A and Ishibuchi H 2007 *Hybrid Evolutionary Algorithms: Methodologies, Architectures, and Reviews* (Berlin: Springer).

Hammermeister K E, Chikos P M, Fisher L and Dodge H T 1979 Relationship of cardiothoracic ratio and plain film heart volume to late survival *Circulation* **59** 89-95.

Collection @ jeju

Han D K and Prosperetti A 1999 A shape decomposition technique in electrical impedance tomography *J. Comput. Phys.* **155** 75-95.

Harris N D 1991 Applications of electrical impedance tomography in respiratory medicine *PhD Thesis* Univ. of Sheffield.

Hemingway H, Shipley M, Christie D and Marmot M 1998 Cardiothoracic ratio and relative heart volume as predictors of coronary heart disease mortality *Eur. Heart J.* **19** 859-69.

Hoffman E A and Ritman E L 1987 Heart-lung interaction: effect on regional lung air content and total heart volume *Ann. Biomed. Eng.* **15** 241-57.

Hoffmeister F and Back T 1991 Genetic algorithms and evolution strategies: Similarities and differences *in PPSN I Proc. 1st workshop on parallel solving from nature* (vol 4961) (Berlin: Springer) pp 455-469.

Holland J H 1975 *Adaptation in natural and artificial systems* (University of Michigan press).

Ider YZ Gencer N G, Atalar E and Tosun H 1990 Electrical impedance tomography of translationally uniform cylindrical objects with general crossectional boundaries *IEEE Trans. on Med. Im.* **9** 49-59.

Ikehata M and Siltanen S 2000 Numerical method for finding the convex hull of an inclusion in conductivity from boundary measurements *Inverse Prob.* **16** 1043-52.

Jin Y and Branke J 2005 Evolutionary optimization in uncertain environments—A survey *IEEE Trans. Evol. Comput.* **9** 303-317.

Collection @ jeju

Jin Y and Sendhoff B 2004 Constructing dynamic test problems using the multi-objective optimization concept *in Applications of Evolutionary Computing, G. Raidl, Ed. et al. New York* (vol 3005) (Berlin: Springer) pp 525-536.

Julier S J and Uhlmann J K 2004 Unscented filtering and nonlinear estimation. *Proc. IEEE* **92** 401-422.

Khambampati A K, Rashid A, Kim S, Soleimani M and Kim KY 2009 Unscented Kalman filter approach to track moving interfacial boundary in sedimentation process using three-dimensional electrical impedance tomography *Phil. Trans. R. Soc. A.* **367** 3095-120.

Khambampati A K, Rashid A, Kim B S, Liu Dong, Kim S and Kim K Y 2010 EM algorithm applied for estimating non-stationary region boundaries using electrical impedance tomography *J.Phys.: Conf. Ser.* **224** 012044.

Kim B S, Kim K Y, Kao T J, Newell, J C, Isaacson D and Saulnier G J 2006 Dynamic electrical impedance imaging of a chest phantom using the Kalman filter *Physiol. Meas.* **27** S81-91.

Kim B S, Isaacson D, Xia1 H, Kao1 T-J, Newell J C and Saulnier G J 2007a A method for analyzing electrical impedance spectroscopy data from breast cancer patients *Physiol. Meas.* **28** S237- 46.

Kim K Y, Kim, B S, Kim M C, Lee K J, Ko Y J and Kim S 2005 Electrical impedance imaging of two-phase flows undergoing rapid transient : part II. Effect of input current pattern *International Communications in Heat and Mass Transfer* **32** 649-57.

Kim K Y, Kim B S, Kim M C, Lee Y J and Vauhkonen M. 2001 Image reconstruction in time-varying electrical impedance tomography based on the extended Kalman filter. *Meas. Sci. Technol* **12** 1-8.

Collection @ jeju

Kim S, Ijaz U Z, Khambampati A K, Kim K Y, Kim M C and Chung SI 2007b Moving interfacial boundary estimation in stratified flow of two immiscible liquids using electrical resistance tomography *Meas Sci Technol* **18** 1257-1269.

Kolehmainen V, Voutilainen A and Kaipio J P 2001 Estimation of non-stationary region boundaries in EIT—state estimation approach *Inverse Prob.* **17** 1937.

LaTorre A 2009 A framework for hybrid dynamic evolutionary algorithms: multiple offspring sampling (MOS) *PhD Thesis* Universidad Politécnica de Madrid.

Lewis J, Hart E and Ritchie G 1998 A comparison of dominance mechanisms and simple mutation on non-stationary problems *in Proc. Parallel Problem Solving From Nature, Amsterdam, The Netherlands* 139-148.

Li X R 1997 Canonical transform for tracking with kinematic models. *IEEE trans. Aerospace and Electronic Systems* **33** 1212-1224.

Louis S J and Xu Z 1996 Genetic Algorithms for Open Shop Scheduling and Re-Scheduling *ISCA 11th Int. Conf. on Computers and their Applications*.

Malmivuo J and Plonsey R 1995 *Bioelectromagnetism.* Oxford university press New York

Mann R, Dickin FJ, Wang M, Dyakowski T, Williams R A and Edwards R B *et al* 1997 Application of electrical resistance tomography to interrogate mixing processes at plant scale *Chem. Eng. Sci.* **52** 2087-97.

McArdle F J 1992 Investigation of cardiosynchronous images of the heart and head using Applied Potential Tomography *PhD Thesis* Univ. of Sheffield.

Ng K P and Wong K C 1995 A new diploid scheme and dominance change mechanism

Collection @ jeju

for non-stationary function optimization *Int. Conf. Genetic Algorithms, Pittsburgh, PA* 159-166.

Oppacher F and Wineberg M. 1999 The shifting balance genetic algorithm: Improving the GA in a dynamic environment *Genetic Evol. Comput. Conf., Orlando, FL* 504-510.

Philbin E F, Garg R, Danisa K, Denny M, Gosselin G, Hassapoyannes C, Horney A, Johnstone D E, Lang R M and Ramanathan K *et al* 1998 The relationship between cardiothoracic ratio and left ventricular ejection fraction in congestive heart failure *Arch. Intern. Med.* **158** 501-6.

Ramsey C L and Grefenstette J J 1993 Case-Based Initialization of Genetic Algorithms *Fifth Int. Conf. Genetic Algorithms*.

Rashid A, Kim B S, Khambampati A K, Liu Dong, Kim S and Kim K Y 2010a Dynamic boundary estimation of human heart within a complete cardiac cycle using electrical impedance tomography *J. Phys.: Conf. Ser.* **224** 012042.

Rashid A, Khambampati A K, Kim B S, Kim S, Kang M J and Kim K Y 2010b An EKF based estimation scheme for sedimentation processes in vessels using EIT-type measurement data *Flow Meas. Inst.* **21** 521-30.

Rashid A, Khambampati A K, Kim B S, Dong L, Kim S, and Kim K Y 2010c A differential evolution based approach to estimate the shape and size of complex shaped anomalies using EIT measurements *GDC/CA 2010 (CCIS* vol 121**)** (Berlin: Springer) pp 206-15.

Rashid A, Kim B S, Khambampati A K, Kim S, and Kim K Y 2011 An oppositional biogeography-based optimization technique to reconstruct organ boundaries in human thorax using electrical impedance tomography *physiol. meas.* **32** 767.

Collection @ jeju

Rechenberg I 1971 Evolutionsstrategie Optimierung Technischer Systeme nach Prinzipien der Biologischen Evolution.

Rolnik V P and Seleghim Jr P 2006 A specialized genetic algorithm for the electrical impedance tomography of twophase flows *J. of the Braz. Soc. of Mech. Sci and Eng.* **28** 378-90.

Ryan C 1997 Diploidy without dominance *Nordic Workshop on Genetic Algorithms, Helsinki, Finland* 63-70

Saleem S and Reynolds R 2000 Cultural algorithms in dynamic environments *2000 Congress on Evolutionary Computation* 1513-1520.

Salomon R and Eggenberger P 1997 Adaptation on the evolutionary time scale: A working hypothesis and basic experiments. In Hao J-K, Lutton E, Ronald E, Schoenauer M and Snyders D *Artificial Evolution: Third European Conf., AE'97* (Berlin: Springer) pp 251–262.

Schwefel H P 1974 Numerische Optimierung von Computer-Modellen. *PhD thesis* Technischen Universitat Berlin.

Seppanen A, Vauhkonen M, Somersalo E and Kaipio J P 2001a State space models in process tomography – approximation of state noise covariance *Inverse Problems Eng.* **9** 561-585.

Seppanen A, Vauhkonen M, Vauhkonen P J, Somersalo E and Kaipio J P 2001b State estimation with fluid dynamical evolution models in process tomography – an application to impedance tomography *Inverse Probl.* **17** 467-484.

Shumway RH and Stoffer D S 1982 An approach to time series smoothing and forecasting using the EM algorithm *J. Time Ser. Anal.* **3** 253-264.

Collection @ jeju

Simon D 2008 Biogeography-Based Optimization *IEEE Trans. Evol. Comput.* **12** 702-13.

Simon D 2009 A probabilistic analysis of a simplified biogeography-based optimization algorithm *Evolutionary Computation* **19** 167-188.

Simon D, Ergezer M and Du D 2009 Population distributions in biogeography-based optimization algorithms with elitism, *IEEE Conference on Systems, Man, and Cybernetics,* San Antonio, TX, 1017-22.

Somersalo E, Cheney M, Isaacson D 1992 Existence and uniqueness for electrode models for electric current computed tomography *SIAM J Appl Math* **4** 1023–40.

Spears W 1992 Crossover or Mutation? *Foundations of Genetic Algorithms Workshop* **2** 221-237.

Steding K, Buhre T, Carlsson M, Engblom H, Mosén H, Wohlfart B and Arheden 2007 Total heart volume independently predicts maximal work capacity in normals and athletes *Circulation* **116** 346-7.

Storn R and Price K 1997 Differential evolution - A simple and efficient heuristic for global optimization over continuous spaces. *J. of Global Optim.* **11** 341-359.

Tossavainen O P, Vauhkonen M, Kolehmainen V and Kim KY 2006 Tracking of moving interfaces in sedimentation processes using electrical impedance tomography *Chem Eng Sci.* **61** 7717-7729.

Trojanowski K and Michalewicz Z. 1999 Searching for optima in non- stationary environments *Proc. Congr. Evol. Comput.,Washington, DC* 1843-1850

Tseng L and Liang S 2006 A hybrid metaheuristic for the quadratic assignment problem *Comput. Optim. and Appl.* **34** 85-113.

Ursem R K 2000 Multi-national GA optimization techniques in dynamic environments

Collection @ jeju

Proc. Genetic Evol. Comput. Conf., Las Vegas, NV 2000 19-26.

Vauhkonen M 1997 Electrical impedance tomography and prior information *PhD Thesis* University of Kuopio, Finland online at http://venda.uku.fi/~mvauhkon

Vauhkonen M, Karjalainen P A and Kaipio J P 1998 A Kalman filter approach applied to the tracking of fast organ boundaries *Proc. 20th Annual Int. Conf. of the IEEE Engineering in Medicine and Biology Society* **20** 1048.

Vauhkonen M, Lionheart W R B, Heikkinen L M, Vauhkonen P J and Kaipio J P 2001 A MATLAB package for the EIDORS project to reconstruct two dimensional EIT images *Physiol. Meas.* **22** 107–11.

Vavak F, Fogarty T C and Jukes K 1996 A genetic algorithm with variable range of local search for adaptive control of the dynamic systems. Proc. the 2nd Int. Mendelian Conf. on Genetic Algorithms.

Weicker K 2003 Evolutionary algorithms and dynamic optimization problems *PhD Thesis* Univ. of Stuttgart.

Weicker K and Weicker N 2000 Dynamic rotation and partial visibility *in Proc. Congr. Evol. Comput., San Diego, CA* 1125-1131.

Wirgin 2004 The inverse crime. ArXiv *Mathematical Physics* e-prints arXiv:math-ph/0401050.

Witsoe D A and Kinnen E 1967 Electrical resistivity of lung at 100 kHz *Med. & Biol. Engng.* **5**, 239-48.

Woldesenbet Y G and Yen G G 2009 Dynamic evolutionary algorithm with variable relocation *IEEE Trans. Evol. Comput.* **13** 500-13.

Young A A and Frangi A F 2008 Computational cardiac atlases: from patient to

Collection @ jeju

population and back *Exp. Physio.* **194** 578-96.

Ziegler R F 1962 Technics for, and the importance of, heart size determination in infants and children *J. Natl. Med. Assoc.* 54: 439-44.

Eckel H 2008 Numerical study of an evolutionary algorithm for electrical impedance tomography *PhD thesis* Georg August University, Göttingen, Germany.

Collection @ jeju